ESCUELA POLITÉCNICA SUPERIOR
DEPARTAMENTO DE QUÍMICA-FÍSICA Y TERMODINÁMICA APLICADA
ÁREA DE MÁQUINAS Y MOTORES TÉRMICOS

NUMERICAL AND EXPERIMENTAL ANALYSIS OF THE ENERGY SAVING AND POTENTIAL OF VENTILATION OF OPAQUE VENTILATED FACADES

PHD THESIS

AUTHOR: FERNANDO PECI LÓPEZ

ADVISOR: Dr. MANUEL RUIZ DE ADANA SANTIAGO

OCTOBER, 2012

TITULO: *NUMERICAL AND EXPERIMENTAL ANALYSIS OF THE ENERGY SAVING AND POTENTIAL OF VENTILATION OF OPAQUE VENTILATED FACADES*

AUTOR: *FERNANDO PECI LÓPEZ*

Campus de Rabanales
Ctra. Nacional IV, Km. 396 A
14071 Córdoba

www.uco.es/publicaciones
publicaciones@uco.es

TÍTULO DE LA TESIS:

NUMERICAL AND EXPERIMENTAL ANALYSIS OF THE ENERGY SAVING AND POTENTIAL OF VENTILATION OF OPAQUE VENTILATED FACADES

DOCTORANDO/A:

D. FERNANDO PECI LÓPEZ

INFORME RAZONADO DEL/DE LOS DIRECTOR/ES DE LA TESIS

(se hará mención a la evolución y desarrollo de la tesis, así como a trabajos y publicaciones derivados de la misma).

Por todo ello, se autoriza la presentación de la tesis doctoral.

Córdoba, ____ de _____ de _____

Firma del director

Fdo.:_____

Para Pilar, Pilar, Fernando y Beatriz,

Contents

LIST OF FIGURES

LIST OF TABLES

Nomenclature:

A_j area of surface j in zone i (m^2)

A_c cross-section area of the air gap (m^2)

C_p pressure coefficient (dimensionless)

C_D discharge coefficient (dimensionless)

c_p specific heat of air (J/kg K)

D_h hydraulic diameter (m)

G_s total solar shortwave irradiation on the façade (W/m^2)

H height of the OVF air gap (m)

h_o exterior convection coefficient ($W/ m^2 K$)

h_{ow} windward exterior convection coefficient ($W/ m^2 K$)

h_{ol} leeward exterior convection coefficient ($W/ m^2 K$)

L 1/5 of the OVF height (m)

$\dot{m}$ mass flow rate (kg/s)

Nu_{Dh} Nusselt number based on the hydraulic diameter (dimensionless)

P_w pressure difference between static pressure on the façade and atmospheric pressure (Pa)

P_i, P_j pressure of zones i and j (Pa)

Q_i net energy rate into air node I (W)

Q_{sj} net energy rate from surface s to air node I (W)

Q_{fk} energy gain due to airflow coming from zone k (W)

q_s solar irradiance incident on the exterior OVF surface (W/m^2)

q_c heat flux into the façade due to conduction (W/m^2)

q_{rs} net solar short wave radiation absorbed by the façade (W/m^2)

q_{rl} net solar long wave radiation absorbed by the façade (W/m^2)

T_{sky} sky effective temperature (K)

T_{so} exterior surface temperature (K)

T_o ambient temperature (K)

T_k temperature of air node k (K)

V_f undisturbed Wind speed (m/s)

$\dot{V}$ air flow rate (m^3/s)

Z_i, Z_j height of nodes i and j (m)

Greek letters

α_s solar absortance of the external OVF surface (dimensionless)

ε long wave emissivity (dimensionless)

ζ dynamic loss coefficient (dimensionless)

λ friction factor (dimensionless)

ρ density of air (kg/m^3)

σ Stefan-Boltzmann Constant 5.6697×10^{-8} ($W/m^2 K^4$)

ABSTRACT

Nowadays the efficient use of energy is a crucial necessity. Buildings are among the greater energy consumers in a country and the ventilation and HVAC systems account for a high percentage of this consumption. A way of reducing the energy consumption of these systems is taking advantage of the renewable energies available. In this document an opaque ventilated façade (OVF) was studied. An OVF takes advantage of the wind force and solar radiation to provide the indoor space with free ventilation and air preheating. The objectives of the study were: find evidence of this possible advantages, quantify the potential of an OVF to provide ventilation and heating in different situations and study the sensibility of the system to variation of the most important parameters. For this purpose an experimental module of OVF was built and monitorized, and a model was configurated and validate with the experimental data. With this model, simulations were carried out to study the performance of the OVF with the variations of estimated parameters and design parameters. It was also tested the performance of the OVF under different climatic conditions in several climatic areas of Spain. The results showed that for any climatic zone the OVF could provide buildings with free ventilation. However the flow rates yielded weren't sufficient to meet the regulation requirement so this system would require mechanical ventilation support. The results also showed that the heating energy consumption could be reduced by two means: preheating the ventilation air and introducing ventilation air in non occupancy periods at a convenient temperature. From the sensibility study it could be concluded that the external and internal convection coefficients, and the solar absortivity were key parameters for predicting the energy savings an OVF could provide.

1. INTRODUCTION

1.1 BACKGROUND

The concern about the efficient use of energy has been increasing in the last few decades. There are economic and environmental reasons involved on this matter. Emissions of greenhouse effect gases and the climate change associated, polluting of inhabitated areas, health problems, etc. are some of the main problems that a bad use of energy can generate. International agreements have been reached in order to try to stop or mitigate these problems, like in the summits of Kyoto, Aalborg or Bali. The Kyoto protocol considered, in a global way, the reduction of emission of gases like CO2, 5% from 2008 to 2012, respect emissions in 1990.

An increasing percentage of the energy consumed in a country is destined to supply residential and office buildings. The increasing population, the improvement of quality of life as well as the increase of the time people spend indoor, have made their energy consumption rise up to the same levels of industry or transport [1]. In the EU the energy consumption of residential buildings reached 40% of the total energy demand [2]. In Spain that percentage was about 25% [3].

Due to this, in the last few years a policy destined to improve energy efficiency in buildings has been developed. Its aim is promoting energy efficientcy in buildings through the improvement of building design, better insulation, better performace of HVAC devices and the use of renewable energy sources where available. HVAC energy consumption accounts for more than half the total energy consumption of a residential or office building [4].

In Spain these objectives are implemented in the Technical Building Code [5] (CTE). The aims of this regulation are limiting the building energy demand through a good building design, installations improvement and the support of renewable energy sources.

A good indoor air quality is essential for getting a high level of comfort inside a building. Air quality influences health and efficiency of inhabitants [6]. People usually spend 80% to 90% of their time indoor. Due to the modern life style, more healthy and comfortable environments are also required. Some of the factors which influence indoor air quality are air temperature, humidity, air draughts and level of pollutants. Regulations contains minimum levels of ventilation depending on the type of activities develop in rooms.

Ventilation can be forced, natural or a mix of them. Nowadays new systems are being studied for accomplishing ventilation requirements while reducing building energy consumption. Natural ventilation uses wind and buoyancy forces to ventilate rooms, reducing the use of mechanical means and therefore reducing energy consumption. The most common way of natural ventilation is cross ventilation. In cross ventilation, air flows through the building windows, door and vents, using the force of the wind, or the stack effect caused by the indoor-outdoor temperature difference.

Natural ventilation has been traditionally implemented using the normal building openings like windows and doors. However this method presents some inconveniences like noise increase, wind draughts or incorrect user operation. One of the most studied alternative ways to ventilate buildings naturally is by using ventilated facades

1.2 THE VENTILATED FAÇADE CONCEPT

A ventilated façade is a double skin façade made up of two layers separated by an air gap. The layers can be opaque or transparent. The air gap normally has an inlet opening through which the ambient air comes in, and one or two exhaust openings for returning the air back to the ambient or driving it into the building. Other types of ventilated facades have also an interior inlet opening, allowing other operation modes. Air flow can be induced naturally through the facade by wind forces or due to thermal buoyancy. Additionally, in sunny days part of the solar radiation absorbed by the facade is transferred to the air in the gap. This heated air can be introduced in the building if it is convenient, thus reducing the heating energy consumption of the building.

Ventilation modes depend on the estate of the façade openings. As it was mentioned above, in a double skin façade there could be up to four openings. In Figure 1 the different operation modes more widely studied are represented, [7] The A) configuration is a traditional façade with an air gap between two solid layers. In double glazed facades this configuration presents overheating problems due to the greenhouse effect. It is also a configuration used in double-pane windows. It has other advantages as indoor noise reduction and in some cases greater insulation level than that of single pane windows. The B) configuration is referred as exterior air curtain. The air gap is ventilated with exterior air and then exhausted back again to the ambient. The aim of this is removing the hot air to prevent overheating. The air flow driving forces are wind pressure and buoyancy. In case C) the air curtain is interior. The air enters the air gap and it increases its temperature as It passes through the façade, removing the heat from the structural elements of the façade or from a specific device placed to absorb solar radiation, for example blinds. The driving force in this case is buoyancy, though mechanical ventilation can also be used. The former cases didn’t

imply ventilation of the adyacent rooms with ambient air. In D) and E) cases the air is received or supplied by the adyacent room. In the first case, named supply window, the air enters the façade and is heated as it passes through the air gap, then it is introduced into the room providing ventilation and heating. The driving forces are wind pressure and buoyancy but mechanical ventilation could also be used if convenient. The E) case is called exhaust window as the indoor air is exhausted through the façade's air gap. The same driving forces as in the previous case are present.

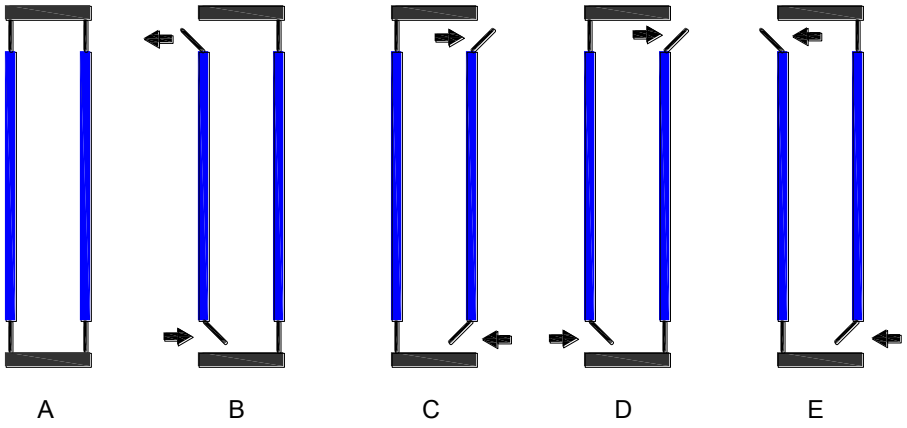

Figure 1. Operating modes in a double skin façade. A) closed air gap, B) Exterior air curtain, C) Interior air curtain, D) Supply window, E) Exhaust window.

1.3 CLASSIFICATION OF VENTILATED FAÇADES

Ventilated facades are classified according to several criteria, like the type of ventilation, the ventilation modes and the partitioning of the cavity [8] . The two first criteria have already been discussed above. According to the partitioning of the air cavity ventilated double façade can be classified as:

- Modular partitioning: The building façade is made up totally or partially of independent ventilated façade modules.
- Storey partitioning: The ventilated façade modules extend across the entire storey façade.

- Shaft-box: Storey modules are linked vertically in order to increase the stack effect.
- Multistorey: There isn't any modularity. The air cavity extends across the entire building façade.

Another classification criteria regarding the materials used for each layer could be:

- Totally glazed ventilated double facades: all the façade layers are transparent.
- Opaque and glazed layers: at least one the layers is opaque, normally the interior one, as in Trombe walls.
- Opaque ventilated façade (OVF). Both layers are opaque.

The most widely studied and implemented type of double skin facade is the glazed double skin façade. This type of facade has become very popular due to its aesthetically pleasing exterior [9]. However, the use of double glazed facades increases the risk of overheating in the hot season [10]. Moreover, glazed double skin facades are generally more expensive and the maintenance costs are higher.

1.4 OPAQUE VENTILATED FACADES

To avoid the disadvantages of using a transparent façade in hot climates, an alternative solution could be using opaque ventilated façades. In an opaque ventilated façade its two solid layers are opaque and solar radiation is absorbed in the external one, thus reducing the overheating risk. Additionally, an opaque ventilated façade can be made of conventional materials, therefore leading to a smaller cost.

Different types of OVF's have been studied in the last few years. In [11] a type of double skin opaque façade called rainscreen was studied. A rainscreen is basically an OVF where the inlet and outlet openings are always open to the exterior. In other paper [12], a multi-storey OVF was assessed using a scaled experimental model. A combination of photovoltaic panels and a ventilated façade was studied in [13]. Finally, in [14], three types of OVF were analyzed to investigate their thermal behavior.

An opaque ventilated façade is basically a double skin façade made up of two opaque layers separated by an air gap. The inner layer works as building insulation whereas the outer layer acts as a solar radiation collector. The air gap normally has an inlet opening by which the ambient air comes in, and one or two openings for exhausting the air back to the ambient or for introducing it to rooms. Natural ventilation can be induced through the facade by the wind flowing around the building, or due to the stack effect, as in the case of traditional cross ventilation. Furthermore, part of the solar radiation absorbed by the exterior layer is transfered to the air in the gap. This hot air moves up as a consequence of buoyancy and can then be introduced in the building or exhausted to the ambient, depending on the climate conditions. Usually these three effects act simultaneously, depending on the weather conditions.

1.5 OBJECTIVES

The work described in this document attempted to reach several objectives about OVF's. First, getting evidence about the claimed advantages of using an OVF as a mean for preheating air and therefore reducing the heating energy demand of a building. In addition to this, evaluating the performance of the same OVF in the hot season in order to know if there are any disadvantages, as OVF is a dynamic system and the capacity to adapt to different weather conditions should be proven. Second, quantifying the potential of an OVF to provide free ventilation and evaluating the ratio of natural ventilation to ventilation requirements by regulations that the system provides.

Third, finding out which climatic conditions are better to install this type of facades and in which ones it wouldn't be worth it to do it as the performace of an OVF will be different depending on the climatic conditions of the location of the building. Finally, obtaining basic design parameters and producing guidelines for the OVF designing process.

The strategy followed in this research was: first obtaining experimental data about the performance of an OVF in order to evaluate its ventilation and heating capacity; next, creating a numerical model which would use the estimated parameters obtained from the analysis of the experimental data previously recorded. A control system was needed at this stage so simulations were carried out to find out a convenient control system that takes advantage of the OVF potentials. Once the numerical model of the OVF was validated against the experimental data, it was included in a real building model for subsequent studies. Simulations in different climatic conditions were carried out and the results obtained were analysed. After this, a sensitivity study of the model outputs to the estimated parameters was carried out in order to know if little variations or errors in the estimated paramaters seriously affected the results. Finally simulations with different values of design parameters were run in order to obtain useful information for the basic design of an OVF.

2. EXPERIMENTAL STUDIES WITH OPAQUE VENTILATED FAÇADES

2.1 INTRODUCTION

Facades, as external building elements, are exposed to the changing atmospheric conditions. The meteorogical variables depend on the location of the building, its climatic characteristics and the season of the year. Although the weather usually follows a typical pattern along the year for a certain location, it usually changes from year to year in a more or less cycling way. The performance of an OVF depends on solar radiation, ambient temperature and wind speed and direction, which are variables that are continually varying in a quite unpredictable way. Therefore the best way of studying the performance of an OVF is by putting it under real weather conditions for the longest time possible.

Two experiences with OVF's were carried out under real weather conditions. In the first one, the experimental module of OVF was install in a homologated test cell; in the second one a module of OVF was installed covering part of the façade of a real building.

2.2 MONITORING AN OVF WITH A PASLINK CELL

An experimental opaque ventilated facade was built up and installed on a PASLINK test cell in order to evaluate its performance under real weather conditions. The PASLINK cell was set up in the Building Quality Control Laboratory of the Vasque Country Government in Vitoria (Spain). The experimental data were measured from the 1st to 19th of September 2009. The tests were done in the framework of the Research

National Proyect *"Integration of industrial construction systems of active ventilated facades to guarantee an efficient energy consumption and indoor air quality. Application to non residential buildings"*.

2.2.1 EXPERIMENTAL SET UP

2.2.1.1 The PASLINK test cell

The PASLINK cell is made up of two adjacent rooms: the service room and the test room, Figure 2. The service room contains all the measure instruments and the pressure control system. The test room is basically a very well insulated room where the heat transfer through all the walls (except for the test probe wall) is measured. The inside surfaces of the test room are covered with heat flux measurement tiles. These tiles measure the heat losses through the insulation walls of the test room. The inside surface temperature and inside air temperatures are measured and the heat loads inside the room monitored. The temperature inside the test room can also be set to a constant temperature as it includes heating and cooling devices, but in the tests carried out in this study the temperature was allowed to vary freely. More details about the construction of the PASLINK cell can be found in [15].

2.2.1.2 The opaque ventilated facade test probe

The test probe of opaque ventilated façade was installed on the south face of the PASLINK test cell. The test probe was 2.71 m width and 2.96 m height and it had three layers: an insulation layer, an air gap and a steel plate. The OVF probe was made up horizontally of three identical modules of 0.9 m width. Each module had an independent air channel, with an 0.9 width and 0.03 m height opening at the bottom and a 0.7 x 0.17 m opening at the top. A schematic of the OVF can be seen in Figure 3 and . The materials used for the layers and its characteristics can be seen in Table 1.

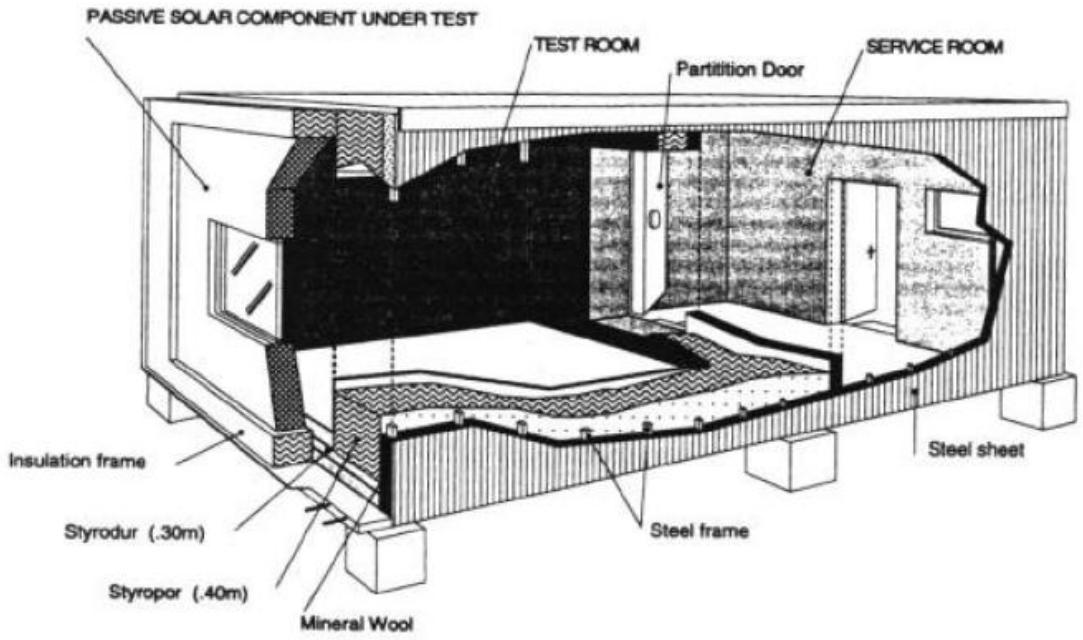

Figure 2. Schematic drawing of a PASLINK test cell.

In order to prevent the effect of wind pressure on the OVF outlet openings, the latter were connected through ducts with a common pipe which was equipped with a fan aimed to maintain a neutral pressure at the façade outlet, [16]. This set up is shown in Figure 5. The difficulty of controlling the pressure difference between the OVF outlet and the atmospheric pressure made it unfeasible. Eventually the fan was used to keep a constant pressure increase. The exhaust pipe was protected from the wind so the wind driving force was only due to the wind pressure at the inlet opening and not by the pressure at the exhaust.

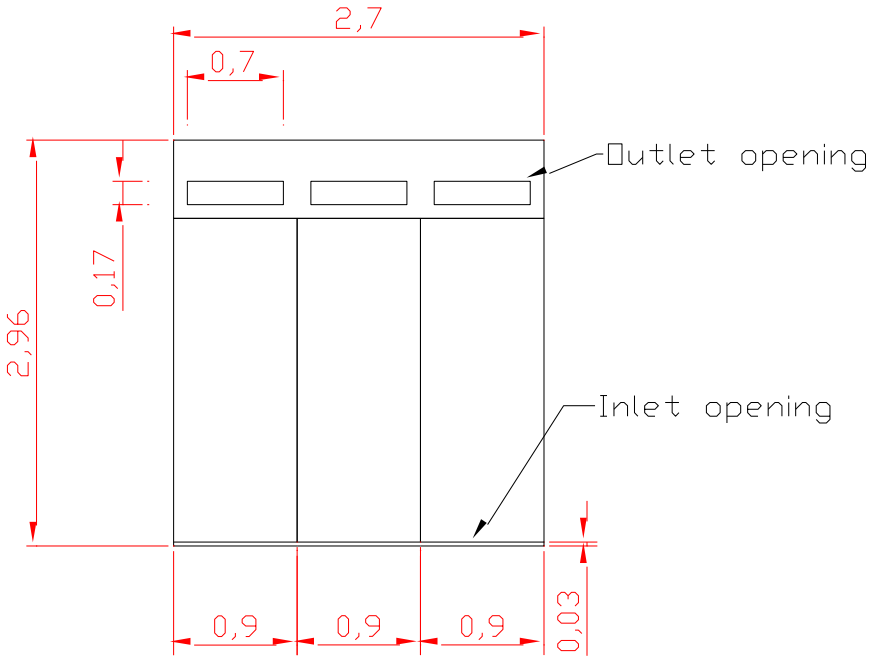

Figure 3. Front view of the test probe of OVF for the PASLINK test.

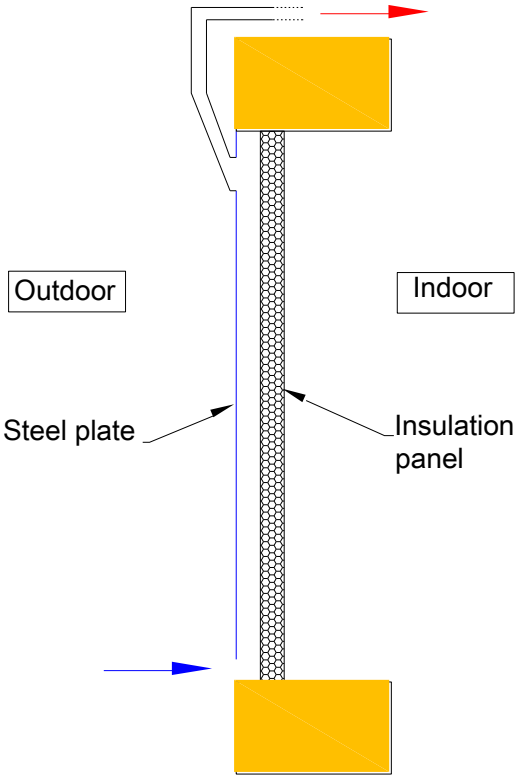

Figure 4. Schematic view of the OVF channel

Figure 5. Pictures of: A) Front view of the OVF. B) Fan. C) Connection of the façade with the common pipe.

Table 1. Thermophysics properties of the materials used in the OVF

	Conductivity (W/m K)	Specific heat (kJ/kg K)	Density (kg/m^3)	Thickness (m)
Galvanized steel	60	0.50	7800	0.002
Insulation panel	0.350	1.80	40	0.10

2.2.1.3 Measurement set up

The temperature of the air inside the OVF was measured using PT100 Ahlborn FP04415 (± 0.2 ºC) probes in five points along the height of the façade. The points of measurements were located equally distant to the steel plate and the insulation layer. These temperature sensors were not shielded due to the small thickness of the air gap. Later, it was found that this affected importantly to the accuracy of the measurements. The increase of the temperature of the air inside the façade was also measured with a 10 measurement point thermopile (± 0.01 ºC). The air flow rate was calculated using the air speed measurement of a thermoanemometer Ahlborn FVA605TA (±0.1 m/s)

located in at mid height of the façade. The locations of the probes are shown in Figure 6. The measurement signals were transmitted to an Agilent data logger. The frequency of measurement was 0.1 Hz.

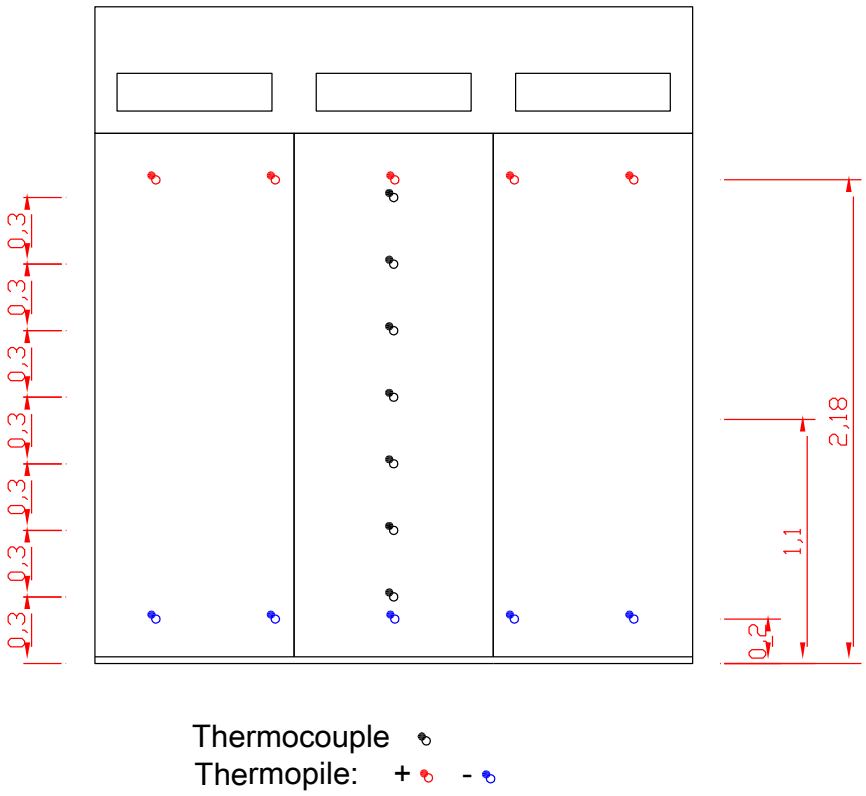

Figure 6. Location of the measurement probes.

The weather data were measured with a meteorological station made up of three shielded ambient temperature sensors (± 0.2 K), a pyranometer with solar tracker for measuring the diffuse horizontal radiation, a pyramometer for the solar horizontal global radiation, a pyranometer for the solar global radiation on the vertical surface facing south, an anemometer installed on a 10 m mast (± 1 m/s), a measure of wind direction (± 10º) in the same mast and a measure of relative humidity (±2%). All the pyranometers were Kipp & Zonen model CMP 11 (± 3 %).

2.2.2 RESULTS AND ANALYSIS

In Figure 7, the increase of air temperature and the flow rate inside the air gap of the OVF during the 19 days of measurements is shown. The weather conditions can also be seen in this figure. Most of the days were sunny days with a global solar radiation maximum up to 740 W/m^2. Only six days were overcast or cloudy days with maximum global solar radiation of around 60-300 W/m^2. The minimum night temperatures were around 8 ºC and the maximum day temperatures were around 35 ºC. The wind speed in front of the south façade of the PASLINK test cell was low, with a mean value of 0.4 m/s. The prevalent wind direction was 150º (Southeast).

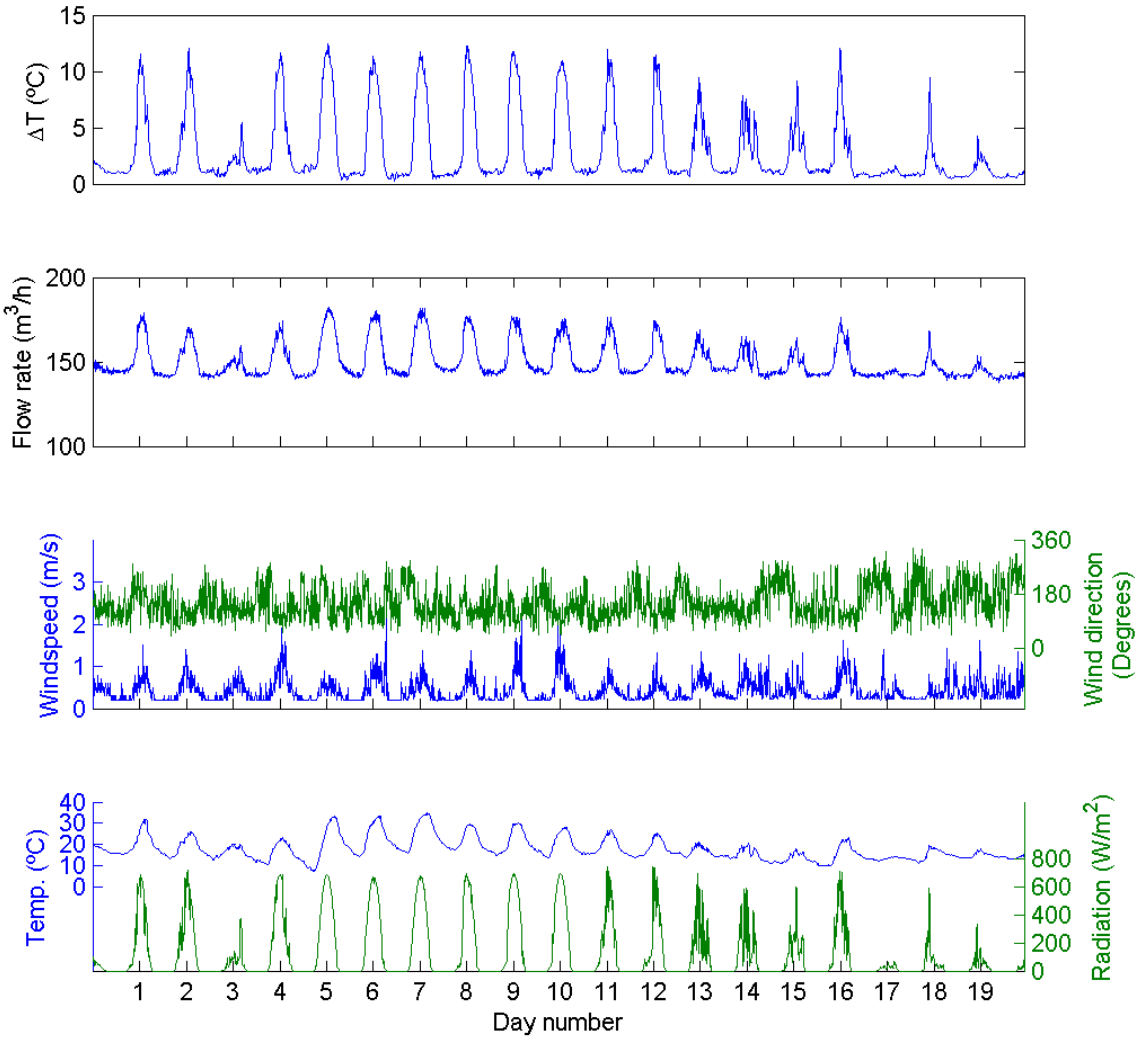

Figure 7. Air Temperature increase inside and flow rate inside the façade. Wind speed and wind direction(0° = north). Ambient temperature and global solar radiation on the façade.

As the OVF channel was open to the ambient air at both ends, the only driving forces possible were wind pressure and buoyancy due to the temperature difference between the air in the air gap and the outside air. It can be clearly seen that the main driving force of the increase in the air flow rate was the buoyancy force. The air inside the façade was heated by the short wave solar radiation absorbed on the exterior steel layer. The days with maximum solar radiation corresponded with the days with maximum air flow rate. The cloudy days like days 3, 17, 18, and 19 had the lower air flow rates. Even in days where the wind pressure was high and the wind direction was favorable, the wind pressure was not enough to increase the air flow rate. The reason of this could have been the small pressure coefficient as the inlet opening was near the ground and the PASLINK test cell was located near a building that sheltered it from wind.

The uncertainty of the measurements of air temperatures and temperature increase inside the façade was affected by the long wave radiation, mainly due to the high temperatures of the steel plate layer. Usually, the temperature probes are shielded from radiation with silvered pipes. Due to the small depth of the air gap it wasn't possible to do that. Therefore the temperature increase measured was probably higher than the real one.

Nevertheless the results evinced the capacity of the OVF of generating an air flow and preheating it. The measurements were taken in a warm season and the ventilation air wouldn't have to be preheated. In this case the hot air flow rate was an example of how the excess of heat could be removed with the exhaust air to the environment. The buoyancy force derived from the heating of air inside the OVF increased the forced ventilation up to 30% in the peak hours.

The wind force in the measurements was found negligible. However it was not possible to measure the pressure coefficient in the inlet opening and in the exhaust so this variable could not be quantified. In later experiments where the wind force was expected to have greater values pressure measurements where planned.

2.2.3 CONCLUSIONS

The following conclusions were reached after analysing the results from the experiment.

- The air was preheated when flowing through the OVF's channel and the maximum temperature increases were around 10 ºC.
- The air flow due to the buoyancy force reached 30% of the forced ventilation provided by the fan.
- The wind force was negligible, however it should have been to be measure to give quantitative data.
- The temperature in the air gap was affected by long wave radiation and it should be shielded so a bigger air gap would be necessary in subsequent experiments.
- It would be necessary to measure the wind pressure in order to evaluate the influence of the wind driving force on the air flow rate.
- The results showed the capacity of the façade of evacuating part of the heat load due to the solar radiation.
- The ventilation mode wasn't used, so it was necessary to do another test in this mode.

2.3 EXPERIMENTAL OVF MODULE ON A REAL FACADE

2.3.1 EXPERIMENTAL SET UP

An experimental opaque ventilated façade module was built and monitored, under real weather conditions, in the Indoor Environmental Engineering Laboratory of the Department of Civil Engineering of the Aalborg University. The module was equipped with sensors for measuring the variables needed to assess its thermal and ventilation performance. Weather data devices were also installed to register the weather conditions during the measurement period. The laboratory building was a one storey building surrounded by other buildings of similar height, and by access roads and trees. The module was attached to the south-west façade which orientation was 126º W. The location of the module was near a building corner. The wind sheltering effect of the own building and other buildings and obstacles was studied through the experimental evaluation of the local pressure coefficient. The module covered a window at the upper part of the wall, which was used to install the ducts for connecting the ventilated air cavity with the indoor space and pass the cables. This window was blinded and insulated after installing the module to prevent air leakages and thermal losses.

The module was made up of a 0.025 m thick wooden plate, a 0.001 m thick completely flat and smooth galvanized steel plate, with a 0.05 m air gap in between. The air gap was closed laterally with a frame of expanded polystyrene panels of 0.15 m thick. The steel plate was screwed to the wooden plate, through the insulation frame, and it was its only support to avoid introducing additional obstacles to the air flow. The overall dimensions of the experimental module are represented in Figure 8 , and the thermophysical properties of the materials used can be seen in Table 2. The module had an inlet opening at the bottom of the steel plate with the same width as the air gap and 0.05 m height. The outlet opening was a hole of the same width as the air gap and

0.15 m height and it was located in the wooden plate at the top of the air gap. This opening was connected with the indoor space through a transition duct, which reduced the cross section of the channel in order to be able to connect a 0.10 m diameter orifice plate for measuring the flow rate.

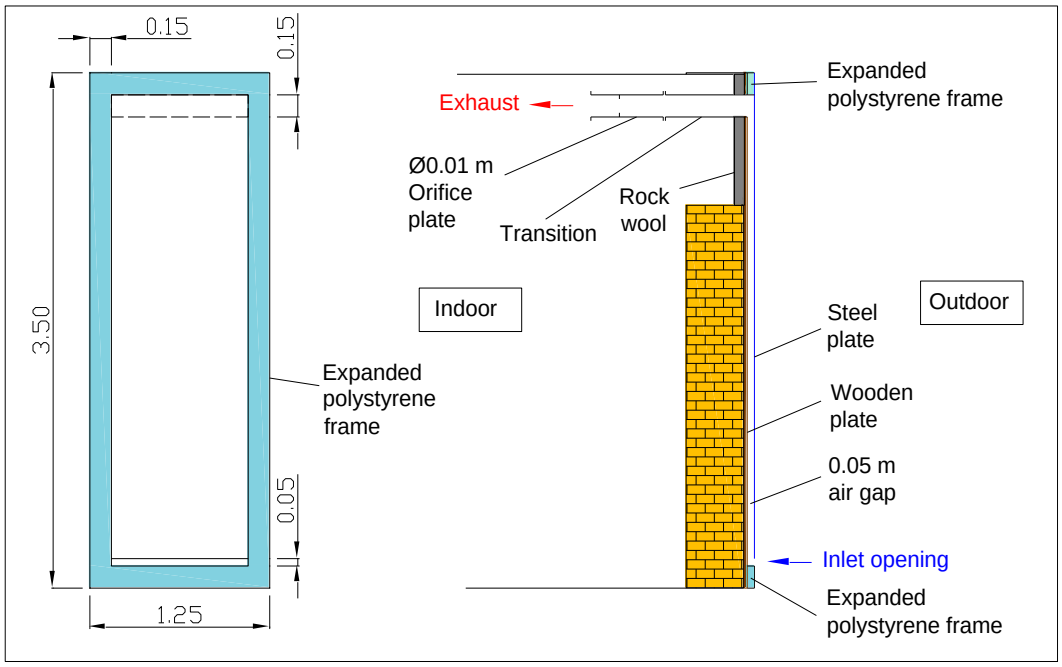

Figure 8. Schematic representation of the experimental OVF module.

Table 2. Thermophysical properties of the materials used in the module of OVF.

Layer	Thickness (m)	Thermal conductivity (W/m K)	Density (kg/m^3)	Specific Heat (J/kg K)
Steel plate	0.001	18	-	-
Air gap	0.05	-	-	-
Wooden plate	0.02	0.14	720	1255

2.3.1.1 Measurement set up

Weather and thermal variables in the façade were measured in the period from 2nd to 20th of June 2010. Data corresponding to different weather conditions were registered, from sunny warm days to cloudy rainy days. The frequency of measurement

was 0.1 Hz. Averaged values were calculated later at 10 min. intervals in order to compare the measurements with the facade model outputs.

Air and surface temperatures inside the façade module were measured in the central axis at five heights using thermocouples type K with accuracy of ±1 ºC. A schematic diagram of the location of the probes is shown in figure 2. The air temperature probes were shielded against long wave radiation with silvered ventilated pipes [17] . Since the steel thermal conductivity was high enough and the plate was very thin, the temperature of the steel plate was supposed to be nearly the same at both sides of the plate. Therefore the steel plate temperature was measured at the inside surface, thus avoiding the solar radiation effects. All surface temperature probes were also protected from long wave radiation with reflective adhesive tape. The room air temperature was also measured using the same method.

Additionally, two horizontal arrays of five thermocouples each were set at two different heights in the air cavity. The aim of these arrays was to measure the temperature profile at the upper and lower part of the air gap for monitoring the air temperature distribution in the cavity and estimating the convection heat transfer coefficient at the inside surfaces of the façade.

An orifice plate was used for measuring the flow rate through the facade. A Ø10 cm diameter was chosen so low flow rates could be measured. For measuring the differential pressure in the orifice a Furness Controls FCO44 0±20 Pa ±2.5% pressure transducer was used. The relative error of flow rate measurements with the orifice plate used was 19%.

The pressure coefficient is an important parameter for modeling the air flow through the façade. This parameter relates the wind speed and direction with the static

pressure on a facade opening. It also reflects the effect of the building shape and the urban environment. The pressure coefficient Cp is obtained from the expression:

$$\boldsymbol{P_w = C_P \frac{\rho V_f^2}{2}} \quad (1)$$

Where Pw is the pressure differential between static pressure on the façade and atmospheric pressure, ρ is the air density (kg/m3), and U is the undisturbed wind speed (m/s). Wind speed and direction are typically measured at the roof height of the building [18].

In order to calculate the pressure coefficient at the inlet opening, three pressure taps were set just below the inlet opening of the module. The average wind pressure differential with respect to the atmospheric pressure was measured. The taps were located far enough to the opening to prevent the airflow to interfere with the measurement and near enough to be representative of the pressure in the opening [19]. The differential pressure between indoor and outdoor was also measured to obtain an estimation of the internal pressure coefficient. Differential pressure transducers Furness FCO44 0±100 ±2.5% Pa were used.

Two thermocouples were set up at the bottom of the cavity, at both sides of an insulation panel, as shown in Figure 9, in order to estimate the exterior average convection heat transfer coefficient. The heat flux through the insulation panel was evaluated from the two temperature measurements using TRNSYS. Then, the exterior convection coefficient was evaluated through the following expression [20]:

$$\boldsymbol{h = \frac{q_s - q_c + \varepsilon\sigma\left(T_{sky}^4 - T_s^4\right)}{T_{so} - T_o}} \quad (2)$$

where qs is the solar radiation absorbed by the exterior surfaced, qc is the heat flux by conduction through the facade, ε is the emissivity of the exterior surface , σ is the Stefan-Boltzmann constant, Tsky is the sky effective temperature, Tso is the exterior surface temperature, and To is the ambient temperature. The sky effective temperature was approximated by the expression [16]:

$$T_{sky} = T_o - 6 \tag{3}$$

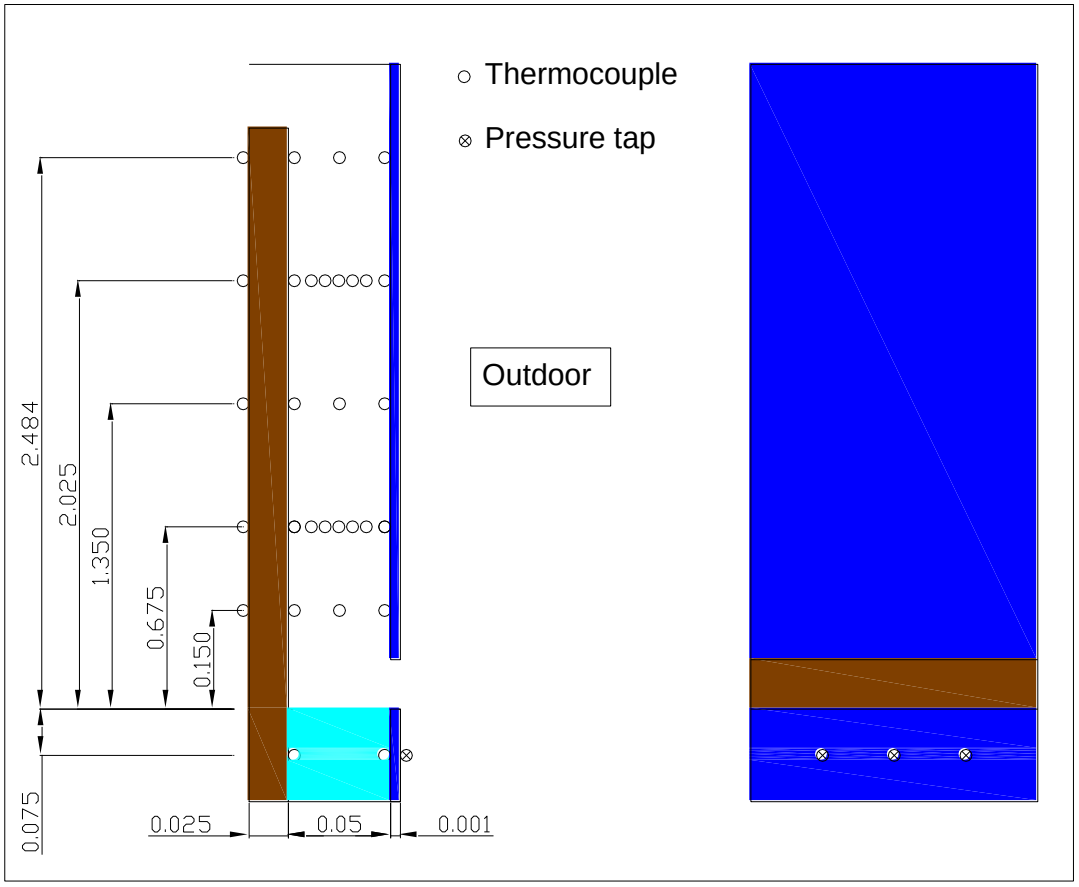

Figure 9. Schematic representation of the positions of sensors in the experimental OVF module. O=thermocouples, X=pressure taps.

Weather variables were also measured. Solar global radiation in the vertical was measured with a Kipp&Zonen pyranometer model CM21 located vertically on the same wall as the experimental module. The local ambient temperature was measured using

a shielded thermocouple. Wind speed and direction were measured using an ultrasonic anemometer Gill Windmaster 3D mounted on a10 m mast just in front of the building.

2.3.2 MONITORING RESULTS

2.3.2.1 Pressure coefficient

Figure 10 represents the average CP values measured as a function of the wind angle respect to the façade normal. To evaluate the dependency of the averaged Cp with the number of sectors used, the values were averaged for sectors of (360/n)º, with n=8, 12 and 16.

For rectangular buildings without any interference of nearby buildings, positive values of CP are expected in the windward side for wind angles from 0º to 60º, approximately, and negative values for angles from 60º to 180º [21]. In the experiment, the CP values obtained were not symmetric with respect to the façade normal direction. For 0º<α<180º CP values were all negative, because the module was sheltered due to the shape of the building and the presence of nearby buildings. For 180º>α>360º the sheltering effect was smaller as there were no buildings in this direction. Values became positive for 250<α<270º, which was a behavior more similar to that of unsheltered buildings.

The results showed in Figure 10 are similar to those obtained with CFD or wind tunnel measurements for buildings with nearby obstacles [22]. However, It has to be taken into account that the experimental values of CP showed in Figure 10 are local, and local pressure coefficients decrease with lower heights, so lower values of CP were expected since the inlet opening was located at the bottom of the wall (Figure 8).

The dependency of averaged CP values on the number of sectors can be neglected for n>8. In this study eight angles were used in simulations.

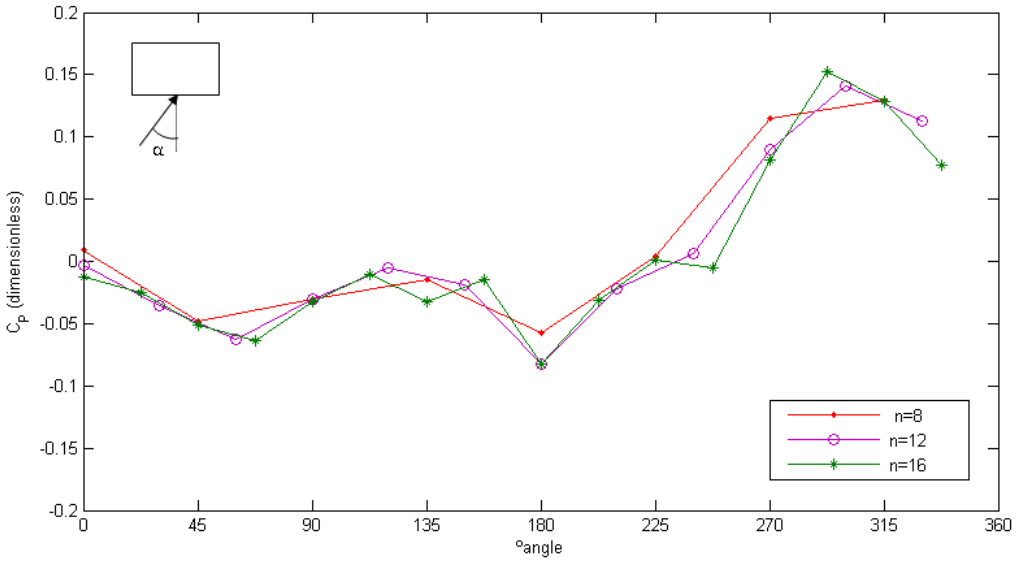

	0º	*45º*	*90º*	*135º*	*180º*	*225º*	*270º*	*315º*
C_p(n=8)	0.001	-0.05	-0.03	-0.015	-0.058	0.0041	0.115	0.1296

Figure 10. Averaged pressure coefficient C_P for divisions of α=360/n.

2.3.2.2 Recorded weather data

Figure 11 shows the exterior temperature, solar radiation on the vertical and the wind speed and direction during the six days measurement period. The solar irradiation represents the sum of direct solar radiation, diffuse solar radiation and ground and surroundings reflected solar radiation. Days 1 and 5 corresponded to overcast days since maximum solar radiation was less than 400 W/m2. Days 2, 3 and 4 corresponded to sunny days, and day 6 was a cloudy day although eventually it became sunny after midday. The peak solar radiation on the façade was around 725 W/m2 without clouds and it oscillates between 70 and 380 W/m2 for cloudy days. Peak ambient temperatures varied for sunny days from 18 ºC to 24 ºC, whereas in cloudy days the maximum temperatures were around 15ºC.The windiest day was Day 1 with peak

values of 9 m/s. In the rest of the days the wind velocity was moderate. The prevalent wind angle was around 300º clockwise from the façade normal.

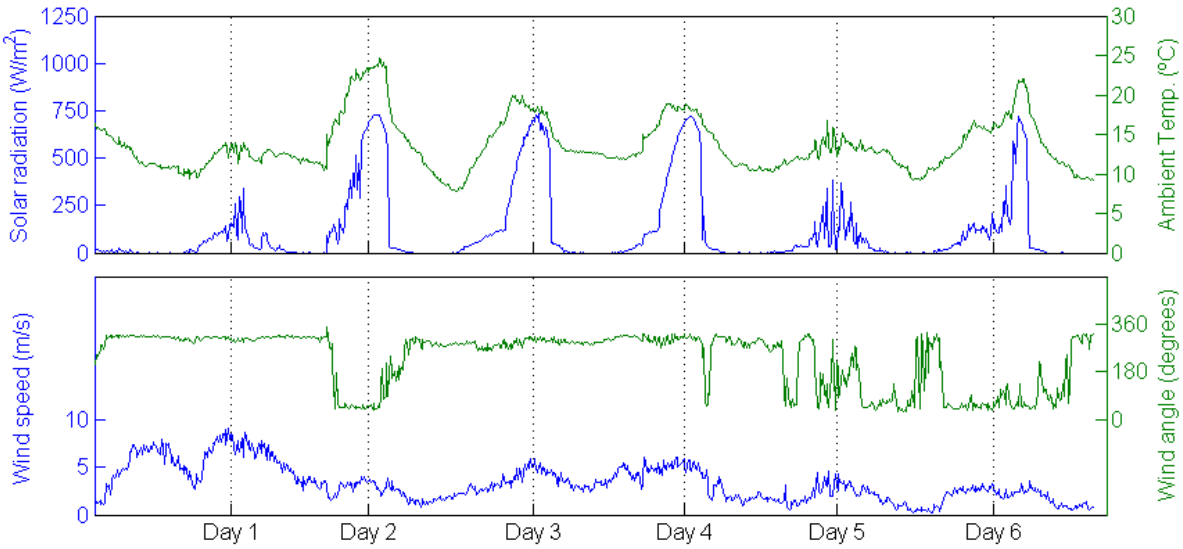

Figure 11. Weather data from the measurement campaign: Solar radiation, ambient temperature, wind speed and direction.

2.3.2.3 Façade monitoring

Figure 12 shows vertical temperature profiles of the air inside the cavity of the experimental façade module. The profiles represented were measured at the maximum solar radiation point of each day. The measurements were made in the middle point between the cavity walls, so the temperatures do not represent, in principle, the average temperature at that height. However the thermal boundary layer develops quickly and the horizontal temperature profile is quite flat by that height as it can be seen in Figure 13, so these measurements can be considered a good approximation to the average values.

Table 3. Weather conditions and flow rate through the OVF for the peak solar radiation time intervals of the six days of measurements.

	Day 1	*Day 2*	*Day 3*	*Day 4*	*Day 5*	*Day 6*
Solar radiation(W/m^2)	341	728	734	720	293	721
Ambient Tempertaure (°C)	14	24	18	18	15	22
Windspeed (m/s)	5.9	2.7	5.2	5.7	3.3	2.3
Flow rate (m^3/h)	18.1	10.8	17.7	17.0	6.4	9.6

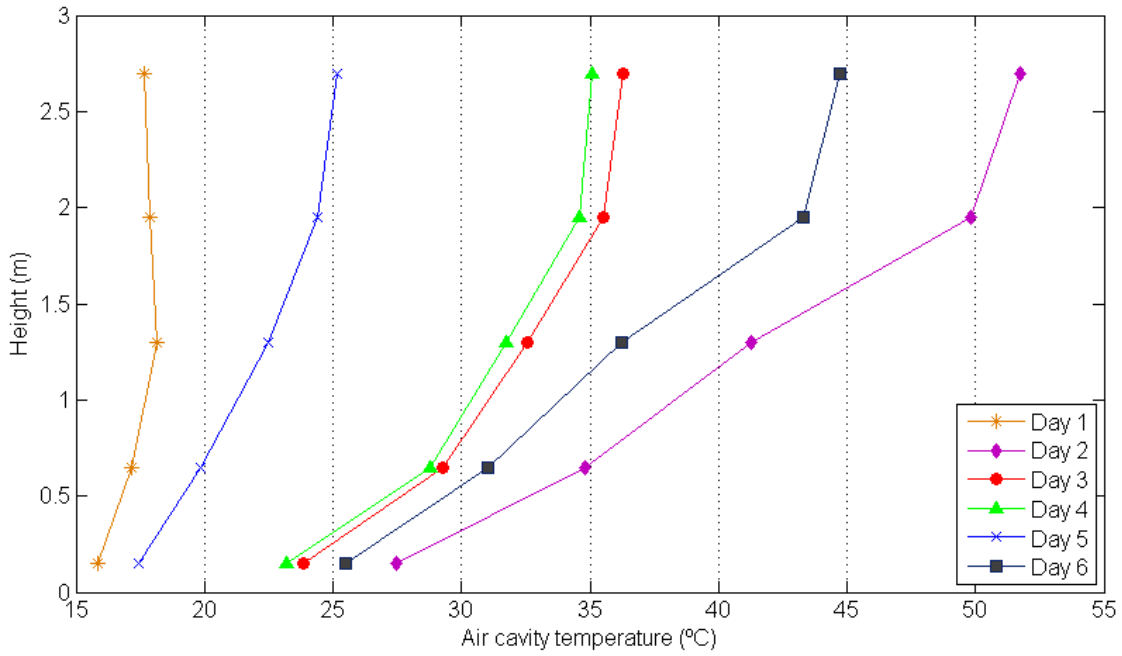

Figure 12. Vertical air temperature profiles in the façade air gap at the point of maximum solar radiation for the six days of measurements.

Figure 13 shows the horizontal temperature profile measured inside the façade module for two different heights. For h=0.63 m, the temperature gradients were negligible near the wooden plate since it was an insulation layer. Nevertheless, in day 2, wooden plate surface was 2 ºC above the air temperature. A possible explanation for this could be that at high temperatures long wave radiation interchange begins to be of the same importance as heat convection, and temperature rises to balance heat transfer.

In the upper part of the cavity, h=2 m, the air temperature profile is practically flat, although there is still a temperature difference of 9ºC between the air next to the steel

plate and the steel plate surface. The temperature decline slightly near the wooden plate for all the cases, probably due to the fact that at this height the wooden panel is worse insulated as it was in front of the window hole. Another explanation could be that buoyancy forces become more and more important as temperature rises. This could induce recirculation of air in the upper part of the façade, mixing up hot and warm air and limiting the temperature gradient.

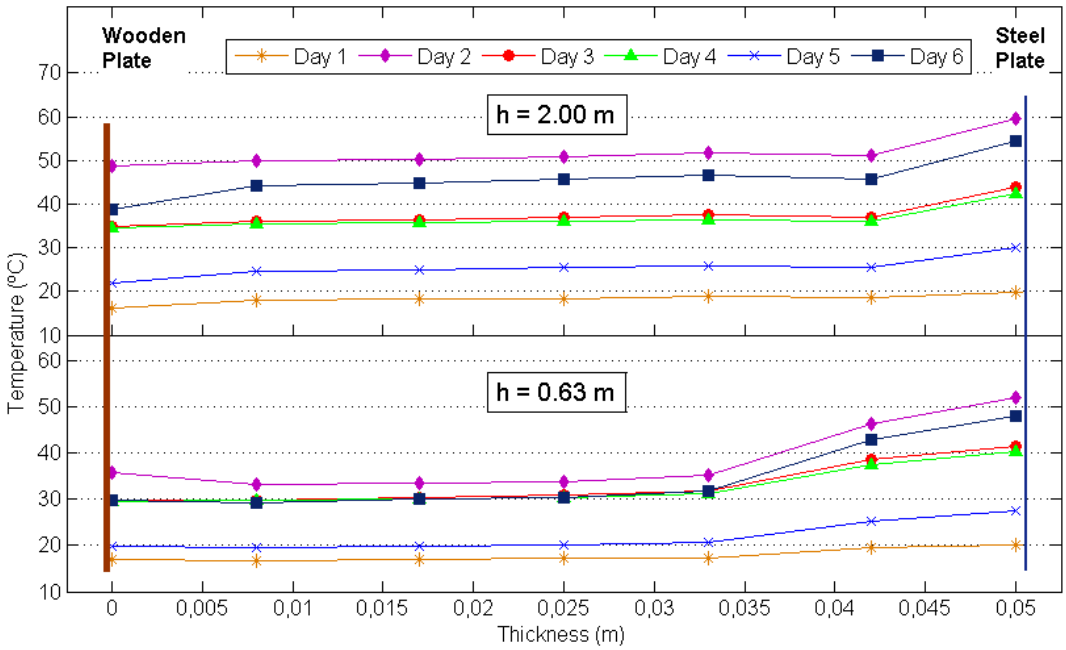

Figure 13. Horizontal temperature profiles of the facade module at two heights for the six days of measurements.

Figure 14 shows the evolution of the horizontal profile at middle height for Day 3. Three stages can be distinguished. During the night the steel plate and cavity air temperature were practically the same whereas the wooden plate surface temperature was higher. At this stage the building was losing energy through the insulation layer as the indoor air temperature was higher than outdoor. When the solar radiation began to raise, a transient stage started in which the steel plate got hotter and hotter until the temperature of the air in the cavity surpassed the wooden plate surface temperature. At this moment the same profiles as shown in figures 4 and 5 remained until the solar radiation started to go down and the inverse transient stage occurred.

In Figure 15 the evolution of cavity air temperatures along the height of the façade is represented. The same temperature stratification as in Figure 12 was maintained all day. Temperature began to rise from the sunrise and reached their maximum by 16:30h. It can be seen that the temperature gradient decreased with height.

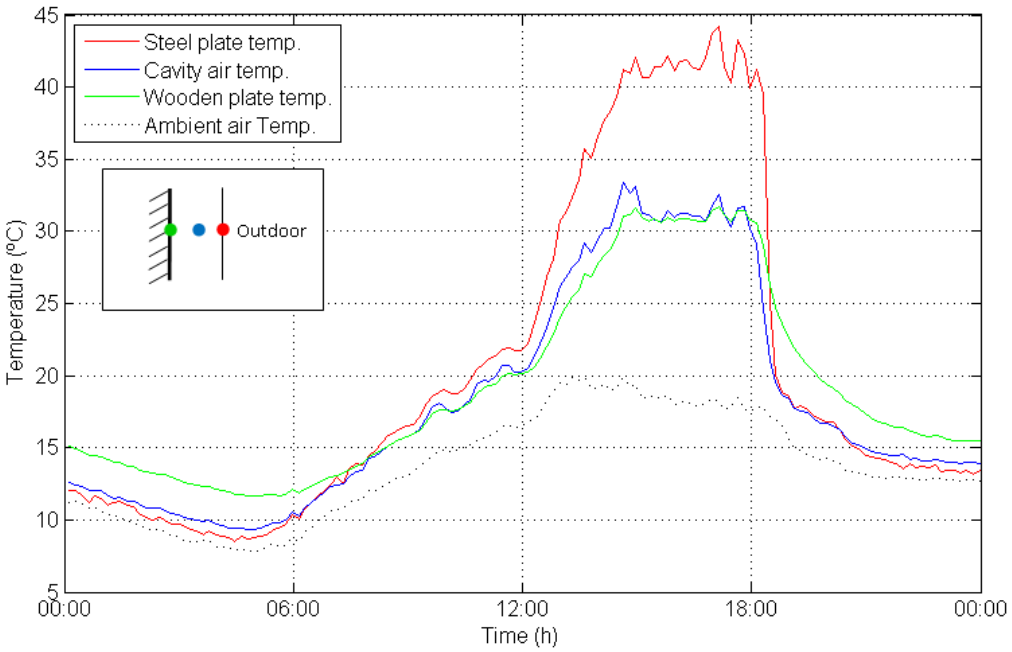

Figure 14. Time evolution of temperatures at the cavity middle height during Day 3.

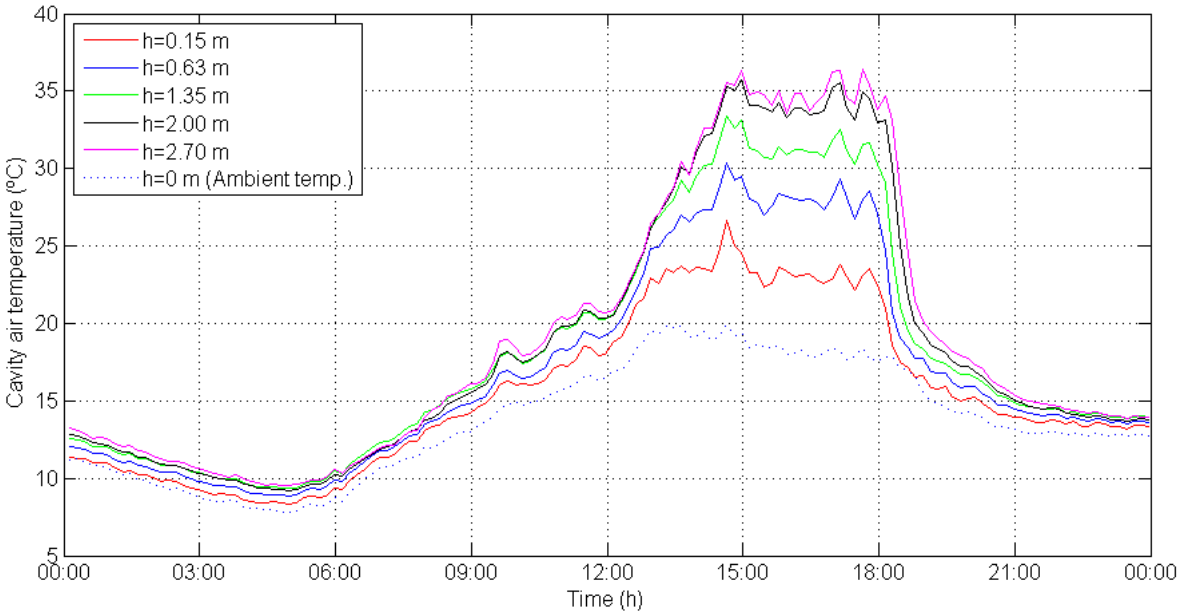

Figure 15. Time evolution of cavity air temperatures along the height of the air gap during Day 3.

2.3.2.4 Conclusions

In this paper the performance of an experimental OVF module was assessed and the experimental data were used to validate a numerical model. The main conclusions from this piece of work are now summarised:

- The performance of the facade depends on the meteorological variables. Wind speed and direction and solar radiation are the driving forces of air flow. If the wind speed is the prevalent driving force temperatures are lower and if buoyancy is the main driving force temperatures rise.
- Air flow rates due to wind forces depend on wind speed and direction but also on the Cp values that are characteristic of geometry and location of the building.
- If wind increases the air flow rates, so does the heat loss due to convection to the ambient air.

2.3.3 STUDY OF THE DISCHARGE COEFFICIENT

In order to estimate the energy saving that an opaque ventilated façade can provide, it is important to have a reliable prediction method for helping in the design process.

The orifice equation is widely used in cross ventilation for evaluation the air flow rate through a facade opening [23] [24]. It is based on the Bernoulli equation with steady, incompressible flow. This equation has been traditionally applied to windows and large openings in facades [25] [26] [27] [28], but also to ventilation stacks [29][30]. Orifice equation requires knowing the discharge coefficient. The discharge coefficient (C_D) depends on several factors and is a characteristic parameter of a particular opening and location. This makes its estimation a difficult task, which affects accuracy of the air flow rate predictions. Nevertheless, the orifice equation is a quite simple approach to the calculation of flow rate through openings and a useful tool for natural ventilation analysis.

In this section the orifice equation is used to evaluate the flow rate through an opaque ventilated façade. The orifice equation is aimed for evaluation of the flow rate through an opening when driving forces are wind and the stack effect, but is not intended for long openings where there is a vertical separation between inlet and outlet and the air is heated as it flows through it [31]. However, it can be used when wind or stack effect are prevailing. In the case of pure buoyancy forces the orifice equation can't be used at all, and another parameter has to be used for evaluation the flow rate through the façade. When all driving forces are of the same order of magnitude, the effect of temperature could be studied by analyzing its effect on the discharge coefficient.

The aim of this study is to find the variable dependency of the discharge coefficient in the cases of forced convection and mixed convection cases, and to propose a coefficient to evaluate the flow rate when buoyancy forces are prevalent. For this purpose, an experimental module of an opaque ventilated façade was constructed and installed on the wall of an existing laboratory façade and the main variables were monitored.

2.3.3.1 Basic equations

The orifice equation relates pressure difference across an opening and the flow rate through it:

$$Q = C_D A \sqrt{\frac{2\Delta p}{\rho}} \qquad (4)$$

where Q is the air flow rate (m^3/s), C_D is the discharge coefficient, A is the opening cross section (m^2), Δp is the pressure difference across the opening (Pa), and ρ is the air density (kg/m^3). Orifice equation is applicable under some assumptions [23] and for pressure differences between two points in an horizontal stream line. In a ventilated façade the inlet and outlet openings are not at the same height. However, considering the whole ventilated façade as a building opening, the pressure difference can be taken between an indoor and an outdoor point at the same height. The pressure difference in equation (4) accounts for all the driving forces that induce airflow through the opening. Following, the three driving forces of air flow through a building opening are explained.

Pressure differences across the opening can be caused by the wind flowing around the building or by the stack effect due to indoor-outdoor temperature differences. Wind creates a static pressure distribution on the envelope of the building. The static pressure on a point of the surface of a building envelope is related to the wind speed and angle through the following expression:

$$\boldsymbol{P_w = C_P \frac{\rho U^2}{2}} \qquad (5)$$

Where CP is the dimensionless pressure coefficient, ρ is the air density (kg/m3), and U is the undisturbed wind speed (m/s). The pressure coefficient depends on location and geometry of the building, and on wind direction [31].

The temperature difference between air inside and outside the building produces the so-called stack effect. It creates a different absolute pressure distribution inside and outside the building [31]. The pressure difference across an opening due the stack effect can be evaluated with the expression:

$$\Delta \boldsymbol{p} = \boldsymbol{\rho_o} \frac{(\boldsymbol{T_o} - \boldsymbol{T_i})}{\boldsymbol{T_i}} \boldsymbol{g}(\boldsymbol{H_{NPL}} - \boldsymbol{H}) \qquad (6)$$

Where ρ_o and ρ_i are the densities of outdoor and indoor air respectively(kg/m3), H_{NPL} is the height of the Neutral Pressure Level (m), H is the height referred to the Neutral Pressure Level (Height where the pressure difference is zero), g is gravity (m/s2), and T_o and T_i are the outdoor and indoor air temperatures (K).

For a sharp-edged orifices, like windows, equation (4) can be evaluated using the sum of the pressure differences due to wind and stack effect. The flow rate can't be calculated as the sum of flow rate corresponding to all driving forces, as its behavior is non linear. For natural ventilation in buildings the overall pressure difference across an opening is given by the expression:

$$\Delta \boldsymbol{p} = (\boldsymbol{C_P} - \boldsymbol{C_{Pin}}) \frac{\boldsymbol{1}}{\boldsymbol{2}} \boldsymbol{\rho U^2} + \boldsymbol{\rho g}(\boldsymbol{H_{NPL}} - \boldsymbol{H})(\frac{\boldsymbol{T_o} - \boldsymbol{T_i}}{\boldsymbol{T_i}}) \qquad (7)$$

where C_{pin} is the internal pressure coefficient.

In an opaque ventilated façade there is another driving force: the natural convection caused by the air heating inside the gap. An opaque ventilated facade is basically a rectangular vertical duct with one of its sides heated by solar radiation. When natural convection inside the air gap is the main driving force, equation (4) can't be used for evaluating the air flow. Usually, CFD models are used for estimating the air flow rate caused by this effect [32] [33]. A simple analysis yields that natural convection flow rate inside the air gap is a function of incoming air temperature (T_o), outgoing air

temperature (T_f) and indoor air temperature (T_i). They can be grouped into the dimensionless temperature:

$$\boldsymbol{T^*} = \frac{\boldsymbol{T_f - T_o}}{\boldsymbol{T_i - T_o}} \qquad (8)$$

The dimensionless expression Gr/Re^2 is used to distinguish between forced and natural convection [34]:

$$\boldsymbol{Gr/Re^2} \begin{cases} \ll \mathbf{1}\ \boldsymbol{Forced\ convection} \\ \approx \mathbf{1}\ \boldsymbol{Mixed\ convection} \\ \gg \mathbf{1}\ \boldsymbol{Natural\ convection} \end{cases} \qquad (9)$$

where:

$$Gr = \frac{g\beta(T_s - T_o)e^3}{\nu^2}$$

$$Re = \frac{ue}{\nu}$$

are the Grashof number and Reynolds number respectively, g is the gravity acceleration(m/s^2), β is the volume expansion coefficient (K^{-1}), Ts is the temperature of the hot wall (K), T0 is the temperature of the incoming air (K), e is the thickness of the air gap (m) , ρ is the air density (kg/m^3), u is the average speed of air in the air gap (m/s), and v is the kinematic viscosity. In this study Gr/Re^2 represents the ratio of buoyancy inside the façade to forced convection due to the wind force and stack effect.

2.3.3.2 Results and discussion

Driving forces

In order to study the effect of each driving force individually, the conditions for the prevalence of one of them over the others were studied through the evaluation of C_D as a function of the buoyancy parameter Gr/Re^2 (6).

Figure 16 represents the variation of C_D with Gr/Re_2 for different values of the stack effect parameter $(T_i-T_o)/T_i$ (°C/°C). It can be seen that when wind force prevails ($Gr/Re^2 \rightarrow 0$) the coefficient diminishes for Gr/Re^2 up to approximately 0.5. From that point the effect of buoyancy is added. This can be seen more clearly when the stack effect is weaker ($0<(T_i-T_o)/T_i<0.25$). For large values of Gr/Re_2 the buoyancy forces can't maintain higher flow rates so C_D diminishes. The variation of the discharge coefficient with $(T_i-T_o)/T_i$ was consistent with the results shown in [35]. When the stack effect in the building prevails the discharge coefficient diminishes considerably.

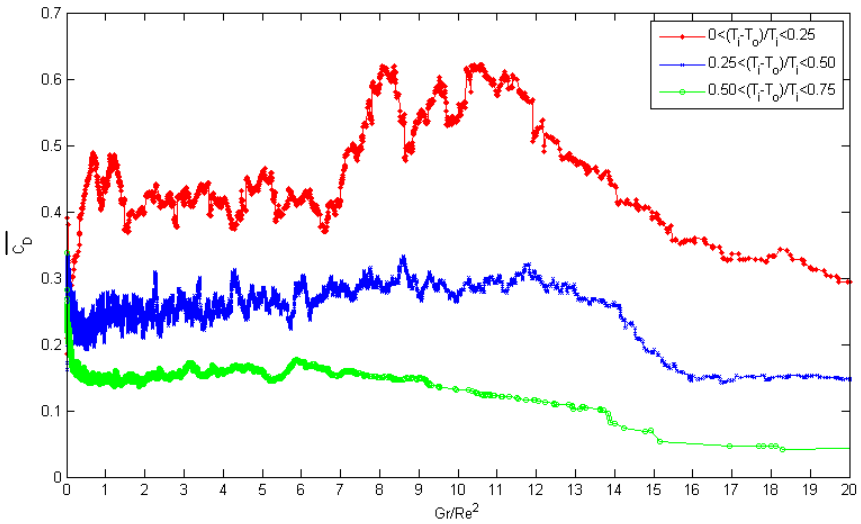

Figure 16. Variation of the average discharge coefficient $\overline{C_D}$ with the buoyancy parameter Gr/Re^2 for different values of the stack effect parameter $(T_i-T_o)/T_i$.

Wind forces

In this section the variation of C_D with wind speed and direction is researched. For this, the stack effect of the building and the effect of buoyancy were minimized by selecting the data where the variation of these driving forces was negligible.

For low values of the free stream velocity ratio, U/u<4, the Reynolds number in the façade has little variation and the discharge coefficient can be represented as a function of U/u. Figure 17 and Figure 18 show the variation of the discharge coefficient

with the free stream velocity ratio U/u for angles from 0º to 180º and from 0º to -180º respectively. Since the variation or Reynolds is limited, the graphs mainly represent the variation of C_D with windspeed. It is noticeable the difference between shielded and unshielded directions. While for the first case the variation of C_D is small, for the latter there are variations around 60%.

For higher Reynolds numbers the variation of free stream velocity ratio U/u is small and the discharge coefficient could represented as a function of the Reynolds. Figure 19 shows that C_D increases with Reynolds, although there are other effects implicitly represented in the graph. but in this study there weren't data for such flow rates.

Similar results can be seen in [29] and [27]. In the latter, a power law relation between C_D and Re was proposed and It was found a critical Reynolds number above which CD became a constant. In this study this point couldn't be compared as there weren't data for such flow rates. In other study, [23] shows a review of discharge coefficients as function of Reynolds for large openings and it is shown that C_D increases up to a certain Reynolds and then decreases slightly. In [36] it is studied the variation of discharge coefficient with wind angle, exhibiting that discharge coefficient could vary up to 60%. Unlike the openings like windows and orifices, a ventilated façade presents a behavior more similar to long openings as ducted air vents or ventilation stacks (chimneys). In [30] the discharge coefficient is represented against Reynolds for a short stack, but the results are not completely comparable as the location of the stack is not the same as that of a façade.

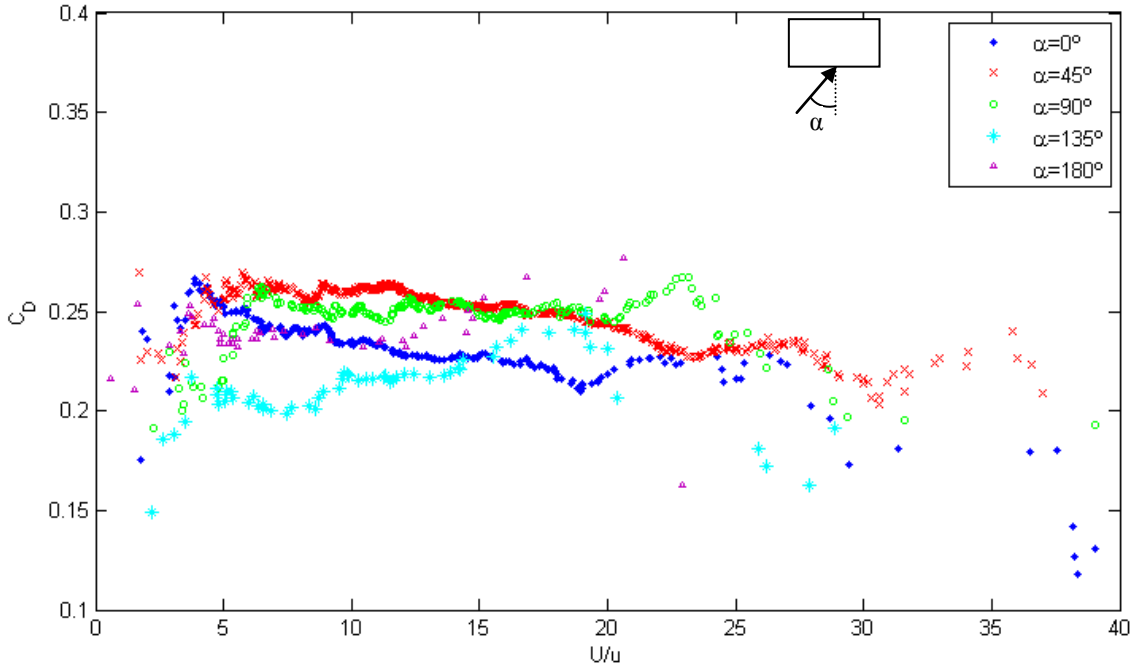

Figure 17. Discharge coefficient as a function of the freestream velocity ratio U/u for angles α=0-180° and, (Ti-To)/Ti<0.5, (Tf-To)/(Ti-To)<6.

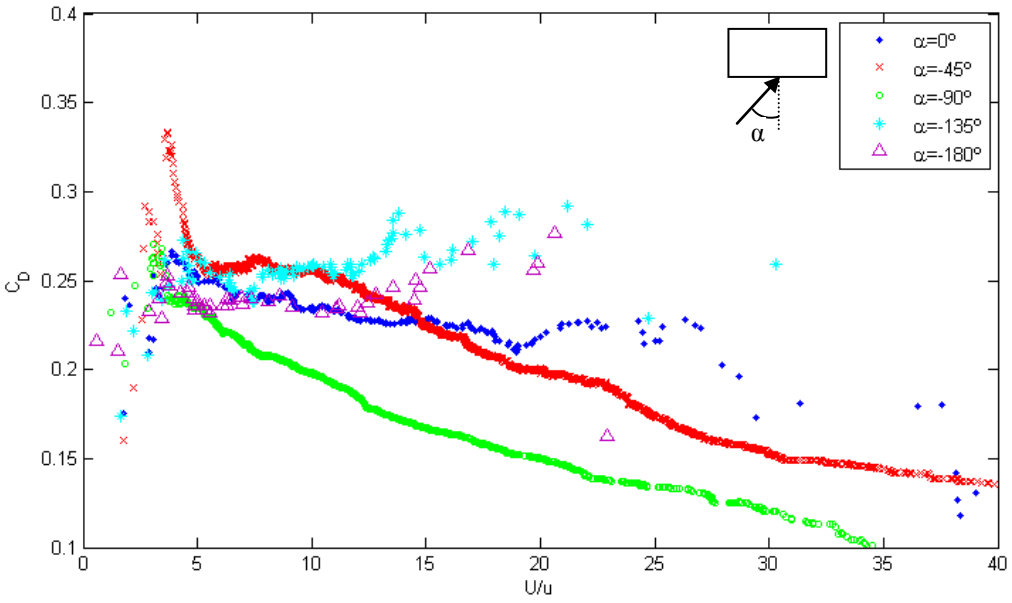

Figure 18. . Discharge coefficient as a function of the free stream velocity ratio U/u for angles α=0 - 180°, (Ti-To)/Ti<0.5, (Tf-To)/(Ti-To)<6.

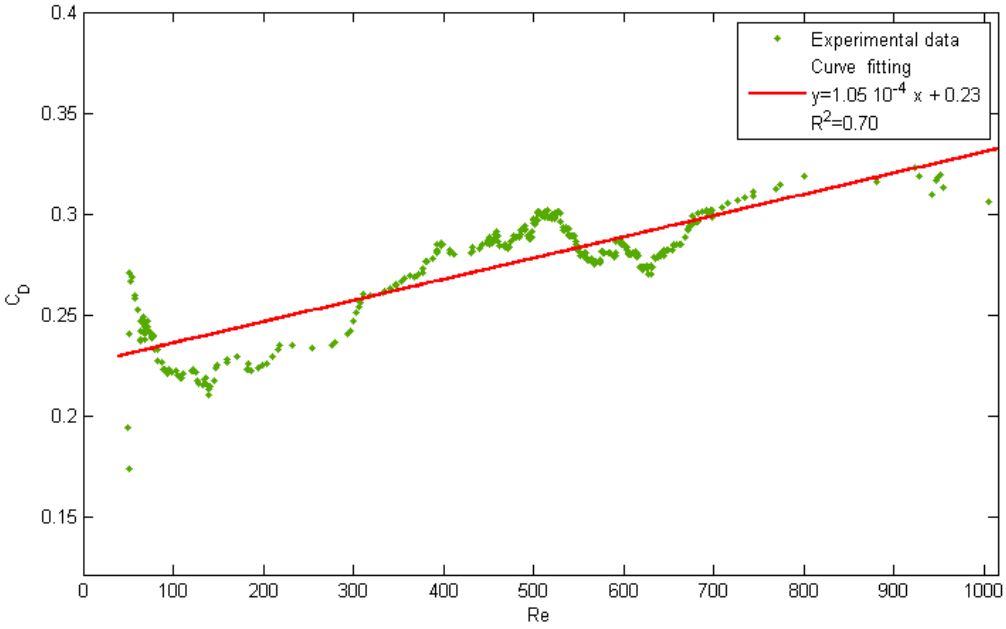

Figure 19. Discharge coefficient as a function of Re in the opening for $0.25<(T_i-T_o)/T_i<0.50$. $(Tf-T_o)/(T_i-T_o)<6$, $U/u<10$.

Natural convection in the air gap

The air flow rate induced by the heated air in the gap depends on the outdoor temperature, the indoor temperature and the temperature of the air in the gap. Should the driving force be pure buoyancy due to the temperature increase in the air gap, the discharge coefficient cannot be used to evaluate the flow rate, as it is not a consequence of the indoor-outdoor pressure difference. Instead, the flow rate is represented in Figure 20 as a function of the dimensionless temperature $T^*=(T_f-T_o)/(T_i-T_o)$, where T_f is the temperature of the air at the facade outlet. Free convection conditions in the air gap were considered by setting the parameter $Gr/Re^2>15$, and by keeping the effect of wind and the stack effect in the building approximately constant. This way, Figure 20 represents the variation of the flow rate with the air temperature at the air gap outlet. The flow rate grows rapidly for $6<T^*<15$ and then it approaches an approximate value of 9 m^3/h for $T^*>15$.

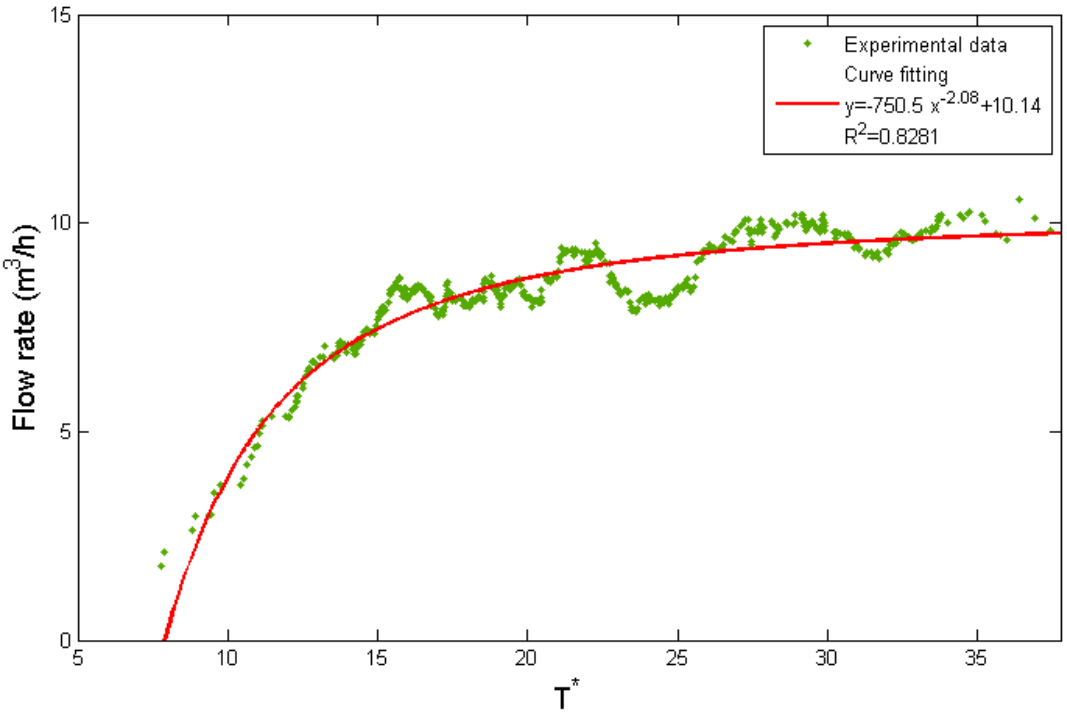

Figure 20. Flow rate through the facade as a function or dimensionless temperature $T^*= (T_f-T_o)/(T_i-T_o)$ for natural convection conditions in the air gap while keeping stack effect and wind force constant.

Mixed convection

Representing the contribution of the wind force, stack effect, and buoyancy in the façade is very complicated. In this section the effect of air temperature in the façade is highlighted by representing the average C_D value, using equation (1), against the dimensionless parameter T*. Since the flow rate induced by natural convection in the façade is not a function of the indoor-outdoor pressure difference, C_D was expected to increase with T*, as flow rate increases while Δp remains unaltered.

Figure 21 shows the general trend of the averaged CD. It increases with T* as it was expected, although the effects of other variables are also implicit in this representation.

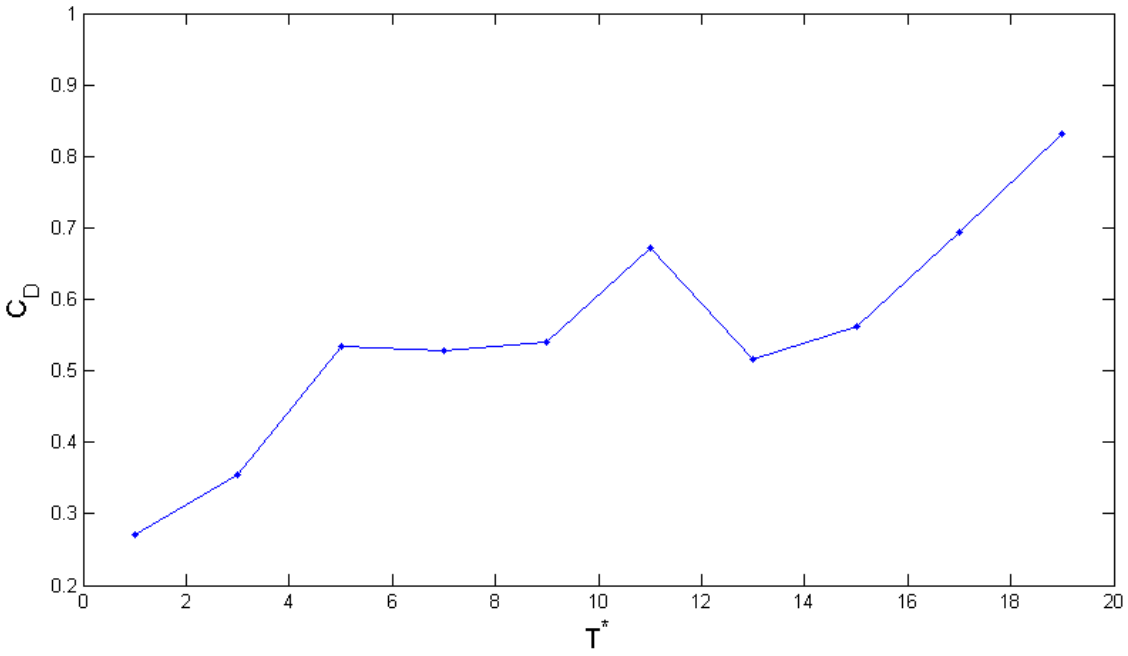

Figure 21. Variation of averaged C_D with T* for mixed convection conditions.

2.3.3.3 Conclusions

Measurements were obtained from an experimental module of FVO under real weather conditions to evaluate the flow rate induced through the study of the discharge coefficient as a function of the variables which it depends on. The measurements were post-processed to represent separately the different driving forces.

First, the flow regime was researched through the evaluation of the parameter Gr/Re^2. It was found that for $0.5<Gr/Re^2<15$ there is an influence of the temperature of the air in the gap on the discharge coefficient. The effect of the air heating in the gap is always positive on the discharge coefficient.

The variables affecting the discharge coefficient were studied independently. For the wind driving force, the discharge coefficient presented a behavior similar to other kind of openings, but with considerable lower values. As the opaque ventilated façade could be considered as a long opening it was expected to depend also on the Reynolds number of the air flow inside the façade.

The discharge coefficient cannot be considered as dependant only on the façade geometrical parameters. It was demonstrated that the urban environment affects it through the pressure coefficient, which depends on the wind angle and the sheltering effect of neighboring buildings.

In the case of mixed convection, it was found that, in general, the averaged discharge coefficient increased when the air was heated in the façade air gap. This means an increase on the air flow rate due to the buoyancy effect created by the solar radiation that impinges the external layer.

The discharge coefficient is a parameter that depends on many variables. It was demonstrated that it’s not only a parameter of the opening, but also depends on external parameters and variables as urban environment and wind speed and direction.

For designing purposes CD can be used in the case of force and mixed ventilation, in the latter case as a function of temperature in the façade air gap. It has been demonstrated that for buoyancy driven ventilation the non dimensional temperature T* can be used to establish the flow rate that a FVO can give.

The complex behavior of the ventilation process in a FVO needs to be researched in a more controlled manner, so the dependency of the discharge coefficient with each parameter could be correlated explicitly.

3. CONFIGURATION AND VALIDATION OF A NUMERICAL MODEL OF AN OPAQUE VENTILATED FACADE

3.1 INTRODUCTION

In this chapter a numerical model of an OVF is described. This numerical model was implemented using a zonal approach software (TRNSYS). The parameters needed in the model were adjusted using information from the experimental data. The simulations outputs were compared to the measurements to evaluate the accuracy of the model predictions.

The zonal approach has been used for simulation of ventilated facades in many ventilated façade studies. The zonal approach is less complicated than CFD models and the accuracy is better than in lumped models [37]. A zonal approach model was used in [11] to assess the performance of a rainscreen façade. Another zonal approach software was used in [38] dividing a transparent double skin façade in several zones and assigning a thermal and air flow node to each one. In the present study the latter strategy was implemented and validated for an OVF using the zonal approach simulation program TRNSYS. This software had been used extensively for studying DSF's as in [39], [40] and [9]. Using the zonal approach allows to model more complex buildings with less programming and computational effort, making simulations feasible for assessing the viability of installing OVF's in a building.

3.2 MODEL DESCRIPTION

A model of the facade module was implemented using the zonal approach building simulation software TRNSYS. The façade air gap was divided into five zones, corresponding to the locations of the temperature probes in the experimental module.

The model calculates the temperatures of all zones and the flow rate through them using the weather data file and the model parameter configuration as input data. Therefore a carefully estimation of model parameters had to be done in order to obtain a good approximation to experimental measurements.

The heat transfer modes considered in the model are conduction through solid walls, convection between surfaces and air, long wave radiation interchange between surfaces and solar radiation on external surfaces.

The total solar short wave radiation absorbed by the façade external layer is calculated using the expression:

$$q_{rs} = \alpha_s \, G_s \tag{11}$$

The external long wave radiation interchange was considered through the effective sky temperature using equation (5). The emissivity of exterior surfaces is fixed at a value of 0.9 in the model. The effective sky temperature had to be modified to account for the lower emissivity of the galvanized steel plate.

$$q_{rl} = \sigma \, \varepsilon \, (T_{sky}^4 - T_{so}^4) \tag{12}$$

The convection heat transfer from the external layer to the ambient air is evaluated through the expression:

$$q_{cv} = h_o(T_{so} - T_o) \tag{13}$$

The OVF model was based on the zonal energy balance carried out in TRNSYS Type 56 and the airflow network solved by TRNFLOW, which is the integration of the model COMIS in Type 56. In each of the 5 subdivisions of the OVF created the energy transfer by convection and radiation between the zone surfaces, and the energy transported by the airflow coming in and going out the zone are balanced to find the

zone air node and surfaces temperatures, and the air flow rate through the OVF. The energy gained by a OVF subdivision air node i due to convection in this model can be calculated with the following expression:

$$Q_i = \sum Q_s + \sum Q_f \qquad (14)$$

where,

$$\mathrm{Q_{sj}} = \mathrm{h\ A_j\ (T_j - T_i)} \qquad (15)$$

are the convection energy transfer terms from the j surface of the zone to the air node i, and

$$\mathrm{Q_{fk}} = \mathrm{\dot{V}\ \rho\ c_p\ (T_k - T_i)} \qquad (16)$$

are the gains due to air flow from the k previous or next OVF subdivisions.

The energy transfer to a wall due to long wave radiation interchange between surfaces in each OVF subdivision is calculated using the star network described in [41]. The conduction through the walls is solved using the transfer function method by Mitalas, which is also described in [41].

The indoor temperature measurements were contained in the weather data file. The indoor temperature depended of uncontrollable factors so it was considered as a model input.

The thermophysical properties used for heat conduction are shown in table 1. The steel plate layer was modeled as a thermal resistance (R=5.5 x 10-5 m2K / W) due to its small thickness and high thermal conductivity. The properties of all materials used in the experiment were considered constant and evaluated at an average temperature. Radiative properties were taken from standard material property tables.

The pressure difference between two nodes comes from the two air flow driving forces: wind pressure and buoyancy. The wind pressure can be evaluated using equation (1). The pressure difference due to buoyancy between two nodes in a vertical line is evaluated with the following equation:

$$P_i = P_j - g\int_{Z_i}^{Z_j} \rho(z)dz \qquad (17)$$

The orifice plate pressure drop curve was used and the pressure loss of the transition duct was measured previously and introduced in the model. The pressure loss in the façade is considered negligible compared with the latter losses at the measured air flow rates.

The OVF channel was modeled as a straight duct. One straight duct was created in the model for each OVF subdivision. The equation for a straight duct is:

$$\dot{m} = A_c\sqrt{\frac{\Delta P\ 2\rho}{\lambda\frac{L}{D_h}+\zeta}} \qquad (18)$$

The inlet and outlet OVF openings were modeled as large vertical openings. The mass flow rate can be calculated from the differential pressure with the expression:

$$\dot{m}_{ij} = C_d\int_0^H \sqrt{2\rho(z)\Delta P(z)}\ w\ dz \qquad (19)$$

where $\dot{m}_{ij}$ is the mass flow rate from node i to node j, Cd is the discharge coefficient, ΔP(z) (positive) is the pressure difference between nodes, w is the opening width and H is the opening height. When ΔP(z) is negative, the air flows in the opposite direction and the mass flow rate is calculated evaluating equation (8) changing the sign of ΔP(z).

3.2.1 CONVECTION COEFFICIENTS

For heat convection in external surfaces a linear correlation with wind speed has been traditionally used. The wind convection coefficient has been widely studied and a compilation of these correlations is presented in [42]. An average linear correlation as a

function of the free stream wind speed Vf was obtained from the experimental measurements:

$$h_{ow} = 4.8 + 1.7\,V_f \quad (\text{windward}) \tag{20}$$

$$h_{ol} = 2.6 + 2.5\,V_f \quad (\text{leeward}) \tag{21}$$

The convection heat transfer problem in the air cavity can be assimilated to the case of parallel plates with one of the plates insulated and the other with constant heat flux. The average Nusselt number correlations depend on the Reynolds and Prandtl numbers for forced convection and on Rayleigh number for free convection. The flow rates in the air cavity were low, with Reynolds numbers under 1600, so the air flow was always laminar [34]. The prevalence of forced or natural convection was studied through the evaluation of the average Archimedes number, Ar = Gr/Re2, for each 10 min time interval of maximum solar radiation in Table 3 along the height of the cavity. The Archimedes number represents the ratio of buoyancy forces to inertial forces. When Ar>>1 natural o free convection is dominant, if Ar<<1 it's forced convection and mixed convection in the case of Ar ≈1. As it can be seen in Figure 22, both forced and natural convection were always present in different proportions. Natural convection was of greater importance in the upper part of the cavity as temperatures were higher there. In windy days as days 1, 3 and 4 the Ar number is lower and both effects were of the same order.

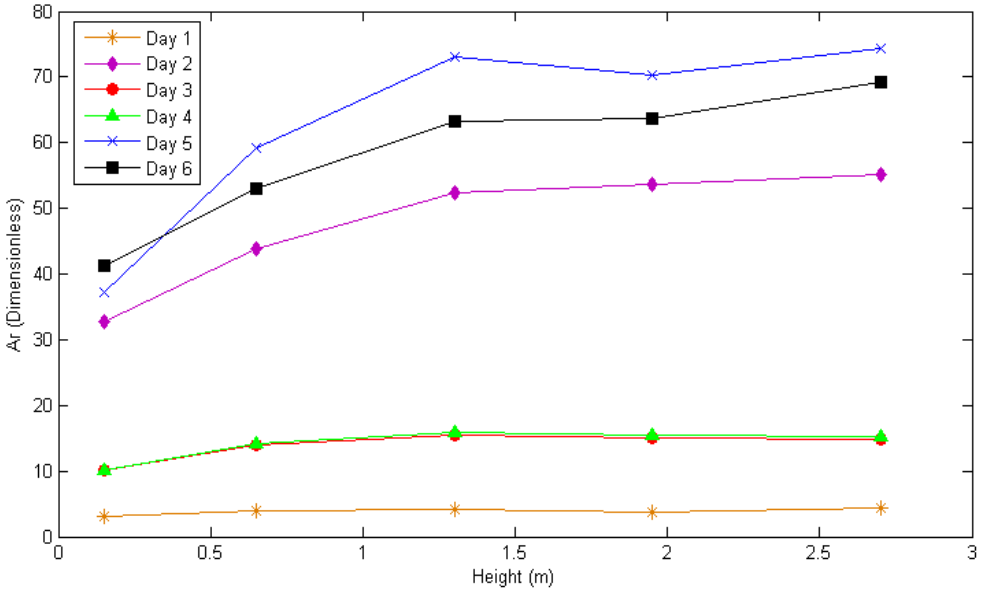

Figure 22. Archimedes number evaluated for the time intervals in Table 3 along the height of the façade cavity.

Using the thermocouples arrays installed in the experimental module, the average convection heat transfer coefficient was estimated by evaluating the temperature gradient near the plate surfaces.

$$Nu_{Dh} = \frac{-D_h \frac{\partial T(x,y)}{\partial y}\Big|_{y=0}}{(T_s - T_o)} \qquad (22)$$

where D_h is the hydraulic diameter of the channel, Ts is the surface temperature and Ta is the average air temperature. An average value of Nu_{Dh}=6.11 was found and this value was used in the numerical model.

3.3 REAL FAÇADE PERFORMANCE AND SIMULATION RESULTS

In order to validate the performance of the numerical model the most important variables were confronted to the experimental data. The exhaust air temperature and the air flow rate were evaluated, as well as the incoming energy supplied by the airstream.

Figure 23 shows the comparison of the experimental data measurements with the simulation ouput for the air temperature at the top of the façade module. This temperature can be considered the temperature of the air that enters the room. The maximum air temperature registered was over 50 ºC and corresponds to midday of Day 2. Air temperature in Days 3 and 4 didn't get so high temperatures despite having the same solar radiation levels. The reason for this was the higher wind speed during those days. In general the more windy the day was the lower temperatures inside the façade there were. It can be also seen comparing Day 1 and Day 5. Both days were cloudy and with similar levels of solar radiation, however Day 1 outlet air temperatures were lower than temperatures in Day 5. Since heat convection from the steel plate to the ambient air depends linearly on the wind speed, the more windy the day the more heat loss to the ambiente air and the lower steel plate temperatures, and therefore the lower air temperatures. Nevertheless the maximum increment of temperature reached more than 10 ºC for Day 3 and Day 4, as it can be seen in Figure 12.

There are not many studies for comparing exhaust air temperature in an opaque ventilated façade. Double skin facades performance regarding solar radiation is similar to the results obtained for opaque ventilated facades [43]. In [9] insuficient solar radiation is related to the lower flow rates. Typically temperatures over 40ºC are reached depending on the season. Air temperature also depends on geometry. Average cavity air temperatures decrease with cavity thickness. However heat loss by convection to the ambient air is lower in transparent façades because the hottest layer, normally the shading device, is inside the cavity and therefore protected from wind. The external layer temperature and hence the air flow temperature is strongly influeced by wind in an opaque ventilated façade.

In order to evaluate the accuracy of the simulation results a linear regression analysis was carried out for the predicted and experimental outlet air temperatures,

Figure 24. The bigger errors were found for the higher temperatures, this was also found for other models [37]. The coefficient of determination was 0.9356 and temperatures from simulation showed good agreement with the experimental results.

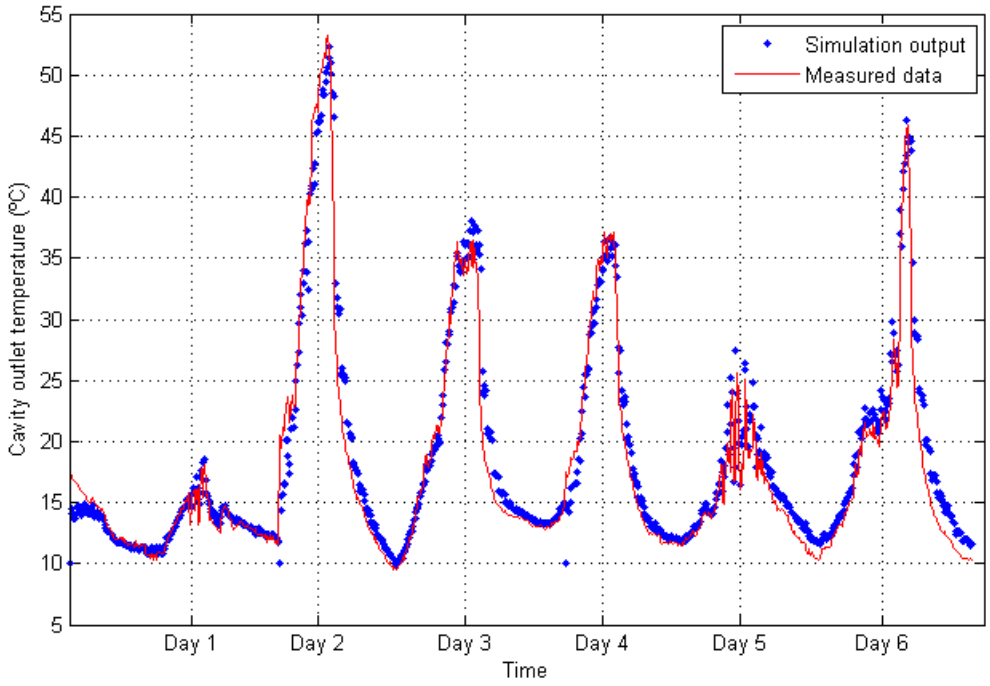

Figure 23. Comparison of exhaust air temperature measured and obtained by simulation

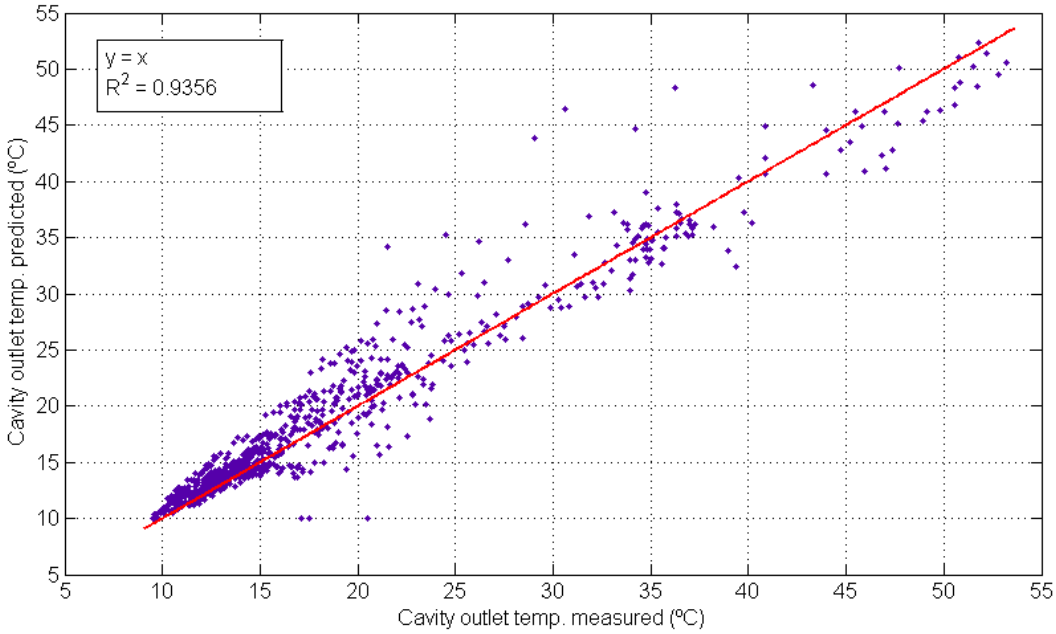

Figure 24. Correlation between exhaust temperature measured and obtained by simulation.

Experimental and simulation results of the air flow rate and energy introduced by the supply air in the room are represented in Figure 26. The range of air flow rate measured was from negative values of – 5 m3/h (inversed flow) to maximum values over 20 m3/h. The average air speed in the cavity had a maximum value of 0.15 m/s. The energy introduced with the ventilation air was higher for the sunny days (Days 2, 3 and 4) with peak values of 130 W. On the cloudy days (Days 1,5 and 6) the energy had values under 50 W.

Low temperatures were expected inside the façade for cloudy days. Sunny days presented high temperature increases in general. It is noticeable that the lowest increases corresponded to the windiest days, due to the increase of the external convection coefficient with windspeed. For the same level of solar radiation, Day 1 temperature rose only 2º whereas increment in Day 5 was 7ºC. Ambient temperature also affected the temperature in the cavity. The increment of temperature in Day 2 was higher than in Day 6 despite having the same peak solar radiation. However the ambient temperature was lower in the later. The maximum vertical temperature increase registered was 24ºC in Day 2.

It can be observed a clear correlation between air flow and energy rate and solar radiation, ambient temperature and wind pressure. On Day 1 the prevalent driving force was the wind pressure. On this day the air flow rate had peak values over 10 m3/h with wind pressure peak values up to 4 Pa and solar radiation under 300 W/m2. On Days 2 and 6 solar radiation was high and wind pressure was almost non-existent so buoyancy was the main driving force. On days 3 and 4 solar radiation was high and wind pressure had moderate values so driving forces are mixed. With the same solar radiation levels as day 2 the air flow rates for days 3 and 4 were slightly greater due to the support of wind pressure.

The linear regression analysis for the air flow rate and the energy of the air flow can be seen in Figure 25 and Figure 27. Bigger errors were expected in both cases due to the high uncertainty in the air flow rate measurements and the difficulty of adjusting all the parameters that affects the air flow rate calculations. The model tends to overpredict the air preheating energy as it can be seen in Figure 27. However, the model has proven to be sensitive to the main air flow driving forces, as it can be seen in Figure 25. The high flow rates that can be seen in Day 4 are due to some tests carried out using mechanical ventilation for trying to control the indoor pressure, and must not have to be taken into account. They were included to provide a continuous source of data to the model.

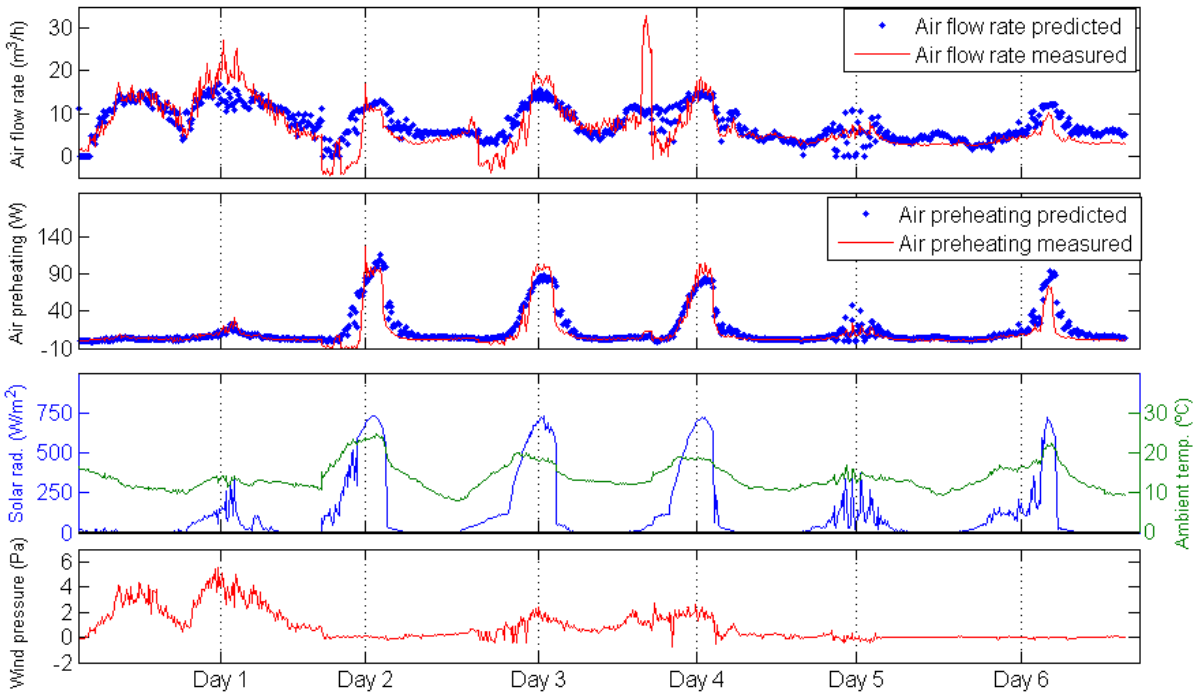

Figure 25. Comparison between air flow rate and energy measured and obtained by simulation.

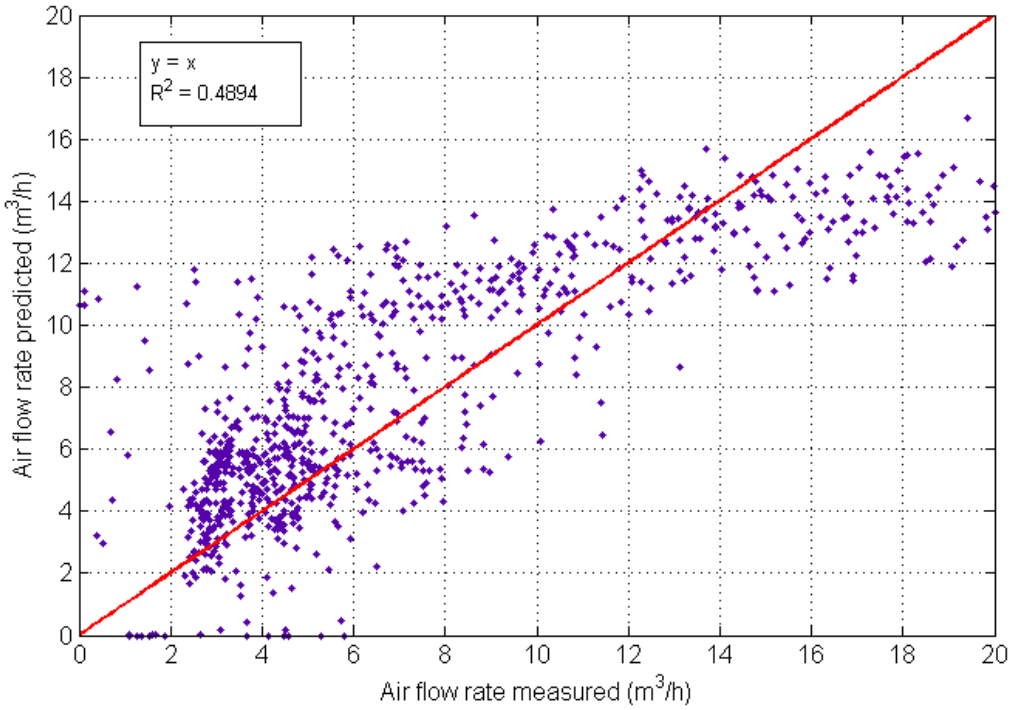

Figure 26. Correlation between air flow rates measured and obtained by simulation.

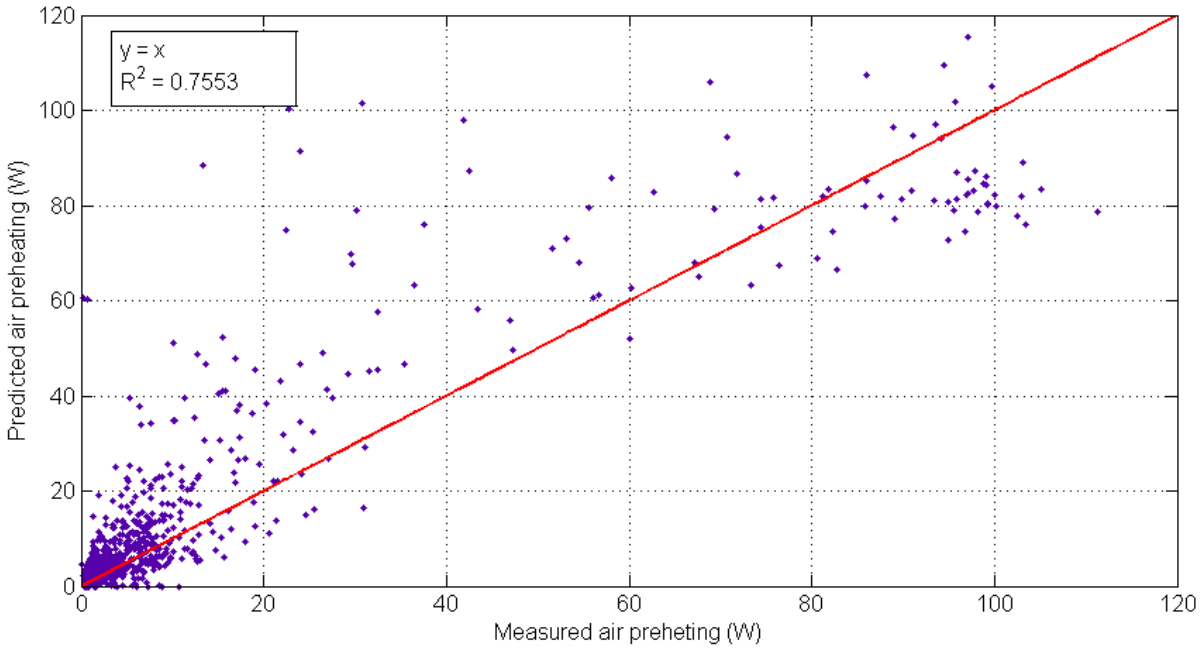

Figure 27. Correlation between energy measured and obtained by simulation.

3.4 CONCLUSIONS

In this chapter experimental data were used to validate a numerical model. The main conclusions from this piece of work are now summarised:

- The model created is sensitive to the driving forces of air flow.
- The outputs of simulation had a good agreement with experimental data. Temperatures were well predicted whereas air flow rate has bigger errors.
- Flow conditions in the cavity corresponded with the analysis from experimental data.
- Having the right parameters it's viable to use the model for analyzing the performance of OVF's, although the air preheating capacity of the façade will be in general overpredicted.

4. PERFORMANCE AND SENSITIVITY ANALYSIS

4.1 INTRODUCTION

The energy demand of a room depends on the inner loads and on the weather conditions among other factors. The inner energy loads depends on the activities developed in the room and on the requirements of ventialtion according to these activities. These requirements are normally established in regulations. Weather conditions are uncontrollable, though there are usually well differentiated seasons with specific characteristics. Generally, in the north hemisphere the Winter corresponds to the heating season and the summer to the cooling season. It is difficult for a passive facade to adapt to both seasons and at the same time having an optimal response. Facades are normally operated manually by opening and closing windows and doors for ventilating rooms, or by raising or lowering shading devices to prevent solar radiation from being absorbed by the room surfaces. Some buildings also include a control system to automatize these tasks up to a certain degree.

An OVF is a dynamic facade element. It can change its operation mode to adapt to the current weather conditions or the room energy requeriments. To do this it is necessary to implement a control system to switch the mode of operation depending on the input variables' values. In order to know which operation mode is more convenient in each case it is pertinent to study the OVF performance under the different conditions that are possible. With this information the key variables for deciding the most convenient operation mode in each situation can be identified.

There are a number of papers about the ventilated façade performance with the variation of the main parameters and variables affecting the system. The study of the

effect of meteorological variables is a key issue to characterize the possible advantages or disadvantages of using a ventilated façade. Somo authors as [10] studied the performance of ventilated facades in different kind of days (overcast, cloudy or sunny). In other studies [44] [7] the effect of the wind speed and direction on the facade was evaluated. In [45] the reponse of a ventilated facade to different weather conditions, using several operation modes, was studied. This way, conclusions can be reached about which operation mode is more convinient under each kind of weather.

Other important group of parameters is that of design parameters. These parameters are those established in the design phase of the project affecting the façade performance. Among these parameters, there are geometrical ones like the thickness of the air gap o the height of the façade, [45] or [7]. The different materials and materials' properties also affect the output variables, mostly their thermophysical properties, like absortivity or emissivity [46].

Other parameters to be studied are those that have to be measured or estimated in some way to be able to evaluate the system performance through a model. Pressure coefficient for the exterior envelope of the building or convection heat transfer coefficients are among these parameters. The estimation of these parameters is essential to build numerical models. A study of the model response to the variation of these parameters is important to establish which parameter should be measured or calculated more accurately and which ones don't have a great influence on simulation outputs. In [7] a parametric study was carried out to establish the sensitivity of a double skin façade model to the key parameters.

In the present study the performace of an OVF was studied under different weather conditions and under the variation of both design and estimated parameteres. The objectives of this study were:

- Gathering information about the performance of an OVF under different weather conditions when using different operation modes in order to design the facade control system.
- Analysing the performance of an OVF in different climatic zones.
- Analysing the sentivity of an OVF model with estimated parameters.
- Analysing the sensivity of an OVF with design parameters.

For this aim, a model of a secondary school building was realized and several cases were defined for doing a sensitivity analisis with the parameters aforementioned.

4.2 METHODOLOGY

A numerical model of an entire building was made with the building energy simulation software TRNSYS. This model was used to study the performance of an OVF under different conditions. Simulations with and without OVF in different parts of the building were made to make comparison studies. In total four studies were carried out: study of the control system, study of performance in different climatic zones, sensitivity study of estimated parameters and sensitivity study of design parameters. Following these studies are described in detail.

4.2.1 THE BUILDING

A secondary school building was selected for the simulations of this study. The chosen bulding was Medina Azahara Secondary School in Córdoba, Spain. This kind of building has several advantages for the design of the simulation cases. First, the schedule of activities in the building and the number or occupants were quite fixed, so the configuration of internal heat loads was easy and very approximated to the real situation. Second, ventilation is an important issue in educational buildings due to the number of people per m^2 who usually occupies classrooms and the effects that poor

indoor air quality can have on the health and performance of students. There are several studies linking indoor air quality and performance of students in a classroom [47] [48].

Medina Azahara Secondary School (MASE) is located in the south of Spain, in the city of Cordoba. Its geographical coordinates are 37º 54' N 4º47' O and its elevation of this location is approximately 125 m. It is a four storey building of rectangular plan view with its longer sides orientated to noreast and southwest. It is situated in a residential neighbourhood near downtown. As it can be observed in Figure 28 the plot of land limits to the north and east with streets and residential buildings of 5 storeys. To the west the school building limits with the sport fields and with an area of gardens. To the south there are several redidential towers.

Figure 28. Picture showing the IES MA and surroundings

The main dimensions in the plan view of the building are shown in Figure 29. The height of the building is 13 m approximately. The layouts of the four floors of the buildings are organized in one logitudinal aisle with classrooms, offices, laboratories and service rooms at both sides of it. In Figure 29 the layout of the first floor of the building can be seen. The main classrooms, with approximately 55 m^2 area each, are situated in the west wing of the building in all floors. In the east wing there are rooms of different sizes destined to laboratories and little classrooms. There are two areas that are out of the builiding central rectangular core. One of these spaces is the auditorium and the other one holds the library and a gimnasium in different floors. In the ground floor there are also offices and the canteen..

The envelope of the building consists of light brown bricks of 5 cm thick, 3 cm of insulation of polyurethane and 7 cm thick airbrick wall, with plaster. The windows glazing is made up of 6 mm thick glass panels.

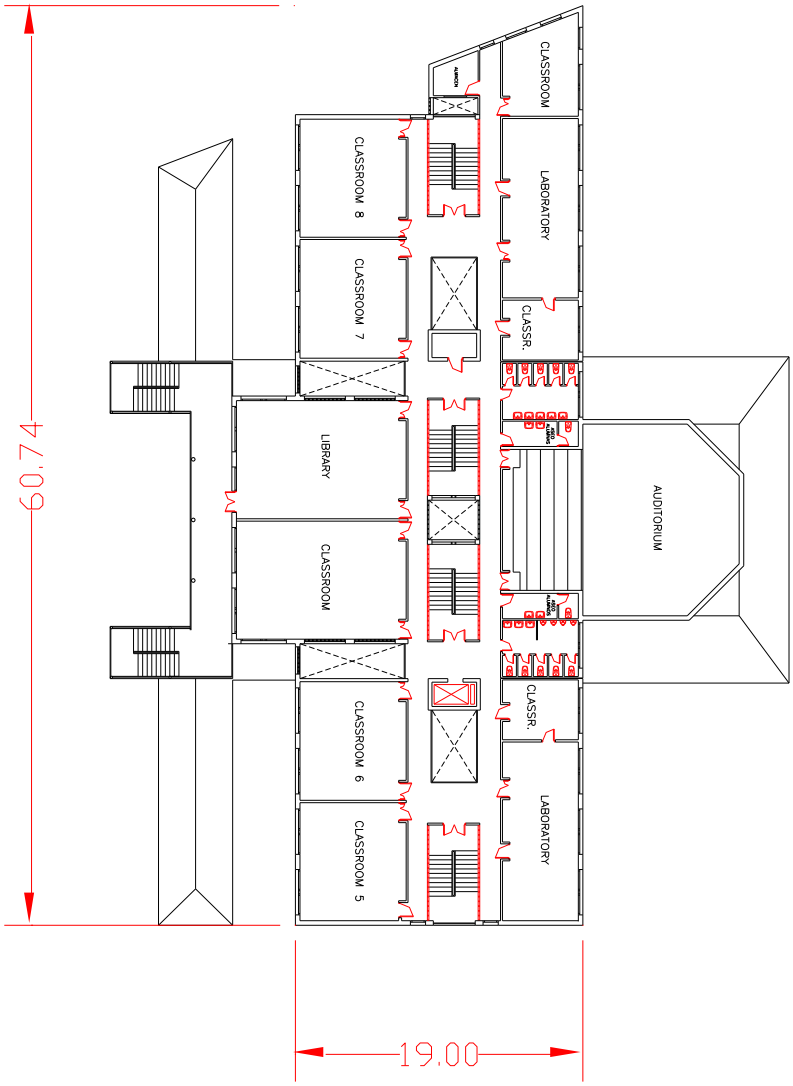

Figure 29. Layout of the first floor of the IES MA building.

Figure 30. Main façade of the IES MA

4.2.2 BUILDING MODELLING

The first step in modeling the building was defining the wall types included in the façade as well as the interior ones. The wall types created are shown in Table 4. The thermophysics properties were obtained from the building project document, except for the solar absortivity, which was obtained from a table of properties of typical construction materials. The long wave properties could not be modified in TRNSYS, so the long wave absortivity for all surfaces remained 0.9. This constituted a source of error, especially when the short wave solar radiation was low, or at nights. However these errors did not affect importantly the results of the simulations, as it can be seen later in section 3.3.

The windows to total façade area ration is approximately 30%. The windows of the building are horizontal sash sliding windows with single pane and with an exterior blind

as shading device. For the studies carried out blinds were not modeled, as they are manual devices and would be normally up to allow the natural light to come in during the day.

The convection heat transfer coeffcient for indoor surfaces was set at the constant standard value 3 W/m^2 K. For the façade surface the convection heat transfer coefficient was calculated from the expressions:

$$h_{ext} = 4.8 + 1.7\ V_f \quad \text{(windward)} \qquad (23)$$

$$h_{ext} = 2.6 + 2.5\ V_f \quad \text{(leeward)}$$

were Vf is the wind speed at the roof's height. The value of the parameters in (23) were taken as average values from empirical expressions found in a literature review about the external convection heat transfer coefficients [42].

4.2.3 OVF MODEL

The model of OVF used for simulations is a zonal approach model and it is described in detail in [49]. However, including the OVF model in a real builing involved certain difficulties. First, the OVF model was based on a model validated previously. This validated model corresponded to a module of 1 m width. In a wider module the velocity field would be modified, thus being more likely that horizontal velocity components parallel to the wall appeared, therfore invalidating the hypothesis of one-dimensional flow. Moreover, it was not possible for a wide module to maintain a rectangular shape on a wall with windows located in most of its length.

Table 4. Thermal and geometrical properties of the walls used in the building model.

	Thickness (m)	Thermal conductivity (W/mK)	Specific Heat (kJ/kgK)	Density (kg/m3)	Solar Absortance (dimensionless)
Exterior walls					
Plaster	0.020	0.26	1.0	900	0.30
hollow brick	0.070	0.42	0.9	1200	
polyurethane insulation	0.030	0.02	1.5	30	
Air gap	0.020	0.02	1.0	1	
Perforated brick	0.115	0.65	1.0	1600	0.36
Interior walls					
Perforated brick	0.115	0.65	1.0	1600	0.30
Hollow brick 7 cm	0.090	0.42	0.9	1200	
Hollow brick 9 cm	0.070	0.42	0.9	1200	0.30
Glazing					
Windows: simple pane	0.006				
Glass security door	0.100				
Concrete slab					
terrazzo of light color	0.010	1.15	1.0	1800	0.30
concrete vault	0.250	1.04	1.0	1460	
plaster	0.020	0.26	1.0	900	0.30
Roofs					
concrete vaults	0.250	1.04	1.0	1460	0.30
semitransparent polycarbonate plate	0.003	0.70	1.2	1200	
concrete	0.010	1.20	1.1	2000	
polystyrene	0.040	0.02	1.5	25	
gravel	0.050	0.70	0.9	1700	0.30
Gymnasium					
Sandwich panel	0.050	0.41	1.5	202	0.34
polyurethane insulation	0.030	0.02	1.5	30	0.30

For the implementation of the ventilated façade two options were studied. The first one was taking advantage of the whole façade opaque surface and using it as a ventilated façade. This option presented the inconvenient of adapting the OVF to the irregular shape of the opaque surface of the building façade. Increasing the complexity of the OVF channel would have made the model uncertainty also increase, due to the differences with the validated OVF model. The second option was trying to fit the 1 m

width and 3 m height validated modules without making any changes in its shape. In order to prevent more uncertainties in the results the latter option was chosen. In Figure 31 a schematic diagram of the position of the modules is shown.

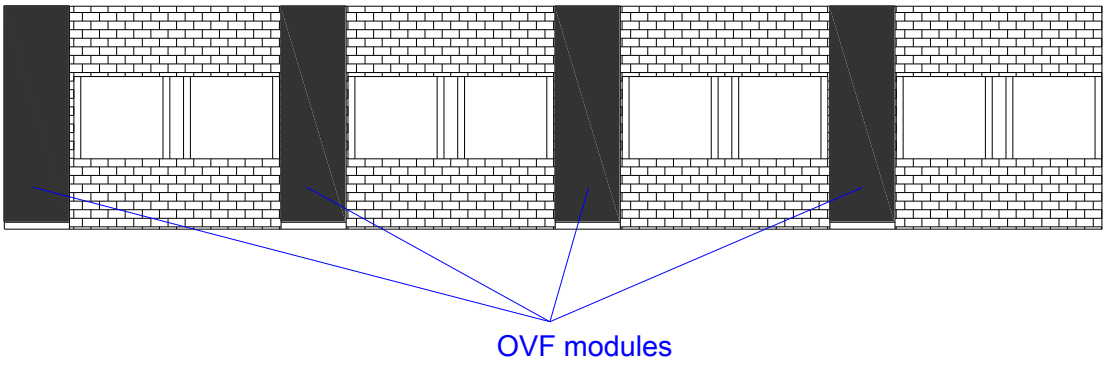

Figure 31. Layout of building façade with 4 modules of OVF.

The OVF modules made use of the existent façade wall as insulation layer and it was only added the external 1 mm galvanized steel plate. Due to its small thickness the steel plate was modeled as a thermal resistance of 5.56 x 10^{-5} m2 K/W. The thickness of the air gap was 0.05 m, which was the same as the one used in the experiments. The side plates were not included in this model because of its negligible area compared to the front face.

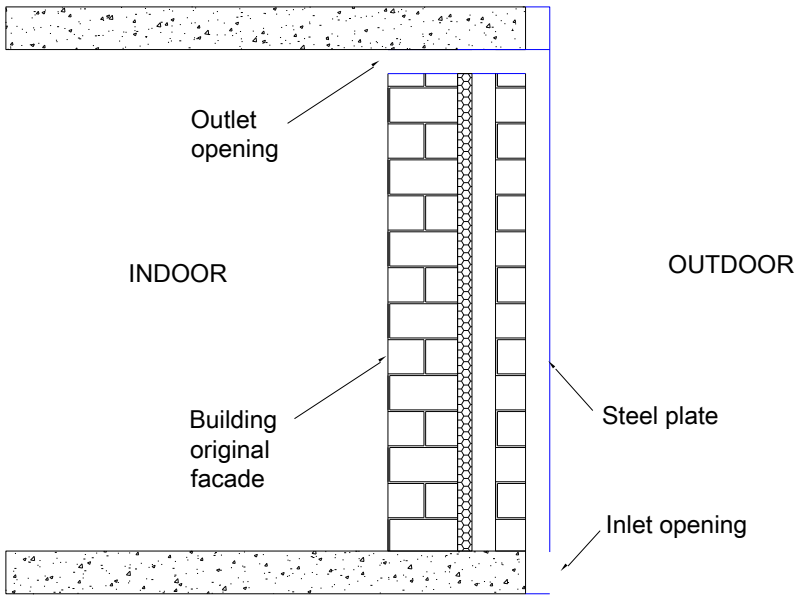

Figure 32. Schematic profile of the OVF module

The channel inside the OVF is modeled like a rectangular duct of 0.05 m^2 cross section and 3.25 m lenght. The mean rugosity was set to 0.1 mm. The connection between the channel and the adyacent room was modeled as a grill opening with a free to close area ratio of 50% and a dynamic loss coefficient of 2.16. The discharge coefficient for all the openings was established as 0.6, which is the recommended value for medium-size holes in facades.

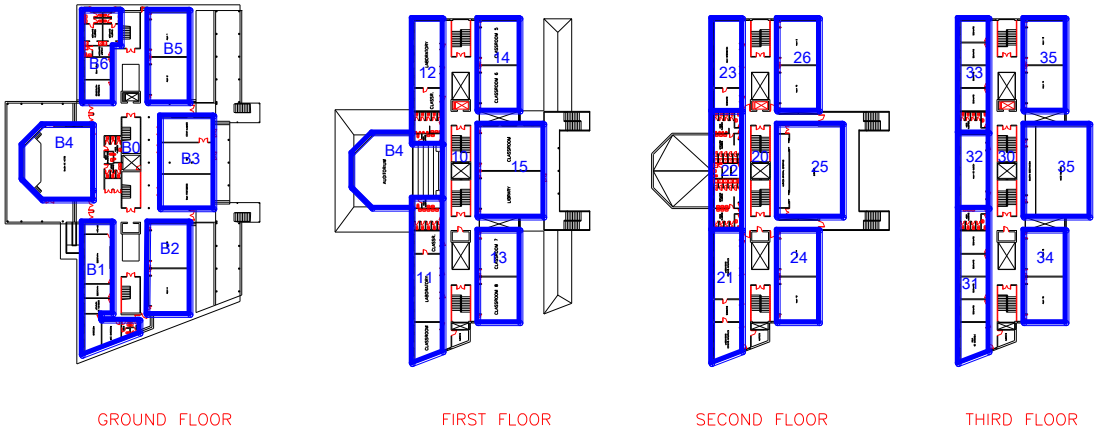

Figure 33. Zone distribution in the TRNSYS model

The zones of the model were created by grouping rooms of similar use. In Figure 33 the layout of termal zones in each floor is shown. There is an aisle zone in each floor which are communicated with each other by the staircase. It was decided that all internal openings between zones, e.g. doors, were always close, as that was the usual situation in the real case.

The pressure coefficients for the envelope of the building were calculated using the software CPCALC+. A plan area density of 10 was taken. The values were calculated in a matriz of 4 x 8 positions in each facade and the average values for each floor were taken. The pressure coeficcient at the roof was considered as the average of two positions as there wasn't a very big difference at any other point. In Table 5 the resulting pressure coefficients are shown.

Table 5. Values of the pressure coefficient

	Cp							
Ground floor	0	45	90	135	180	225	270	315
EN_N	0.0668	0.0220	-0.0451	-0.0216	-0.0205	-0.0216	-0.0451	0.0220
EN_E	-0.0984	0.0191	0.0587	0.0191	-0.0984	-0.0471	-0.0445	-0.0471
EN_S	-0.0205	-0.0216	-0.0451	0.0220	0.0668	0.0220	-0.0451	-0.0216
EN_W	-0.0984	-0.0471	-0.0445	-0.0471	-0.0984	0.0191	0.0587	0.0191
First floor								
EN_N1	0.0365	0.0120	-0.0565	-0.0273	-0.0258	-0.0273	-0.0565	0.0120
EN_E1	-0.1180	0.0126	0.0383	0.0126	-0.1180	-0.0566	-0.0535	-0.0566
EN_S1	-0.0258	-0.0273	-0.0565	0.0120	0.0365	0.0120	-0.0565	-0.0273
EN_W1	-0.1180	-0.1180	-0.0535	-0.0566	-0.1180	0.0126	0.0383	0.0126
Second floor								
EN_N2	0.1602	0.0518	-0.0529	-0.0249	-0.0248	-0.0249	-0.0529	0.0518
EN_E2	-0.1134	0.0601	0.1860	0.0601	-0.1134	-0.0531	-0.0527	-0.0531
EN_S2	-0.0248	-0.0249	-0.0529	0.0518	0.1602	0.0518	-0.0529	-0.0249
EN_W2	-0.1134	-0.0531	-0.0527	-0.0531	-0.1134	0.0601	0.1860	0.0601
Third floor								
EN_N3	0.4205	0.1321	-0.0623	-0.0278	-0.0293	-0.0278	-0.0623	0.1321
EN_E3	-0.1479	0.1228	0.3905	0.1228	-0.1479	-0.0661	-0.0694	-0.0661
EN_S3	-0.0293	-0.0278	-0.0623	0.1321	0.4205	0.1321	-0.0623	-0.0278
EN_W3	-0.1479	-0.0661	-0.0694	-0.0661	-0.1479	0.1228	0.3905	0.1228
Roof								
EN_H	-0.0150	-0.0160	-0.0210	-0.0160	-0.0150	-0.0160	-0.0210	-0.0160

The activity in the different rooms was configured using a usual schedule in a secondary school that opens at 8:00 am and closes at 15:00 pm. The school was considered close from 15:00 pm forward and at weekens, and without any occupancy or internal heat gain at all. All the classrooms use on a daily basis, zones B2, B5, 13, 14, 24, 26, 34, 35, have the same occupancy schedule as the school building. The schedule is the same all the year round so the performance of the OVF can be compared in all seasons, despite of the fact that the building would be normally close in the summer. In Table 6 the schedule of all zones are shown. In this table it can also be seen the number of occupants for each zone in the cases when the ventilation rates required are a function of this number. For the model zones in which two main classrooms were grouped, a number of 75 occupants was established.

The thermal loads considered in each zone were the ones due to occupants and lights. For the occupants load the values in the ISO 7730 standard were used. The lights were considered on during all the occupation period. The lights load was set 19 W/m2, with a fraction of 40% as convective heat gain (fluorescent tubes). In the service zones gains due to electrical appliances were also considered.

The ventilation rates was calculated from the requirements by the spanish Building Technical Book [5](Código Técnico de Edificación, CTE) and the Book for Thermal Installation in Buildings [50] (Reglamento de Instalaciones Térmicas de Edificios ,RITE), in its document IT1.1.4.2.3, Minimun External Ventilation Air Flow Rate. The resulting values can be seen in Table 6.

The heating and cooling systems were set to maintain the minimum temperatures in the winter and the máximum temperatures in the summer. The control system included a hysteresis to prevent the system from becoming unstable. The setting temperatures were drawn from the CTE. The setting temperatures were 21 ºC in the winter and 26 ºC in the summer.

Table 6. Ventilation requirements, occupation and schedule of utilization of the rooms

Room	Use	Flow rate requirement per unit (l/s unit)	Units	value	Ventilation flow rate requirement (l/s)	Volume (m^3)	ACH (h^{-1})	Schedule	Frecuency
B0	CORRIDOR	0.83	m^2	462.3	383.7	1502.48	0.92	8:00-9:00 10:00-11:00 14:00-15:00	Daily
B1	OFFICE	12.5	Nº occupants	5.0	62.5	451.75	0.50	9:00-13:00	Daily
B2	CLASSROOM	12.5	Nº occupants	75.0	937.5	367.25	9.19	8:00 - 15:00	Daily
B3	BAR	8	Nº occupants	20.0	160.0	477.00	1.21	10:00 - 11:00	Daily
B4	AUDITORIUM	12.5	Nº occupants	100.0	1250.0	923.00	4.88	10:00 - 12:00	1 day/week
B5	CLASSROOM	12.5	Nº occupants	75.0	937.5	380.25	8.88	8:00 - 15:00	Daily
B6	CHANGING ROOM	0.83	m2	97.0	80.5	315.25	0.92	12:00-14:00	Daily
10	CORRIDOR	0.83	m2	342.0	283.9	1112.00	0.92	8:00-9:00 10:00-11:00 14:00-15:00	Daily
11	CLASSROOM	12.5	Nº occupants	75.0	937.5	459.00	7.35	8:00 - 15:00	Daily
12	LABORATORY	12.5	Nº occupants	37.0	462.5	352.00	4.73	10:00-12:00	Daily
13	CLASSROOM	12.5	Nº occupants	75.0	937.5	360.50	9.36	8:00 - 15:00	Daily
14	CLASSROOM	12.5	Nº occupants	75.0	937.5	360.25	9.37	8:00 - 15:00	Daily
15	LIBRARY	12.5	Nº occupants	37.0	462.5	580.80	2.87	8:00 - 15:00	Daily
20	CORRIDOR	0.83	m^2	342.2	284.0	1112.22	0.92	8:00-9:00 10:00-11:00 14:00-15:00	Daily
21	LABORATORY	12.5	Nº occupants	37.0	462.5	364.70	4.57	10:00-12:00	Daily
22	CHANGING ROOM	0.83	m^2	105.0	87.2	341.14	0.92	12:00 - 14:00	Daily
23	IT CLASSROOM	12.5	Nº occupants	37.0	462.5	266.58	6.25	8:00 - 10:00	Daily
24	CLASSROOM	12.5	Nº occupants	75.0	937.5	360.50	9.36	8:00 - 15:00	Daily
25	GYMNASIUM	12.5	Nº occupants	37.0	462.5	1080.76	1.54	12:00 - 14:00	Daily
26	CLASSROOM	12.5	Nº occupants	75.0	937.5	360.25	9.37	8:00 - 15:00	Daily
30	CORRIDOR	0.83	m^2	342.2	284.0	1112.22	0.92	12:00 - 14:00	Daily
31	CLASSROOM	12.5	Nº occupants	37.0	462.5	364.70	4.57	8:00 - 15:00	Daily
32	CLASSROOM	12.5	Nº occupants	37.0	462.5	341.15	4.88	8:00 - 15:00	Daily
33	CLASSROOM	12.5	Nº occupants	37.0	462.5	266.60	6.25	8:00 - 15:00	Daily
34	CLASSROOM	12.5	Nº occupants	75.0	937.5	360.50	9.36	8:00 - 15:00	Daily
35	CLASSROOM	12.5	Nº occupants	75.0	937.5	360.25	9.37	8:00 - 15:00	Daily

4.2.4 CASE STUDIES

Control system study

The first study done with the building model was the simulation of the building using each of the operation modes. Sixteen days of a typical meteorological year in Cordoba were selected. The selection was done depending on the season of the year, the level of solar radiation and the average wind pressure on the OVF, for the four orientations of the façade where the OVF was installed. These days are shown in Table 7. The wind pressure values were obtained using the pressure coefficients in Table 5. Two levels (high and low) were considered for each weather variable. The case studies can be seen in Table 8. The same days were simulated without OVF to carry out a comparative study.

The operation modes of the OVF considered were:

a) OVF close completely.
b) Top opening open to the exterior. The ambient air enters the façade through the bottom opening and returns to the ambient through the top opening.
c) Top opening open to indoor. Ventilation of the adyacent room with air from the OVF air gap. The air is exhausted from the room through a ventilation stack ending at the roof.

In order to study the effect of the wind pressure coefficient simulations were made where the OVF was installed in the ground floor with lower pressure coefficients and the top floor, with the highest pressure coefficients.

In the cases in which the OVF remained close or the ventilation air did not flow through the building, the required ventilation flow rate is guaranteed by mechanical means. In the cases where the inner opening was open, natural ventilation is used for ventilating the room. This way the natural ventilation air flow rate could be obtained. However, as it can be seen in section 4.3, the natural air flow rate is insufficient to cover the ventilation requirements in the occupation period. Three cases with forced ventilation were added, Table 8, to study the performance of the OVF when mechanical ventilation is used to assure the ventilation requirements.

The heating season was established from the 1st of November to the 21st of March. The cooling season was from 21st of May to 23 of October. The rest of the period was left without heating or cooling, which is quite a realistic scenario.

For all the cases the simulations were made under a typical meteorological year in Córdoba. The meteorological data were obtained from the software Meteonorm.

The aim of this study was to obtain data about the behavior of the OVF under different meteorological conditions and seasons of the year. With this information a basic control system was configured in order to take advantage of the natural ventilation in the most favourable conditions and to avoid the disadvantages in the non favourable conditions.

Table 7. Selected days for simulation

Day	Code	Season	Direct solar radiation	Wind pressure
Day 1	WHH	Winter	High	High
Day 2	WHL	Winter	High	Low
Day 3	WLH	Winter	Low	High
Day 4	WLL	Winter	Low	Low
Day 5	SHH	Spring	High	High
Day 6	SHL	Spring	High	Low
Day 7	SLH	Spring	Low	High
Day 8	SLL	Spring	Low	Low
Day 9	SMHH	Summer	High	High
Day 10	SMHL	Summer	High	Low
Day 11	SMLH	Summer	Low	High
Day 12	SMLL	Summer	Low	Low
Day 13	AHH	Autumn	High	High
Day 14	AHL	Autumn	High	Low
Day 15	ALH	Autumn	Low	High
Day 16	ALL	Autumn	Low	Low

Table 8. Cases

CASES	OVF ORIENTATION	OVF	EXTERIOR OPENING	INTERIOR OPENING	MODEL ZONE	VENTILATION
1	W	NO	-	-	B2	FORCED
2	W	SI	CLOSED	CLOSED	B2	FORCED
3	W	YES	OPEN	CLOSED	B2	FORCED
4	W	YES	CLOSED	OPEN	B2	NATURAL
5*	W	YES	CLOSED	OPEN	B2	NATURAL
6	E	YES	CLOSED	OPEN	B2	NATURAL
7	E	YES	OPEN	CLOSED	B2	FORCED
8	E	YES	CLOSED	CLOSED	B2	FORCED
9	E	NO	-	-	B2	FORCED
10	S	YES	CLOSED	OPEN	B2	NATURAL
11	S	YES	OPEN	CLOSED	B2	FORCED
12	S	YES	CLOSED	CLOSED	B2	FORCED
13	S	NO	-	-	B2	FORCED
14	N	YES	CLOSED	OPEN	B2	NATURAL
15	N	YES	OPEN	CLOSED	B2	FORCED
16	N	YES	CLOSED	CLOSED	B2	FORCED
17	N	NO	-	-	B2	FORCED
18	S	YES	CLOSED	OPEN	34	NATURAL
19	S	YES	OPEN	CLOSED	34	FORCED
20	S	YES	CLOSED	CLOSED	34	FORCED
21	S	YES	CLOSED	OPEN	34	FORCED

Study of the performance of an OVF in different climatic zones

For this study one city for each climatic zone was selected. The climatic zones in the CTE are classified regarding the climatic severity in the winter and in the summer. In Figure 34 the climatic zones in Spain according with this classification can be seen. Table 9 shows the towns selected in each climatic zone for this study. The aim of this study was to get the variations in ventilation rates and energy demand for heating and cooling when installing the OVF with the control system described in section 4.3.1.

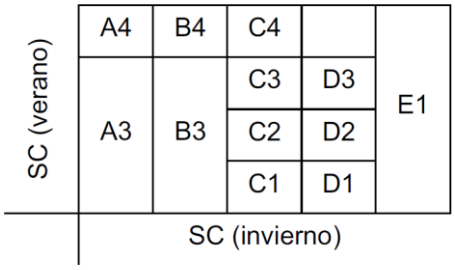

Figure 34. Cimatic zones according to CTE

Table 9. Selected towns for each climatic zone.

Climatic Zone	Town
A3	Cádiz
A4	Almería

Climatic Zone	Town
B3	Valencia
B4	Córdoba

Climatic Zone	Town
C1	Oviedo
C2	Orense
C3	Granada
C4	Badajoz

Climatic Zone	Town
D1	Vitoria
D2	Salamanca
D3	Zaragoza

Climatic Zone	Town
E1	Burgos

Meteorological data were obtained from a tipical meteorological year (TMY) for each location using the software Meteonorm 5.1. These data were formatted and used as input in the building simulation software TRNSYS.

For the whole year simulations the model was simplified thus reducing the computing time. An individual classroom was modeled and simulated. The adyacent spaces were modeled as boundary conditions. An intermediate floor was selected for

the simulated room. The classroom was suppoused to be surrounded by rooms with similar thermal conditions.

The heating and cooling seasons were eliminated. Heating as well as cooling were used whenever necessary to keep the desired temperature in the room during the occupation periods.

The operation modes simulated were:

a) Without OVF
b) With OVF and natural ventilation only.
c) With OVF, natural ventilation and mechanical ventilation to meet the ventilation requirements during the occupation periods.

From the case b) the natural ventilation rates that can be reached with the OVF were obtained. In case c) it can also be quatified the heating and cooling savings when the mechanical ventilation is used trhough the OVF.

Sensitivity analysis of estimated parameters.

For this study a set of estimated parameters used for the model using former experimental results were selected. The objective of this study was to establish the variability of the simulation results as a function of the variation of the studied parameters. This allowed to determine the parameters that have to be estimated with better accuracy or which ones needed a better experimental study.

For this study three parameters were selected: the convection heat transfer coefficient for the external façade surfaces, the convection heat transfer coefficient for the surfaces inside the OVF and the pressure coefficient in the inlet and outlet opening

of the room ventilation air path. Pressure coefficients were estimated from the CpCalc+ software, and the convection heat transfer coefficients were estimated empirically from a previous experiment [49]. The treatments considered for this study can be seen in Table 10.

Table 10. Case study for sensitivity analysis of estimated parameters

	Cases							
	1	2	3	4	5	6	7	8
External convective coefficient	Low	Low	Low	Low	High	High	High	High
Internal convective coefficient	Low	Low	High	High	Low	Low	High	High
Pressure coefficient	Low	High	Low	High	Low	High	Low	High

	High value	**Low value**
External convective coefficient (W/m^2 K)	11.1 + 6 V	3.7 + 2 V
Internal convective coefficient (W/m^2 K)	2.5	0.83
Pressure coefficient	Ground floor level*	Third floor level*

*see Table 5

For this analysis the same simplifiied model as for the former study was used. The simulations were carried out for a typical meteorological year in Cordoba. The following outputs were obtained:

- Heating demand
- Cooling demanda
- Total energy demand
- Average room temperature in the non occupancy period in Winter and summer.
- Air flow rate through the OVF in the non occupancy periods.
- Average air temperature increase inside the OVF when naturl ventilation is used to ventílate the room.

With these data an ANOVA study was carried out to obtain the sensitivity of the outputs with the input parameters.

Sensitivity analysis of design parameters

For this study only two design parameters were chosen. The reason of studying so few parameters was that the numerical model was validated with a defined geometry. Modifying the value of more design parameters could lead to unknown performance of the model. Thus the only parameters that can be modified are those which are not susceptible of affect the results of the numerical model in an unexpected way. The parameters chosen were the global heat transfer coefficient of the insulation OVF layer and the absortivity of the external surface of the steel plate layer of the OVF. These two parameters didn't affect the geometry and therefore the validation of the numerical model was still valid.

Table 11. Case study for sensitivity analysis of design parameters

	Cases			
	1	2	3	4
Insulation (U)	Low	Low	High	High
Solar absortivity	Low	High	Low	High

	High value	**Low value**
Insulation (U, W/m^2K)	0.162	0.486
Solar absortivity (dimensionless)	0.45	0.95

The simulations were made for a typical meteorological year in each case. The outputs obtained in the simulations were the following:

- Heating demand
- Cooling demanda
- Total energy demand
- Average room temperature in the non occupancy period in Winter and summer.
- Air flow rate through the OVF in the non occupancy periods.

- Average air temperature increase inside the OVF when naturl ventilation is used to ventílate the room.

Through an ANOVA analysis information about the sensitivity of the system with the chosen parameters was obtain. With the results of this study it was posible to propose some recomendations about the design processs.

4.3 RESULTS

4.3.1 CONTROL SYSTEM

In this section the graphics of the outputs for the types of days shown Table 7 and the cases in Table 8 are presented. The heating demand in the winter and the cooling demand in the summer are represented for each case and type of day, along with the air mean temperature of the zone and its relative humidity. The free ventilation flow rate in the natural ventilation mode is also presented. Finally the weather data variables, like wind pressure, ambient temperature and solar radiation, are shown. For the sake of brevity only the most representative days are shown as the behavior in the other cases is quite similar.

Winter

In all the cases it was observed that the building performed in the same way in the operations modes in which the inner opening was close or whithout OVF. There were only remarkable differences between the natural ventilation case and the rest. Adding a steel plate layer of 25% of the total surface of façade of the room did not affect significatively the heat transfer through the façade, as the original facade of the building had a good enough insulation so adding another layer did not imply a notable difference.

The differences between different facade orientations were not significant either. The south orientation had a heating demand slightly lower in some cases, Figure 36. However the prevalent heat load was the occupation and therefore external weather conditions were not so influential.

It can be seen that the natural ventilation flow rates were in all cases insufficient to meet the regulation requirements. The required ventilation flow rate for the zone studied (B2) according to Table 6 was 3377 m3/h. The maximum flow rate observed was around 600 m^3/h, which accounts for 18% of ventilation needed.

In the winter period the reduced level of ventilation made the cold air load to be lower and therefore the heating load to be lower too. For the same reason the relative humidity rose until it saturated just after the beginning of the occupancy period. When designing the control system the mínimum required ventilation would have to be supplied by mechanical means and this way keeping indoor conditions under appropriate comfort levels. In the cases with mechanical ventilation humidifying the air was needed in order to meet the comfort levels. After the occupancy period, it took around one hour for the humidity levels to go down to values close to 50%.

At the beginning of the occupancy period the zone temperature rose up to the set temperature. Then the temeperature kept constant while the heating was on. In the natural ventilation case, due to the scarce ventilation, the indoor temperature exceeded the set temperature, Figure 36. This, along with the high relative humidity involved low comfort conditions for the occupants of the room.

The heating demand had a maximun at the beginning of the occupancy period, due to the strong cold air load that is introduced with the outdoor ventilation air. As the time went by and the temperature of the outdoor air was increasing, the heating demand

diminished up to the end of the occupancy period. At this moment the temperature dropped sharply and continued diminishing as the ambient temperature decreased.

The ventilation flow rate curve in the case of natural ventilation followed the same shape as the temperature difference between indoor and outdoor. This indicated that the main driving force of the air flow in those cases was the buoyancy due to the indoor-outdoor temperature difference, or stack effect. In the cases where the wind pressure was significant the effect of the wind can be considered as a disturbance in the flow rate, but the stack effect was prevalent all over the day, Figure 36. In the cases where the wind pressure was negative, it can be seen that this effect balanced and even surpassed the buoyance force so the flow rate got eventually inverted Figure 35. The low short wave solar radiation did not affect significatively the flow rate curve, which means the buoyancy force due to the temperature increase inside the OVF is negligible compared to the stack effect of the building.

When the wind pressure was low, the stack effect maintained a minimum ventilation flow rate of around 300 m^3/h. In the occupancy period, it rose abruptly when the heating system and the occupation load were turned on. The profile of the flow rate was quite definite when the wind force was low, as in Figure 38. In some cases the wind pressure became the prevalent force at times but although it reached high peak values it was not enough to cover the ventilation requierements, Figure 37.

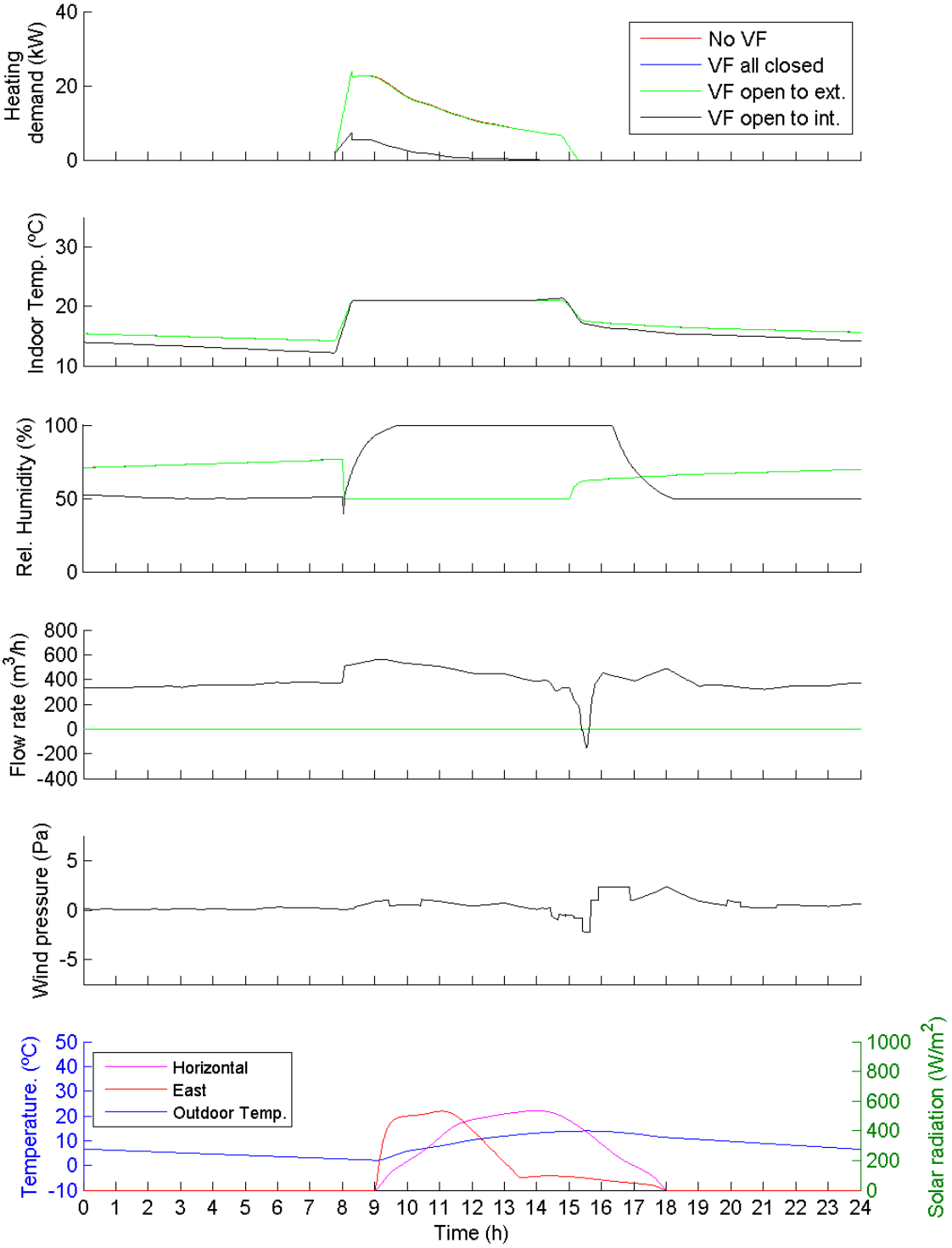

Figure 35. Heating demand and natural ventilation flow rate for case WHH, East orientation.

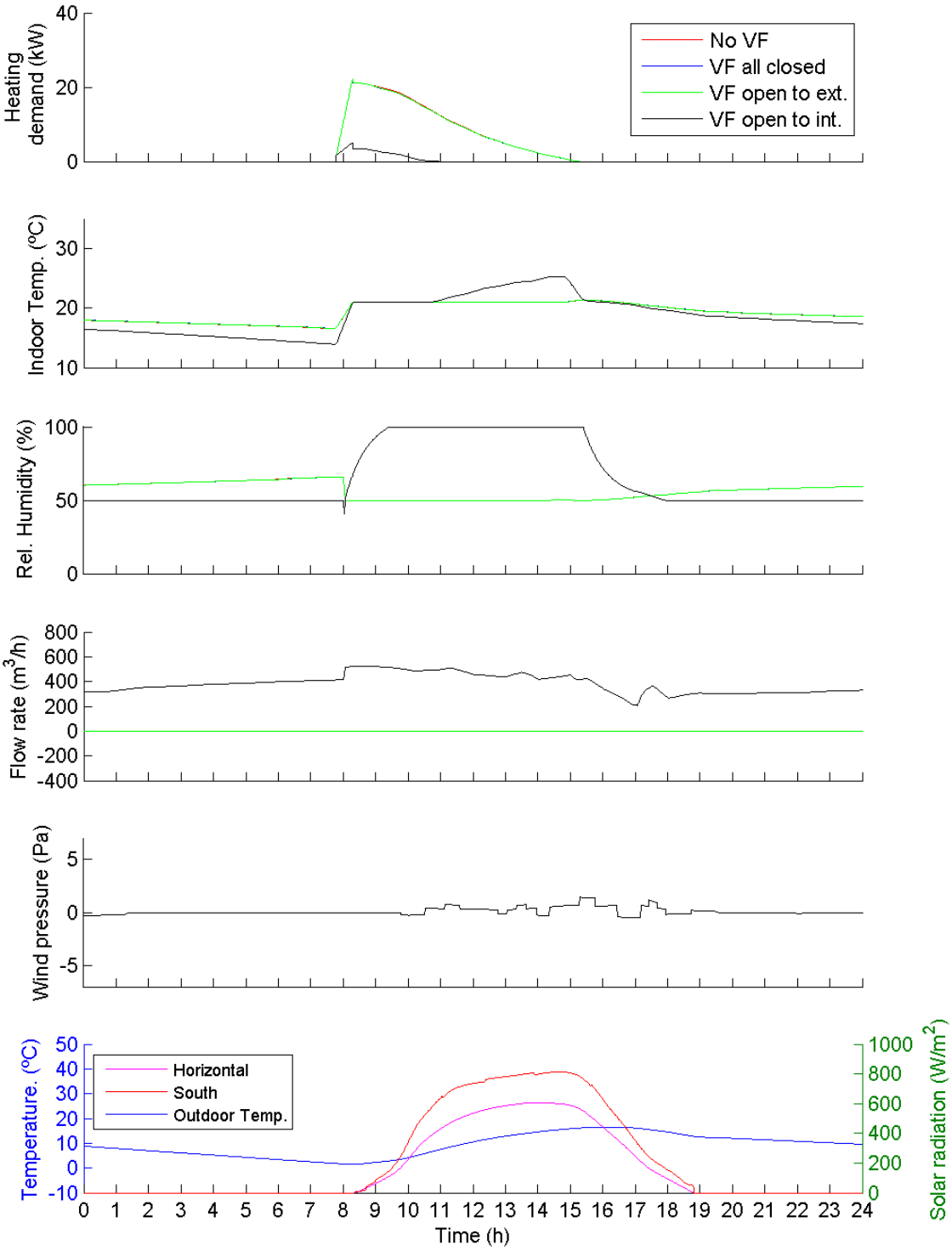

Figure 36. Heating demand and natural ventilation flow rate for case WHH, south orientation.

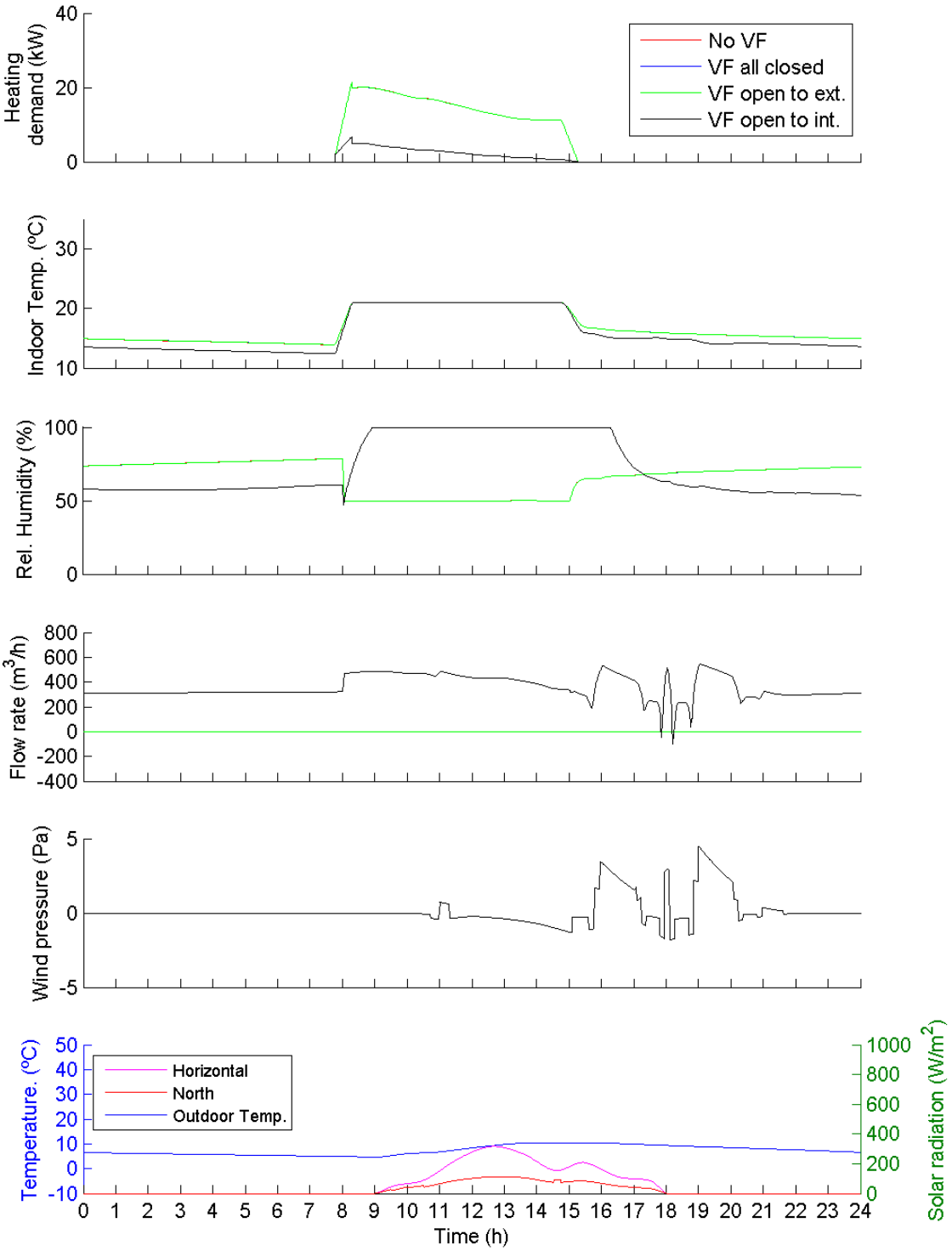

Figure 37. Heating demand and natural ventilation flow rate for case WLH, north orientation.

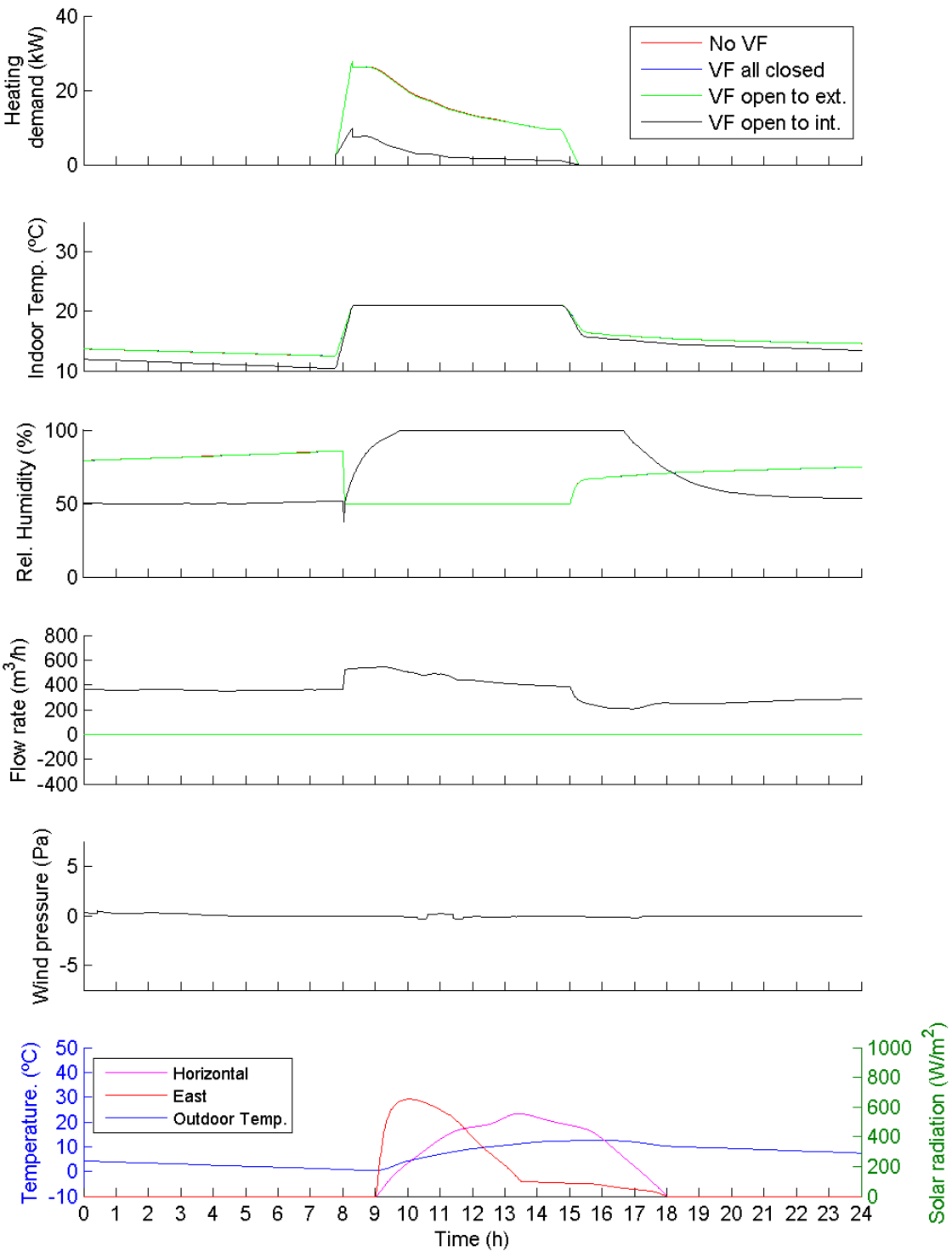

Figure 38. Heating demand and natural ventilation flow rate for case WHL, east orientation.

Spring

During this period of the year the heating was only available at the beginning of the season and the cooling at the end. On the central days their use wasn't available because the temperatures were usually moderated. In this season the ambient temperature begins to rise and so do the indoor temperatures. However the temperature difference between indoor and outdoor decreases. This makes the stack effect lower and it is no longer the main driving force for natural ventilation. The trend of the curve was not the same as that of the indoor temperature, Figure 39.

In the cases where the wind pressure was significative, the natural flow rate profile was the same as the wind pressure. Thus, the wind pressure became the prevalent driving force, Figure 40. When the wind pressure got negative values, the flow rate was inverted.

In the mechanical ventilation cases the cold flow rate at the beginning of the occupancy period made the temperature drop sharply and then it rose progressively until the end of the period, Figure 39. This allowed the average room temperature to maintain values around the required temperature without additional energy consumption. In the natural ventilation mode it can be seen that the temperatures rose above 25 ºC, and the humidity ratio reached high values during the occupancy period. This made the indoor conditions unacceptable.

In the days of spring where the cooling system was on, Figure 41, the energy demand was greater than that in the natural ventilation mode, as the room was ventilated with outdoor air at a temperature lower than the indoor air temperature. Mechanical ventilation used outdoor air at a minimum temperature at the beginning of the occupancy period. As the ambient temperature was rising, a point was reached when it was necessary to turn on the cooling system. The cooling demand increased

as the outdoor temperature increased. When it occured the energy demand of the mechanical ventilation case was greater than that in the natural ventilation mode, as the ventilation rate was much lower. Furthermore, the ventilation air passing throught the OVF was preheated and it became an additional heat load.

In Figure 42 it can be observed that when the temperature difference between outdoor and indoor air was inverted, and there wasn't enough wind pressure on the façade, the flow rate through the OVF was very low. This caused oscilations in the numeric model solution. The low ventilation rate also made the relative humidity to evolve more slowly after the occupancy period.

In the natural ventilation mode, the free night ventilation made the temperature a few degrees lower than in the case without natural ventilation at the beggining of the occupancy period. In warm days this constitutes an advantage as the temeperature reached at the end of the working time will depend on the intitial temperature first time in the morning.

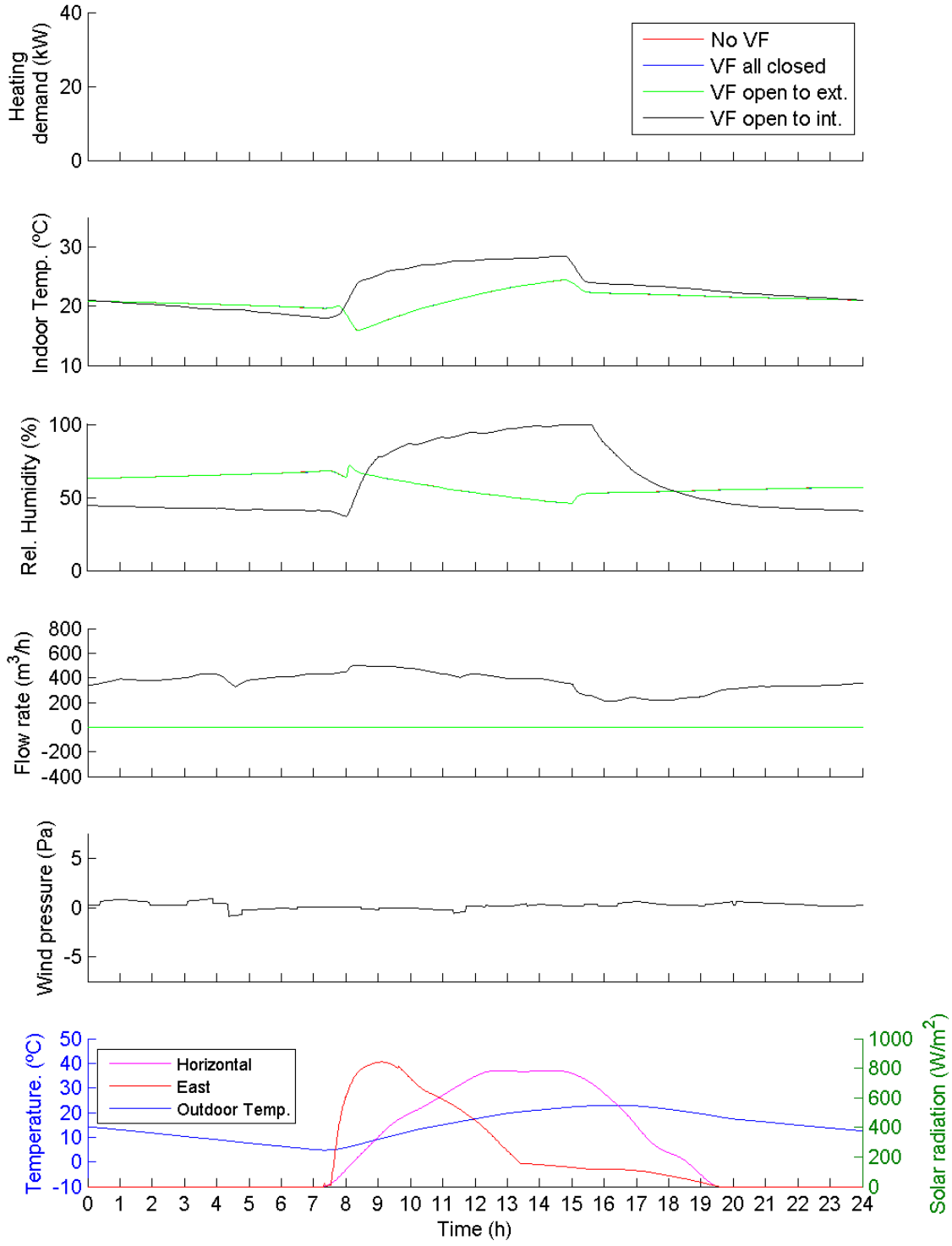

Figure 39. Heating demand and natural ventilation flow rate for case SHH, east orientation.

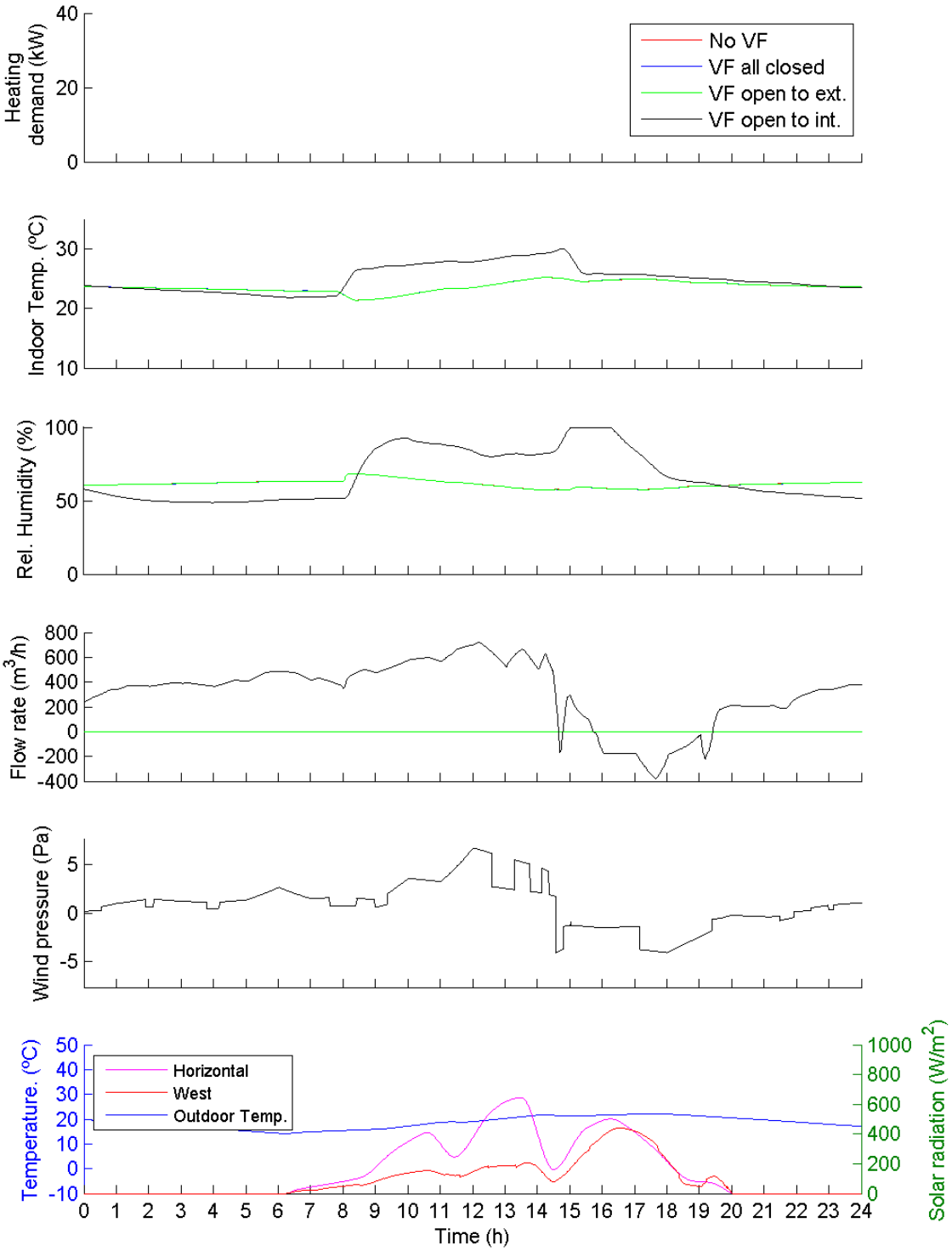

Figure 40. Heating demand and natural ventilation flow rate for case SLH, west orientation.

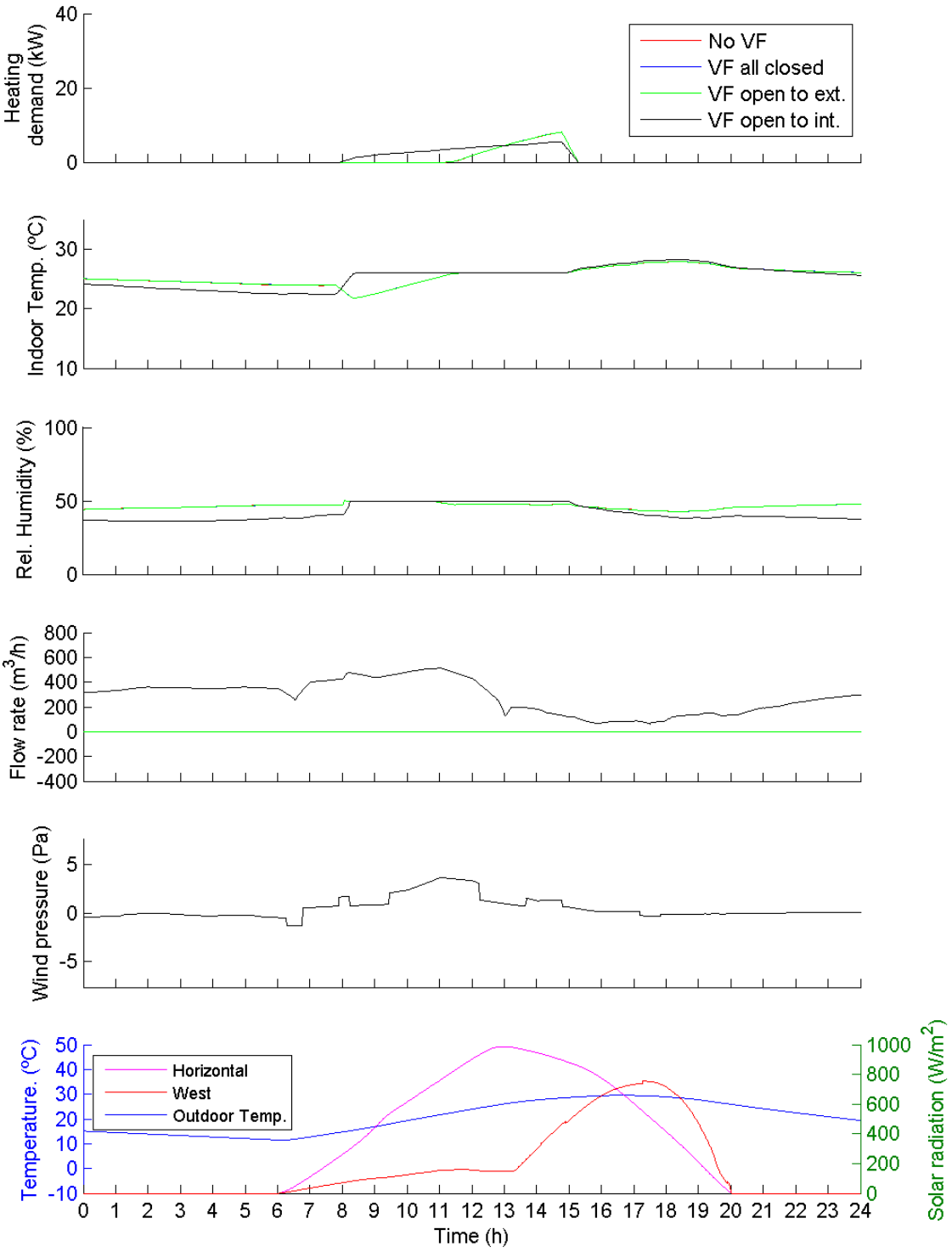

Figure 41. Heating demand and natural ventilation flow rate for case SHH, west orientation.

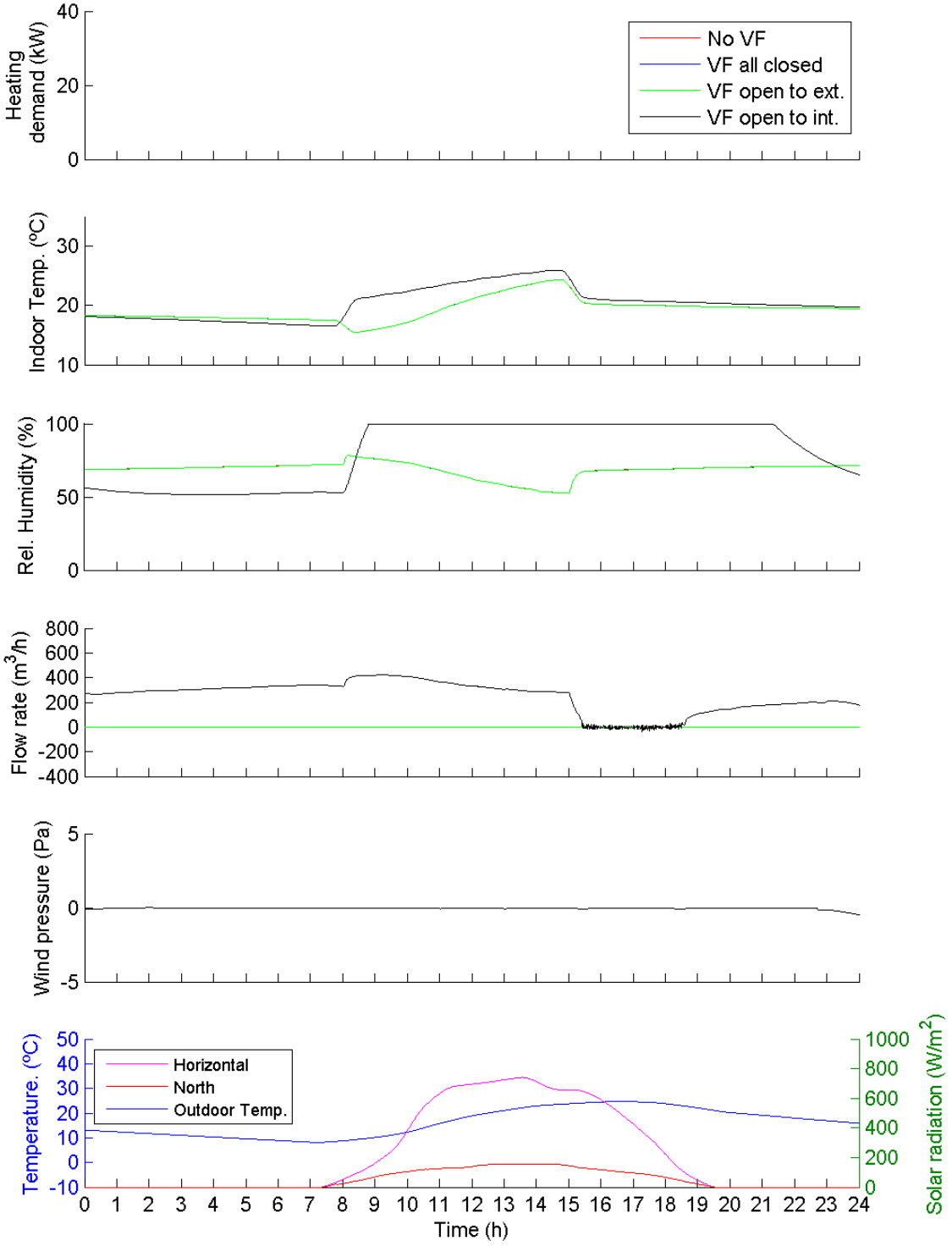

Figure 42. Heating demand and natural ventilation flow rate for case SHL, north orientation.

Summer:

In this season the cooling energy demand was found to have similar values in all cases despite of the fact that the required ventilation rates were not accomplished either. The reason of this is that the main heat load of the zone were the occupants. In the case of mechanical ventilation, cooling was not necessary until the exterior temperature rose sufficiently. The system took advantage of the fresh air in the morning, but it became a heat load at the end of the occupancy period, when the exterior temperature was higher. In the case of natural ventilation, as ventilation was a small heat load, the cooling requirements were destined to balance only interior heat loads that remained constant.

The relative humidity was kept constant, regardless of the ventilation rate, as in this case humidity was controlled by the cooling system.

The temperature difference between indoor and outdoor in the summer diminished further and in almost all the cases it ended up inverted, creating at the end of the working period an important inverse flow rate in the case of natural ventilation, Figure 43. In some cases the effect of the wind was able to stop this process and keep the direct air flow from the OVF to the room, as it can be seen in Figure 44. At night the flow rate increased due to the stack effect as the temperature difference between indoor and outdoor became positive as the outdoor temperature decreased.

Night free ventilation resulted of key importance in the summer. Figure 45 shows that ventilating at night with ambient air at a lower temperature, a lower temperature was achieved at the beginning of the occupancy period. This way the energy demand is reduced as the cooling system turned on later. The more night ventilation existed the night before, for example due to wind pressure, the greater the energy savings the day after. Therefore it is convinient ventilate the room when the ambient temperature is

near its minimum. This way the heat loads stored in the structured of the building can be removed.

At the end of the occupancy period the external heat loads made the temperature rise above the set point, especially in the west orientation, Figure 44, as at that time the zone received an important amount of short wave solar radiation. Maintaining natural ventilation in this situation results counterproductive, though in this case the effect is not very important as the flow rate was not very high. However, once the temperature inside the OVF drops to a low level it is convenient to ventilate.

In Figure 46 it can be observed that the room temperature was over 30ºC during the night, due to the high ambient temperature. Due to this, the temperature of the air at the beginning of the occupancy period was the same in all cases, regardless of the ventilation rates. It can also be seen that when the OVF was open to the exterior the cooling demand was slightly lower than the case without OVF or with the external opening closed. This could be caused by the solar radiation shielding effect and by the heat removing effect of the ventilation to the ambient of the heated air inside the OVF. When the weather is hot it is always convinient to open the façade to the exterior to avoid overheating.

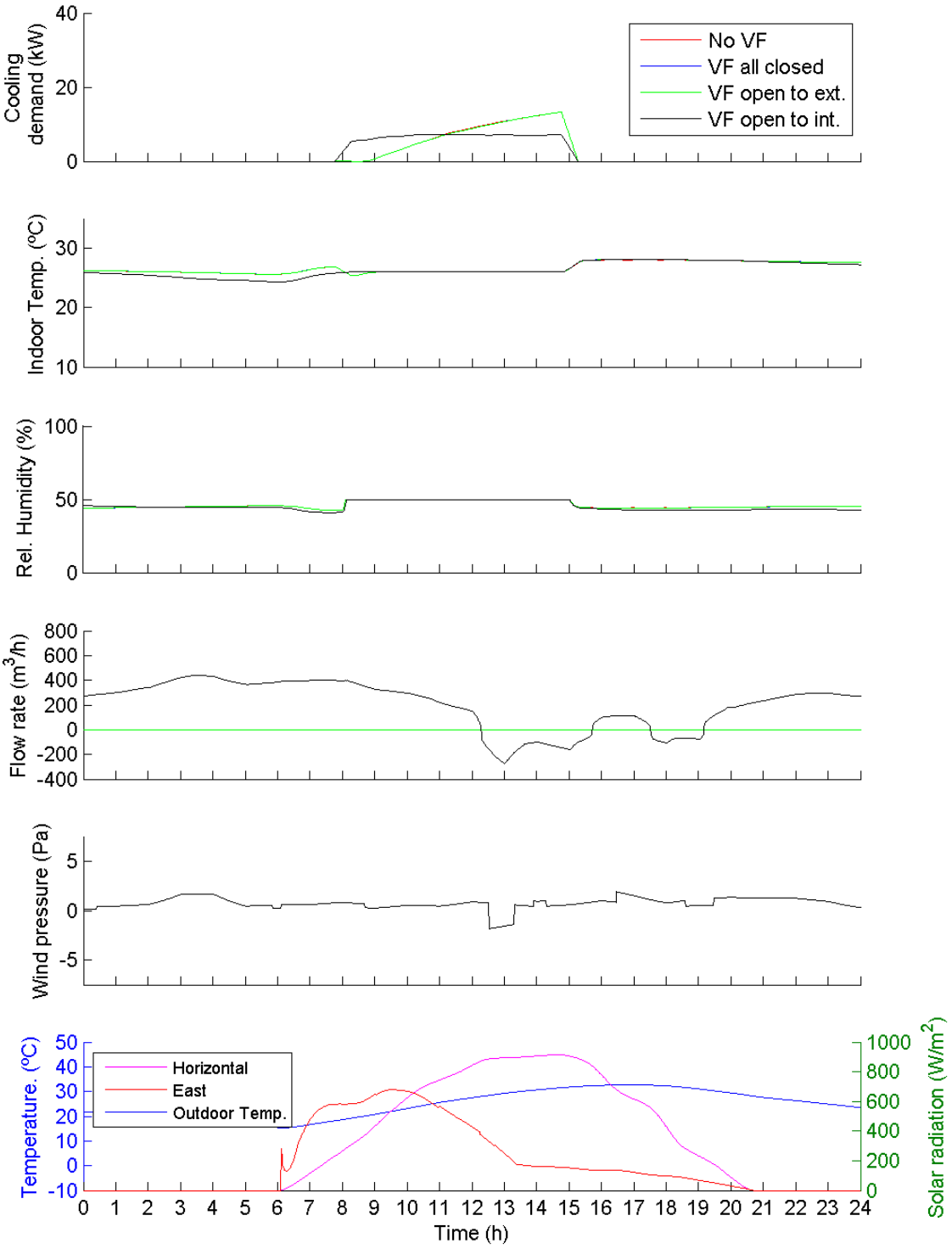

Figure 43. Heating demand and natural ventilation flow rate for case SMHH, east orientation.

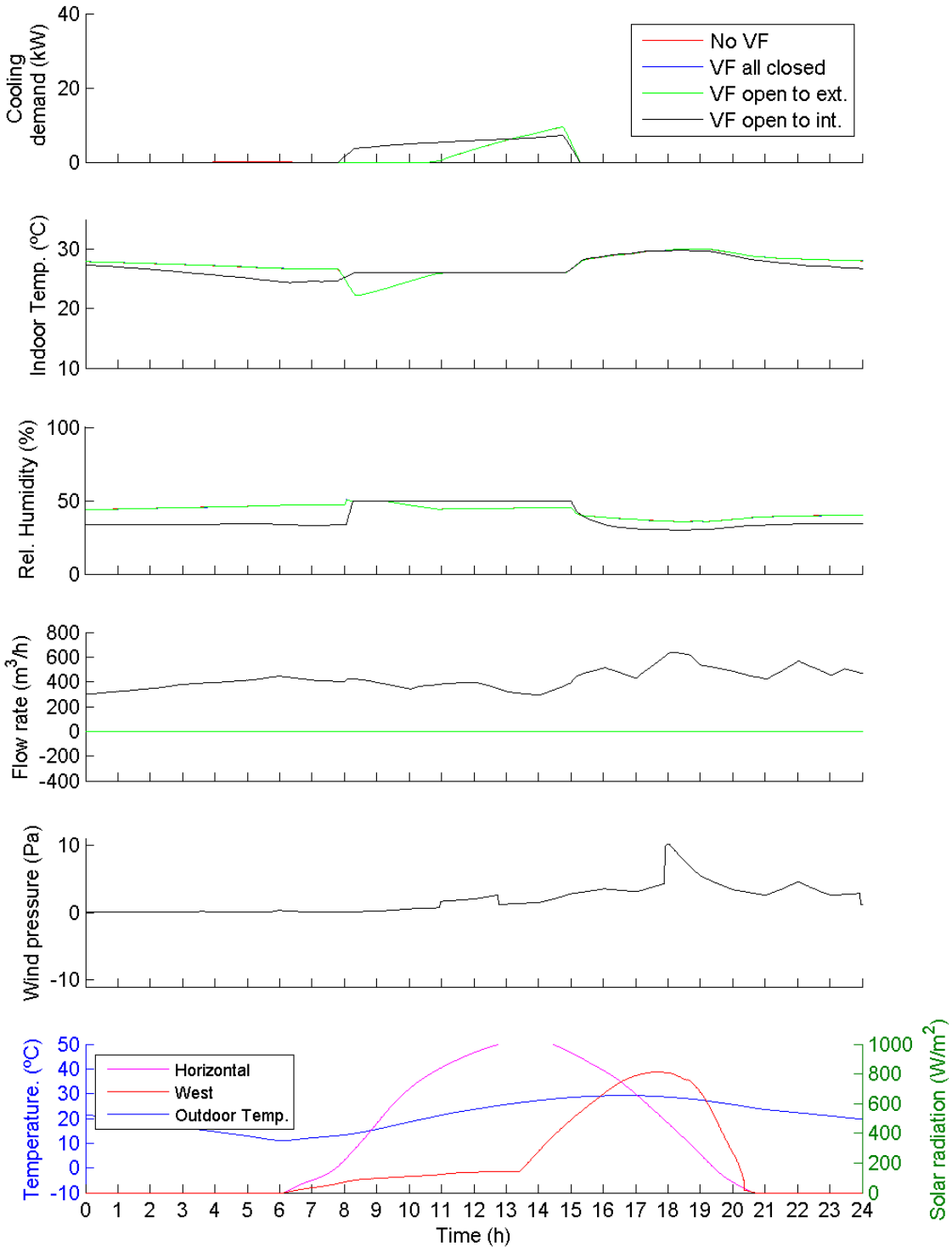

Figure 44. Heating demand and natural ventilation flow rate for case SMHH, west orientation.

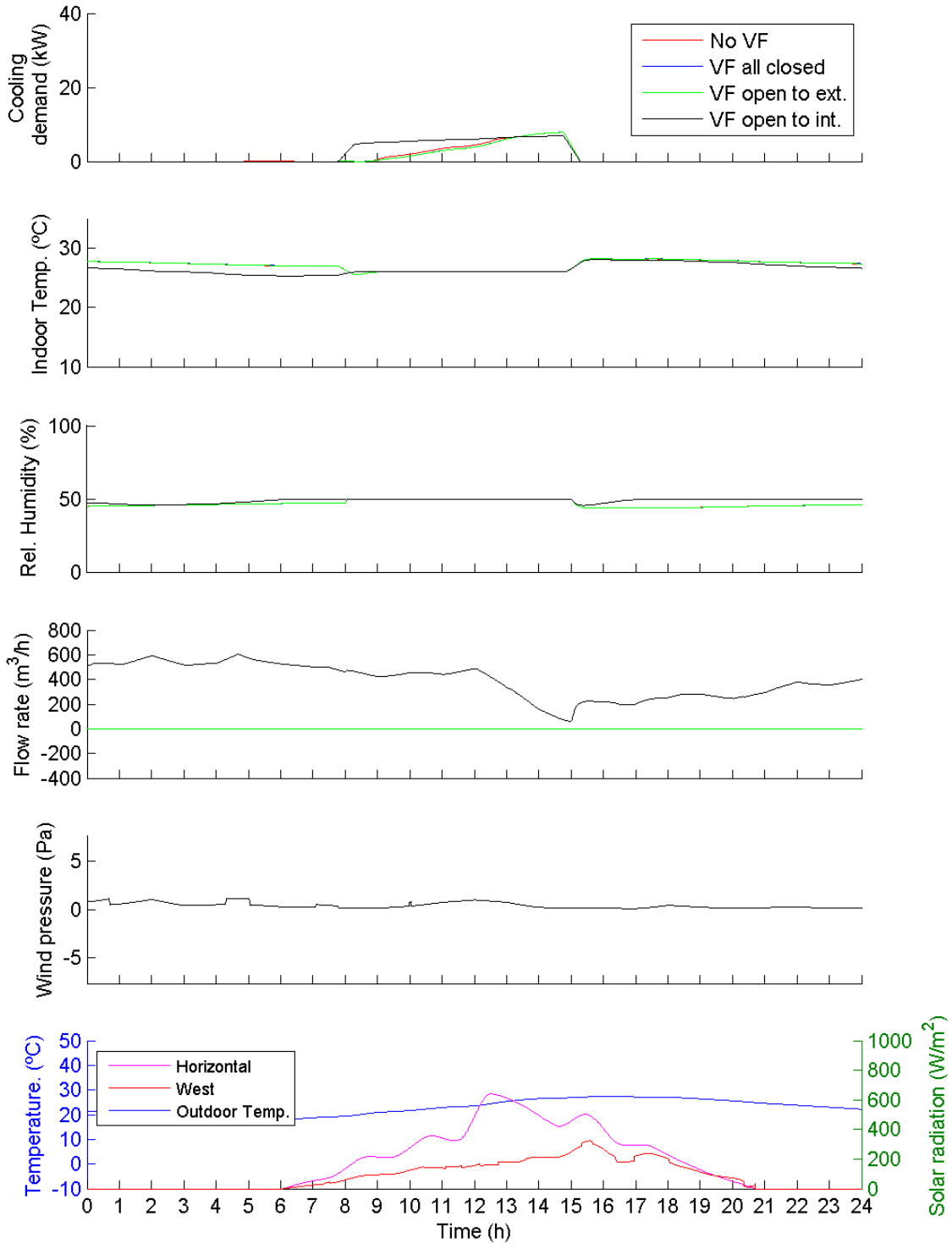

Figure 45. Heating demand and natural ventilation flow rate for case SMHH, east orientation.

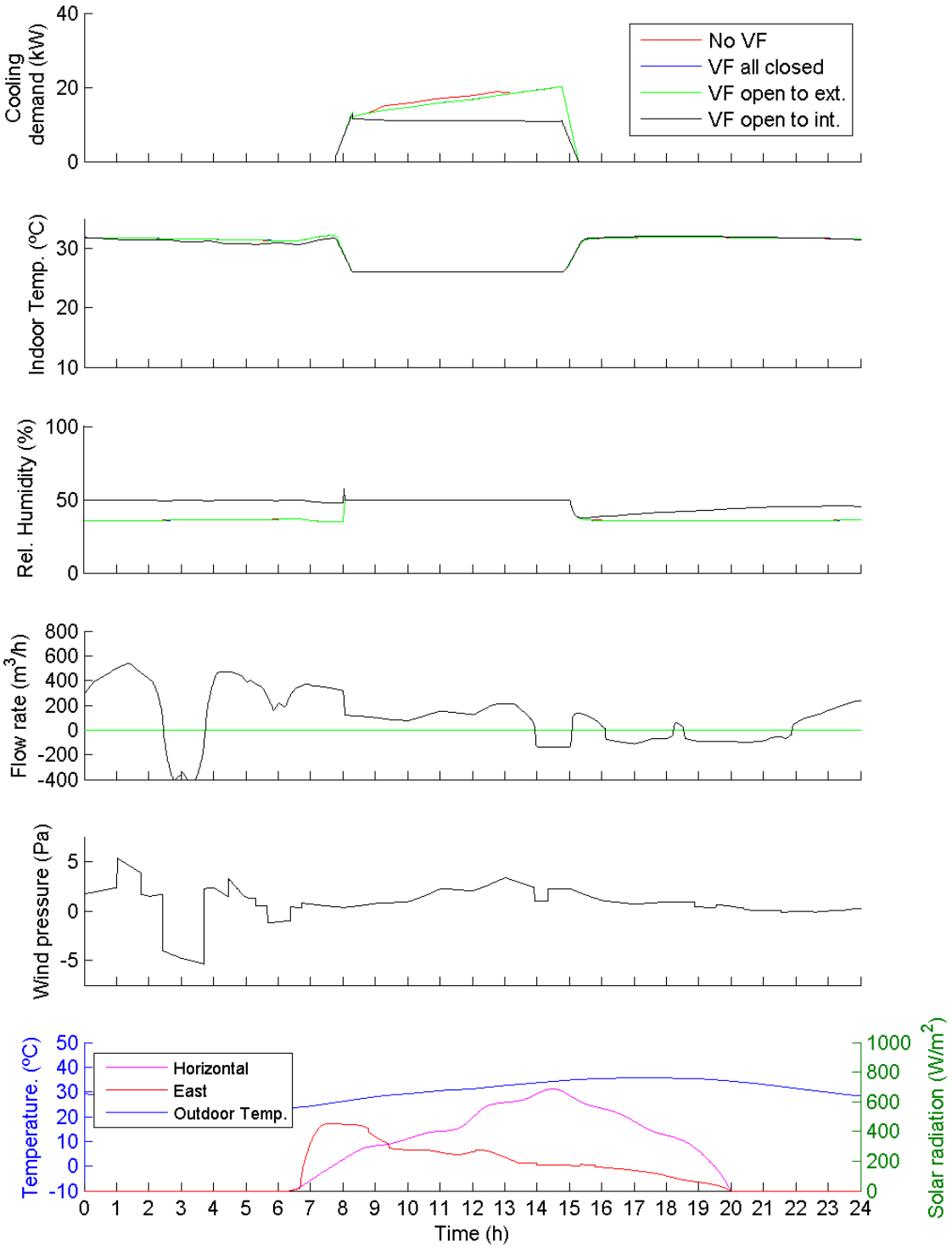

Figure 46. Heating demand and natural ventilation flow rate for case SMLH, east orientation.

Autumn

In general, the model behaved the same way as in spring. It was noticeable the day represented in Figure 47. The mechanical ventilation at the early morning made the room temperature fall so that the cooling system didn't need to be turned on all along the occupancy period. The room temperature remained around the set point. This confirms the recomendation of ventilating the room with ambient air when its temperature is around its daily minimum.

Closure

In a general manner, the trends observed in the results presented so far were quite similar to those of other studies about natural ventilation in buildings. Several authors, as [51], have reached the conclusion that natural ventilation at nights in hot seasons removes the heat stored in the massive elements of the building during the day, reducing the heat loads for the next day. In [52] the same decreasing temperature effect can be seen when night ventilation is used, and moreover it is pointed out that night ventilation with double skin facades doesn't have security problems, as in the caso of traditional windows. In other study, [53] it was concluded that night ventilation in the summer was independent of the wind direction. This is due to the fact that the main driving force is the stack effect. In [54] night mechanical ventilation is also recommended as the energy consumption of the ventilation system is lower than the savings in the cooling system the day after.

Regarding day ventilation, in [55] the authors coincided in the recommendation of ventilation in the early morning in the summer, just before beginning the working period. However, the day ventilation was conditioned by the outdoor air quality and the external noise level. In other study,[56] it was recommended day ventilation through

buffers, in other words massive elements that store heat in some way. An OVF could make the same effect as these buffers.

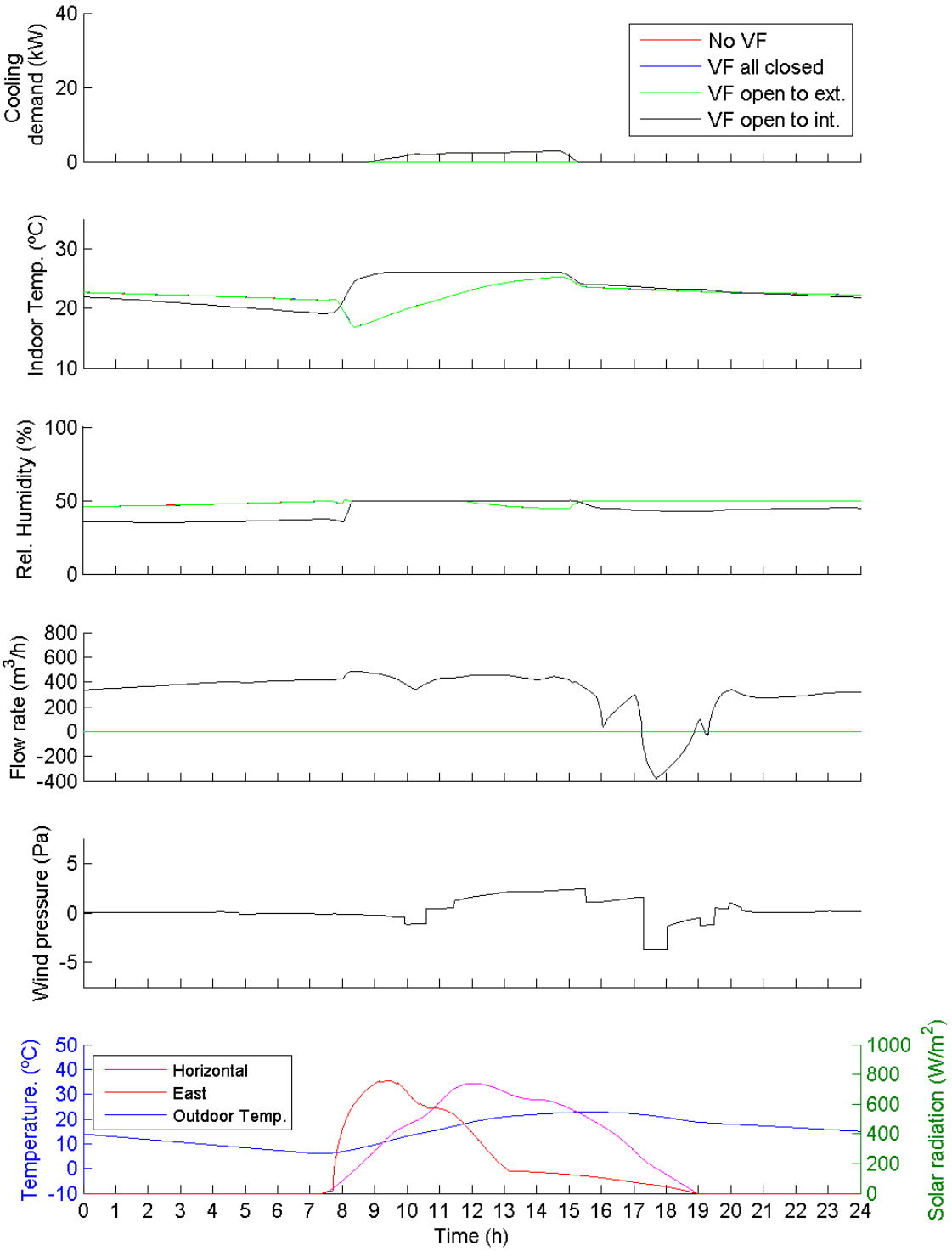

Figure 47. Heating demand and natural ventilation flow rate for case AHH, east orientation.

The shape of the curves of cooling and heating coincided with the results of simulations realized in [56]. In the witner there was a heating peak in the morning and the heat demand diminished as the outdoor temperature rose. In the summer the cooling demand was very low or even zero first time in the morning and it rose along the morning simulstaneously with the outdoor temperature. In other studies it was indicated that natural ventilation influence positively on reducing the cooling energy demand [57].

In the graphics shown so far it can not be appreciated the energy savings that an OVF could provide when working with mechanical ventilation. It will be highlighted in later chapters. However, [58] remarked that solar walls were able to preheat the ventilation air, among other advantages.

In [59], it is pointed out that in the case of moderate temperatures, natural ventilation only was enough to maintain adequate indoor air conditions.

Design of the control system

From the simulations carried out it can be concluded that when the OVF tested could not provide the flow rate required in regulations, mechanical ventilation had to be used. Natural ventilation was then used to smooth the temperature profiles during the rest of the time. In the winter it is convenient to ventilate when temeperatures are near the day maximun, and thus elevating the minimum tempetarure the day after. Additionally, the air was preheated when passing through the OVF. However, ventilating in the summer thorugh the OVF added an additional heat load and This is not convenient as long as the solar radiation and the ambient temperature are high. It can even be convient to use mechanical ventilation in the morning to delay the start of the cooling system.

From these results a control system was established to operate the OVF along the year in subsequent simulations. This control system acts over the interior and exterior OVF openings. The inner opening was always kept open during the occupation period as it was mandatory to provide ventilation to the occupants while they were developing their activities. In the winter season the inner opening was also opened in the non occupancy period when the temperature inside the OVF exceeded 21ºC (with a hysteresis cycle). In the summer season the inner opening was opened (with a hysteresis cycle) when the temperature of the air inside the façade was under 23ºC. This way free ventilation is used to save heating and cooling energy for the next occupation period.

4.3.2 STUDY OF THE PERFORMANCE OF AN OVF IN DIFFERENT CLIMATIC ZONES

In Table 12 the annual energy demands for heating and cooling are presented, as well as the total energy demand per m^2. In Table 13 the results of the simultions carried out for the 12 climatic zones indicated in Figure 33 can be seen. The table shows the increases on heating demand in the winter and cooling demand in the summer. Next to the heat demand it is shown the percentage of heat load provided by the preheated ventilation air through the OVF in the occupancy period. This preheated air was a support for the heating systems in this case. Beside the cooling demand it is shown the percentage of the total cooling load that correspond to the heat introduced with the preheated ventilation air coming from the OVF in the occupancy period. In this case the preheated air implied an additional cooling load.

Table 12. Heating, cooling and total energy demand per unit surface.

Climatic zone	City	Heating Demand (kWh)	Cooling Demand (kWh)	Total energy demand per m^2 (kWh/m^2)
A3	**Cádiz**	1125.20	1448.88	45.97
A4	**Almería**	503.40	2700.15	57.21
B3	**Valencia**	1358.61	2422.07	67.51
B4	**Córdoba**	1578.01	3016.82	82.05
C1	**Oviedo**	3433.82	221.07	65.27
C2	**Orense**	3390.34	296.69	65.84
C3	**Granada**	2679.73	1600.16	76.43
C4	**Badajoz**	2012.73	2333.43	77.61
D1	**Vitoria**	4870.12	437.06	94.77
D2	**Salamanca**	4878.76	797.05	101.35
D3	**Zaragoza**	3300.90	1750.88	90.21
E1	**Burgos**	6331.37	354.25	119.39

Figure 48 shows the average daily temperature in the cases of building with and without OVF, without taking into account the occupancy period, as in these periods the temperature was controlled by the cooling/heating device. The temperature was floating during the non occupancy period and it was affected by the preheated ventialtion air in the winter and the fresh air in the summer.

Table 13. Comparison of thermal behavior of the building with OVF with respect to the case without OVF.

Climatic zone	City	Δ heating demand (%)	Air supply preheating in the winter (%)	Δ cooling demand (%)	Extra load in the summer (%)
A3	**Cádiz**	-23.9	7.3	-13.5	15.6
A4	**Almería**	-23.0	7.6	-5.0	10.7
B3	**Valencia**	-26.4	7.3	-3.8	14.4
B4	**Córdoba**	-29.7	8.0	-10.8	14.4
C1	**Oviedo**	-21.0	6.4	-3.4	48.5
C2	**Orense**	-24.4	6.6	-9.3	39.9
C3	**Granada**	-40.1	7.3	-14.3	18.0
C4	**Badajoz**	-28.7	6.8	-14.1	11.7
D1	**Vitoria**	-20.3	5.7	-12.7	29.8
D2	**Salamanca**	-24.0	5.6	-17.4	22.0
D3	**Zaragoza**	-19.4	4.7	-17.9	9.7
E1	**Burgos**	-18.9	4.8	-20.7	18.7

Table 14. Air flow rate results

Climatic zone	City	Air flow rate accomplished (no mechanical ventilation) (%)	Air flow rate (no occupancy period) (%)
A3	**Cádiz**	55.7	8.7
A4	**Almería**	17.4	6.4
B3	**Valencia**	25.4	6.9
B4	**Córdoba**	20.5	6.6
C1	**Oviedo**	30.4	9.9
C2	**Orense**	31.1	10.3
C3	**Granada**	50.0	8.5
C4	**Badajoz**	24.0	7.5
D1	**Vitoria**	29.6	9.6
D2	**Salamanca**	29.0	8.8
D3	**Zaragoza**	27.0	8.1
E1	**Burgos**	29.5	9.8

The heating demand was lower for all climatic zones when the OVF was used, from 19% to 40% approximately. In the zones with a low winter severity (A, B and C) the saving percentages are in average greater than those of the zones with greater winter severity (D and E). It can also be observed that more energy was obtained from the OVF in the towns with lower winter severity.

The cooling demand decreased also for all climatic zones when the OVF was used. However, the saving percentages were in general lower tan in the case of heating. It can be seen that as a rule of thumb the percentage of cooling saving increased with the climatic severity, except for the zones A4 and C4, in which it decreased respect to the A3 and C4 cases respectively. The additional thermal load due to the ventilation through the OVF followed the opposite trend. Cases C1 and C2 can be highlighted, with loads of 49% and 40% of the cooling load respectively.

In the case with OVF and natural ventilation only, it can be observed that the ventilation rates were insufficient to cover the regulations requirements in all zones. The greater value, case A3, reached 55%, but this percentage is an yearly average so there were times when the ventilation rates were very lower and other were higher. There wasn’t a marked trend for this variable respect to the climatic zones.

In Table 14 it is shown the percentage of required ventilation rate that was accomplished only with natural ventilation in the occupancy periods and the flow rate that circulated trhough the room during the non occupancy periods in the case when the mechanical ventilation was used in the occupancy periods.

The average percentage of natural ventilation in the non occupancy periods was lower than in the occupancy periods. In the winter, with no occupation, there were lower flow rates as the buoyancy forces depends on the indoor-outdoor temperature

difference, and this differences decreased when the heating systems was stopped. In the summer the temperature difference was lower and even negative, so the flow rates were also lower.

However, as deduced from Table 13 and Figure 48, ventilation at high temperatures in the winter and at low temperatures in the summer caused the average temperature in the non occupancy period to rise in the winter and to lower in the summer, and implied energy savings in heating or cooling for the next day. It can be observed in the graphics that in all cases the average temperature with OVF was in general greater in the winter and lower in the summer, than the case without OVF.

The average natural ventilation reached using OVF was over 20% of the required by regulations in almost all cases. The reason of this could be the prevalence of internal loads over the external ones. In other studies the impact of internal on the natural ventilation potential has been studied, [59] [60]. In other studies it has been proven that the key factor for having a high natural ventilation potencial is the indoor-outdoor temperature difference [61], which is closely related to internal thermal loads. In [60] it is shown that when outdoor temperatures were moderate or high, the natural ventilation potential decreased.

The effect of night ventilation has been studied widely. Many authors coincide about the effectiveness of night ventilation in providing better indoor air conditions during the day, and in reducing the consumption of the cooling system. In [59] the natural ventilation potential was studied for several climatic zones. It was concluded that in the cold zones natural ventilation could be enough to cool a building in the summer. It was also concluded that the zones with lower ambient temperatures have greater potential for natural ventilation. In other studies it was concluded that in the south Europe areas night ventilation was not enough and it was recommendable to use mechanical

ventilation during the night to reduce the cooling energy during the day. In [62] it is shown that the cooling load could be reduced by an average of 12 kWh/m2.

During the day natural ventilation can support the heating system in the cold season by using a OVF. In the summer, some studies coincide about the decrease of cooling savings and even the increase of them, when the ambient temperature was high [60]. In the case of an OVF the risk of overheating was found greater due to the preheating process inside the OVF. The energy savings were found greater in extreme climates [63]. This can also be seen in the results of the present study.

From the results obtained in this section it can be concluded that there is a potential of natural ventilation in all the climatic zones studied. However, the natural ventilation during the occupancy period is not enogh to meet the requierements of regulations, and it is necessary to use mechanical ventilation. Besides, natural ventilation in the non occupancy period, when conditions are favourable, implies energy savings in the winter and in the summer in all the climatic zones studied. It was also found that preheating the ventilation air as it passes through the OVF in the winter during the occupancy period reduces the heating load around 6%. The only adverse effect is the increase in the cooling load during the occupancy period in the summer when the ventilation air passes through the OVF.

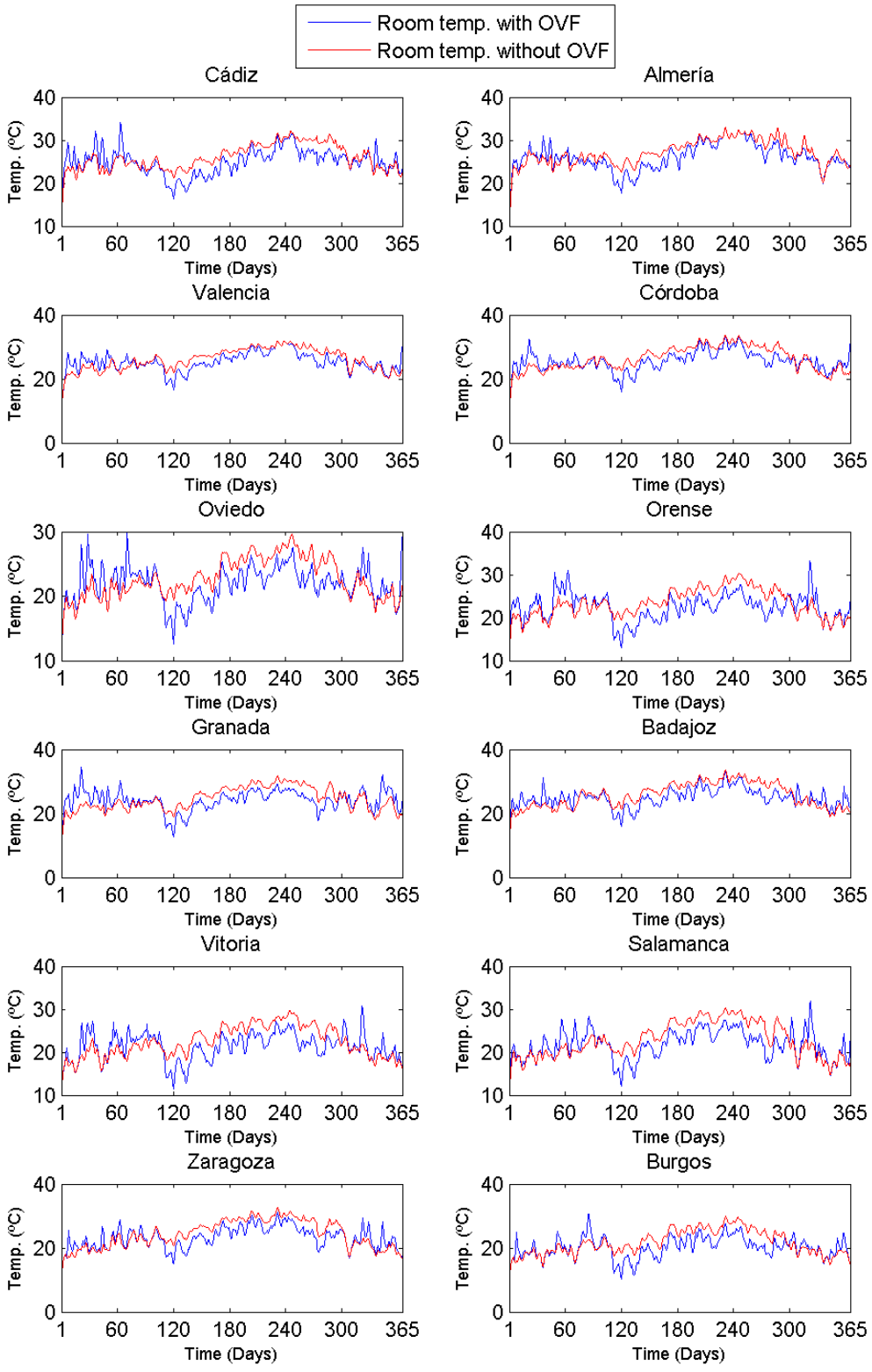

Figure 48. Day average temperature out of the occupation period.

4.3.3 SENSITIVITY ANALYSIS OF ESTIMATED PARAMETERS.

In this section the effect of the variation of the estimated parameters on the model outputs are studied. Simulations were carried out using the combinations of parameters showed in Table 10. The results are presented as scatter plots and the ANOVA results are also shown and discussed.

Effect on the energy demand

In Figure 49, Figure 50 and Figure 51 the yearly heating, cooling and total energy demand values are represented against the low and high levels for the convective heat transfer for the external surface of the steel plate, the internal convective heat transfer coefficient inside the OVF and the pressure coefficient on the façade inlet opening. These parameters were introduced in the OVF model after being estimated from experimental data or, as in the case of the pressure coefficient, from a numerical model software.

To facilitate the analysis, the ANOVA method was used, which allowed to study the variability of the outputs with the inputs variations. The interactions between different parameters were also studied. Table 15Table 16 Table 17 shows the results of these analyses for the heating, cooling and total energy demand.

In general it is observed that the variability of the energy demand respect of the variation of the parameters studied was not strong. The greater variability was due to the convective heat transfer coefficients, as it can be seen in the ANOVA results. The pressure coefficient, and therefore the effect of the flow rate, had little effect compared with the convection coefficients. Moreover, the effect of the interaction between the exterior and interior convection coefficients was high, for heating as well as for cooling energy demand. The effect of the internal convection heat transfer coefficient was always greater than that of the external one.

It can be appreciated that the effect of a greater external convective heat transfer coefficient was raising the heating demand and reducing the cooling demand. This is due to the greater heat transfer to the ambient air and less heat transfer to the air entering the building, and therefore greatet supply of heat by the heating system. Besides, the more heat is transfer to the ambient air in the summer, the lower the heat load, as the ventilation air is not heated so much. The combined effect of low external convection heat transfer coefficient and a high internal convection heat transfer coefficient had a positive effect on the heating demand, but negative on the cooling demand, and viceversa.

As it can be observed in Figure 49, when increasing the internal convection heat transfer coefficient there was a lower thermal resistance for the heat flow to the air inside the OVF. This air was then introduced in the room, decreasing the heating system consumption. In the cooling season the effect was similar. See Figure 50. In this case the air is preheated before going in the building and it added a thermal load, so the cooling demand rose.

In Figure 49 it can be observed that the heating demand increased when the pressure coefficient increased. A greater pressure coefficient means that with the same wind pressure on the façade, a greater flow rates pass through the OVF. During the occupancy period the flow rate was kept constant by mechanical means, so it was never affected. During the non occupancy period the flow rate increase could make the average temperature of the air to drop, reducing the effect of free preheating. For the same reason, in Figure 50 it can be seen that the cooling demand was reduced slightly. The effect on the total energy demand was small because the heating and cooling effects compensate each other.

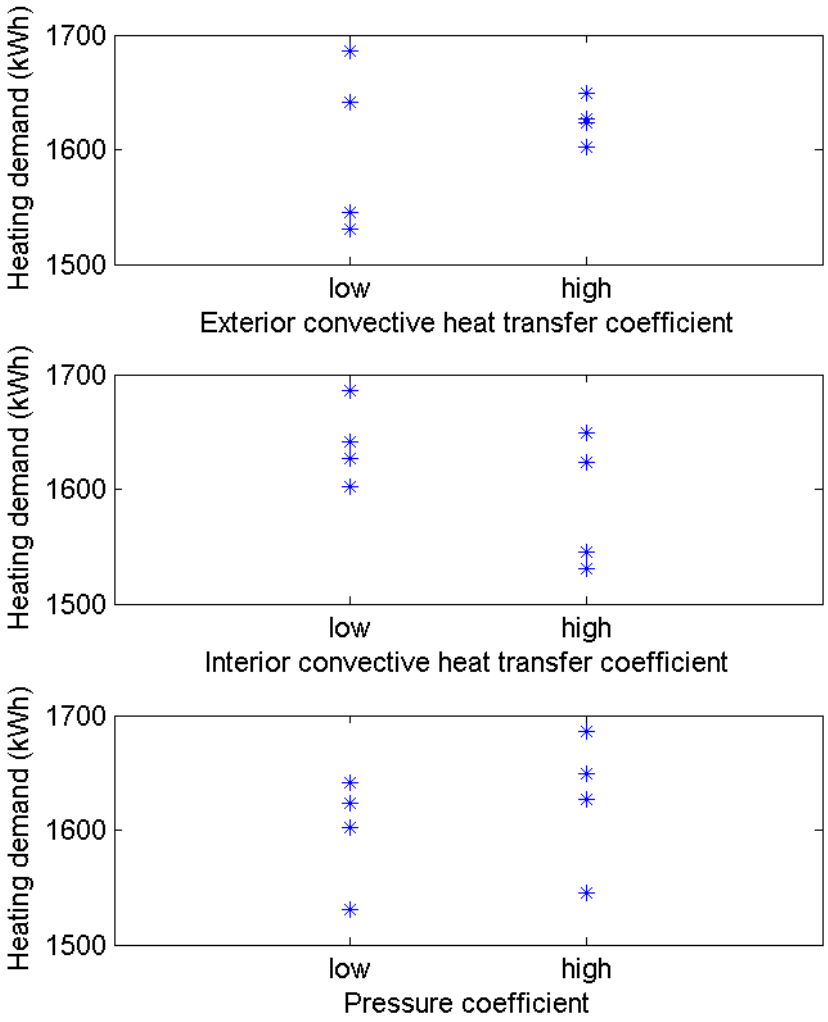

Figure 49. Scatter plots of yearly heating demand depending on the parameters studied

Table 15. ANOVA analysis results for heating demand

Parameter	Sum Sq.	d.f.	Mean Sq.	F	Prob>F
External convective coefficient(X1)	1222.92	1.00	1222.92	10.16	0.19
Internal convective coefficient(X2)	5397.73	1.00	5397.73	44.84	0.09
Pressure coefficient(X3)	1465.84	1.00	1465.84	12.18	0.18
X1*X2	10909.07	1.00	10909.07	90.63	0.07
X1*X3	10.80	1.00	10.80	0.09	0.81
X2*X3	107.95	1.00	107.95	0.90	0.52
Error	120.37	1.00	120.37		
Total	19234.68	7.00			

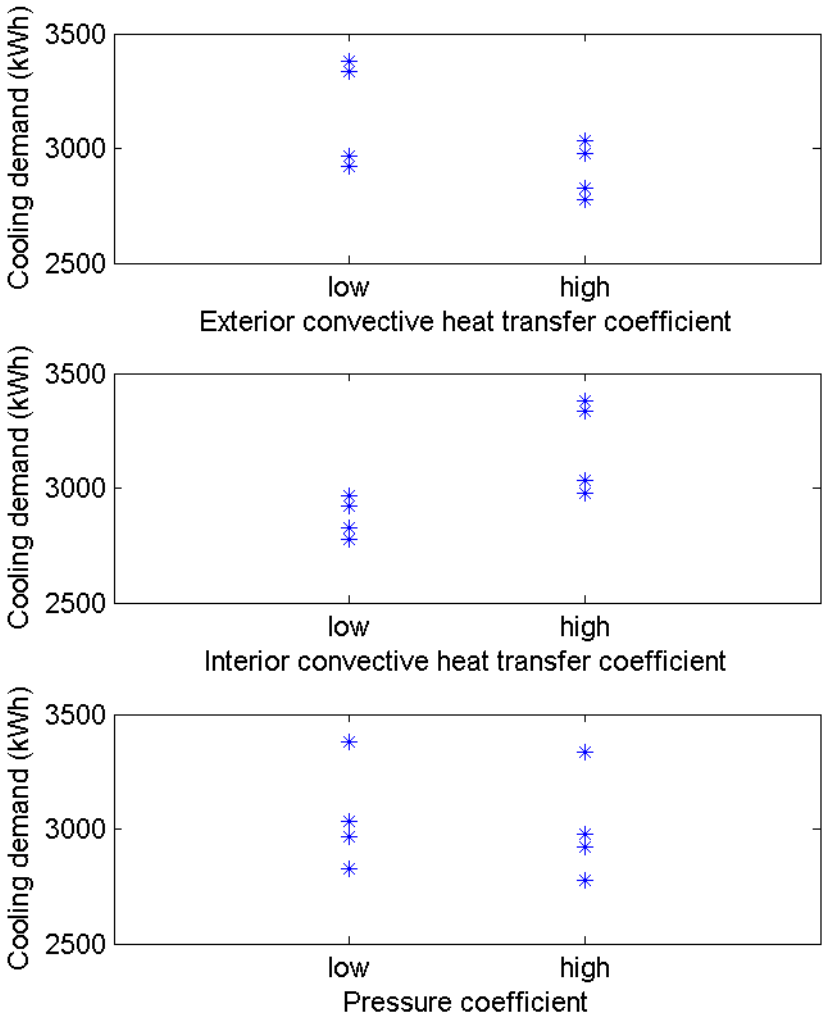

Figure 50. Scatter plots of yearly cooling demand depending on the parameters studied

Table 16. ANOVA analysis results for cooling demand

Source	Sum Sq.	d.f.	Mean Sq.	F	Prob>F
External convective coefficient(X1)	122786.07	1.00	122786.07	59715.79	0.0026
Internal convective coefficient(X2)	192959.57	1.00	192959.57	93843.98	0.0021
Pressure coefficient(X3)	5017.13	1.00	5017.13	2440.03	0.0129
X1*X2	21203.25	1.00	21203.25	10311.99	0.0063
X1*X3	38.71	1.00	38.71	18.83	0.1442
X2*X3	12.35	1.00	12.35	6.01	0.2466
Error	2.06	1.00	2.06		
Total	342019.13	7.00			

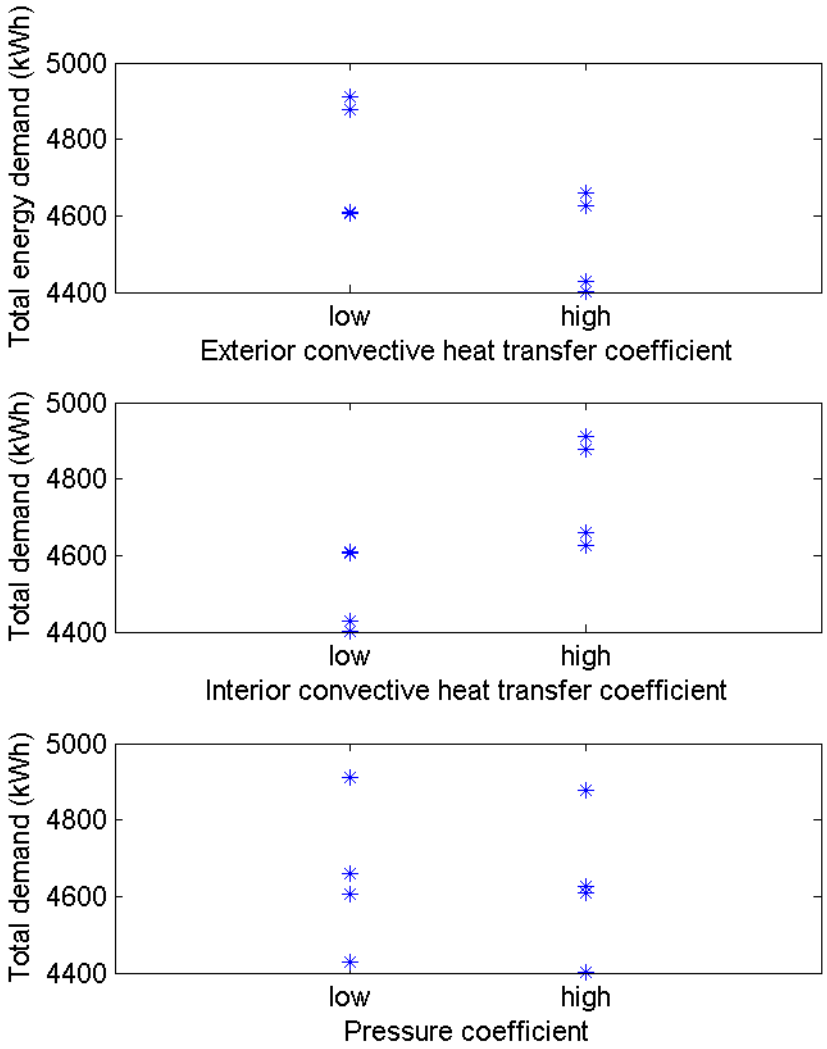

Figure 51. Scatter plots of yearly total energy demand depending on the parameters studied

Table 17. ANOVA analysis results for total energy demand

Source	Sum Sq.	d.f.	Mean Sq.	F	Prob>F
External convective coefficient(X1)	99501.23	1.00	99501.23	1093.86	0.0192
Internal convective coefficient(X2)	133811.39	1.00	133811.39	1471.05	0.0166
Pressure coefficient(X3)	1059.20	1.00	1059.20	11.64	0.1815
X1*X2	1694.71	1.00	1694.71	18.63	0.1449
X1*X3	90.41	1.00	90.41	0.99	0.5010
X2*X3	193.33	1.00	193.33	2.13	0.3827
Error	90.96	1.00	90.96		
Total	236441.24	7.00			

Average room temperature in the non occupancy period

The average temperature of the air in the studied zone during the non occupancy periods gives a measure of the thermal load reduction that is achived ventilating when the weather conditions are favourable. In this section the resultant values of the room average temperature in the non occupancy period are analyzed. To prevent the summer and winter average temperature to balance each other, they are represented separately.

The average room temperature rose no more than 1.5 ºC when the external convection heat transfer coefficient level changed from low to high. During the non occupancy periods the outdoor temperatures were greater than the indoor temperatures for long periods. This means the heat transfer direction was from outdoor to indoor. A greater external convection heat transfer coefficients then means that heat transfer was enhanced, and the temperature rose, Figure 52. In the night time the indoor-outdoor temperature difference was negative and the heat transfer direction it to outdoor, and thus the indoor temperature decreased. However the external convection coefficients tended to be greater during the day, as it was when the wind speed is higher. The global effect was to raise slightly the room temperature. It has to be taken into account that the external convection coefficient affects calculation of heat transfer through the part of the façade without OVF and through the window panes.

The effect on the cooling load was the opposite. During part of the non occupancy periods the exterior temperature was lower than the interior temperature, for example, at night, and the heat transfer was to outdoor. Rising the external convection coefficient had the effect of improving the heat transfer and the room temperature decreased. However, in the non occupancy periods the external temperature was also high at times which made the heat gains to rise either. The global result was found to be

favourable to an average decrease of temperatures, but the variation was even smaller than for the summer case (no more than 0.5 ºC).

The increase in the internal convection heat transfer coefficient in the winter made that, in the non occupancy periods and when the indoor-outdoor temperature difference was positive, the heat losses through the façade were higher. In this case the heat gains did not compensate the heat loss when the indoor-outdoor temperature difference was negative. In the summer the room temperature rose for the same reason. The heat transfer during the non occupancy period had a greater effect than the heat transfer to the outdoor, when the temperature difference becomes negative. The temperature variation was small as it can be seen in Figure 52 Figure 53. The effect of the pressure coefficient was not significative.

ANOVA analysis, Table 18 Table 19, quantified the temperature variation when changing the studied parameters. The analysis confirmed that the room average temperature variation was negligible. Therefore, variations in the estimated parameters does not seriously affect the calculation of room temperature.

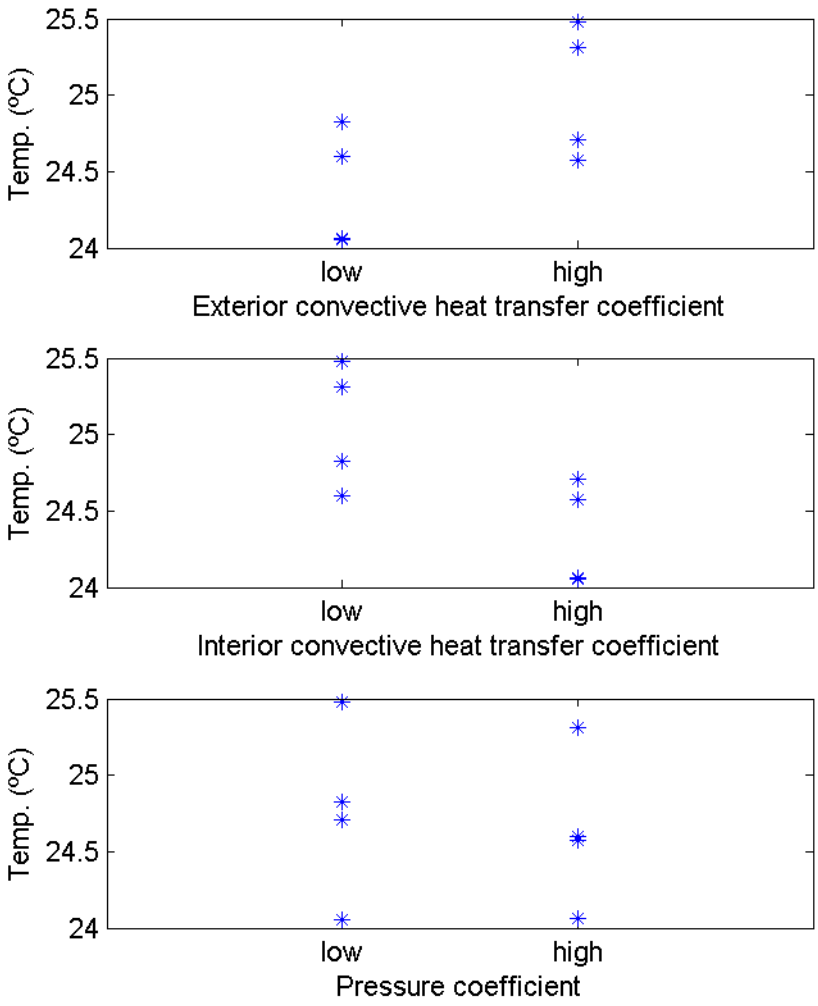

Figure 52. Scatter plots of winter mean temperature of the room depending on the parameters studied

Table 18. ANOVA analysis results for averaged room temperature in the no occupancy period during winter.

Source	Sum Sq.	d.f.	Mean Sq.	F	Prob>F
External convective coefficient(X1)	0.81	1.00	0.81	168.02	0.0490
Internal convective coefficient(X2)	1.00	1.00	1.00	207.01	0.0442
Pressure coefficient(X3)	0.03	1.00	0.03	7.23	0.2266
X1*X2	0.00	1.00	0.00	1.04	0.4945
X1*X3	0.00	1.00	0.00	0.21	0.7262
X2*X3	0.01	1.00	0.01	1.77	0.4103
Error	0.00	1.00	0.00		
Total	1.86	7.00			

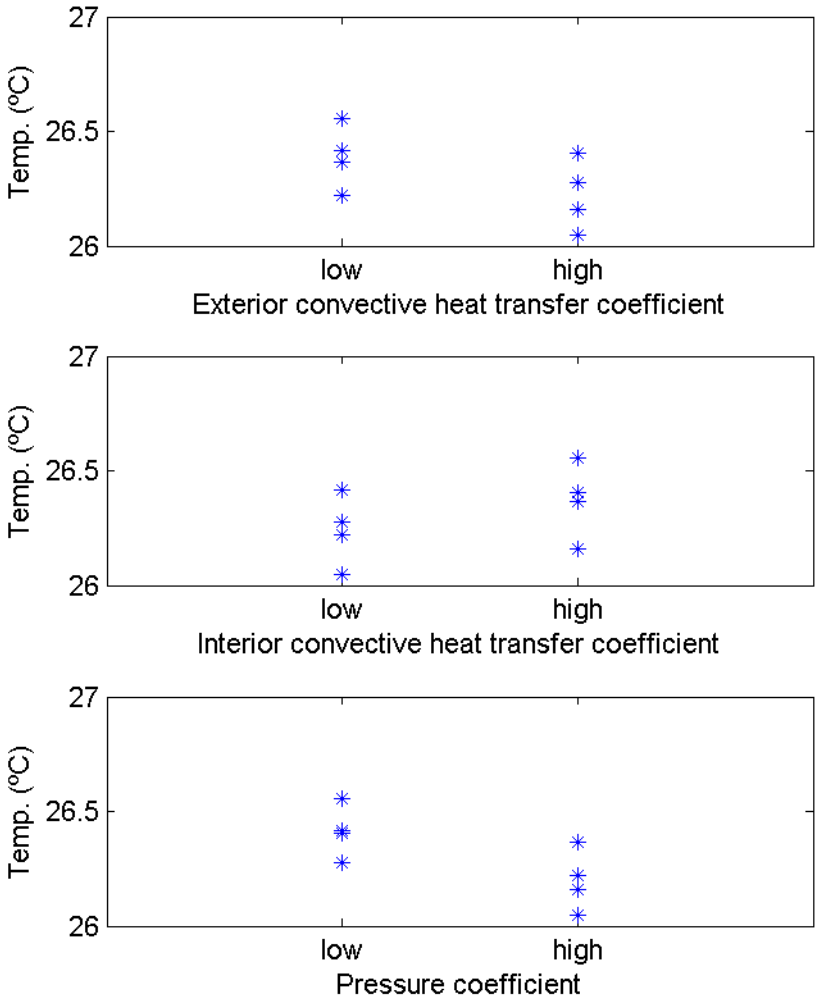

Figure 53. Scatter plots of summer mean temperature of the room depending on the parameters studied.

Table 19. ANOVA analysis results for averaged room temperature in the no occupancy period during summer.

Source	Sum Sq.	d.f.	Mean Sq.	F	Prob>F
External convective coefficient(X1)	0.06	1.00	0.06	656.91	0.0248
Internal convective coefficient(X2)	0.03	1.00	0.03	389.18	0.0322
Pressure coefficient(X3)	0.09	1.00	0.09	1068.80	0.0195
X1*X2	0.00	1.00	0.00	2.55	0.3560
X1*X3	0.00	1.00	0.00	11.89	0.1797
X2*X3	0.00	1.00	0.00	0.41	0.6375
Error	0.00	1.00	0.00		
Total	0.18	7.00			

Ventilation flow rate during the non occupancy period

In this section the effect of the estimated parameters on the ventilation flow rate during the non occupancy period is studied. The ventilation flow rate in the non occupancy periods is a measure of the free heating and free cooling that can be obtained during the day in the winter and during the night in the summer, respectively.

The effect of both external and internal convective coefficients in this case was found negligible, see Figure 54. The flow rate was mainly affected by the wind pressure coefficient. A high pressure coefficient means a greater flow rate for the same wind pressure on the OVF inlet. Therefore a correct estimation of the pressure coefficient is needed to obtain an acceptable approximation to the real natural ventilation flow rates. In the ANOVA analysis, Table 20, the variability of the flow rate was explained mainly by the pressure coefficient. It can also be observed that the external convection heat transfer coefficient had a greater influence than the internal convection coefficient. In other words, the heat losses to the ambient had a greater influence in the air flow rate than the heat transfer to the air inside the OVF.

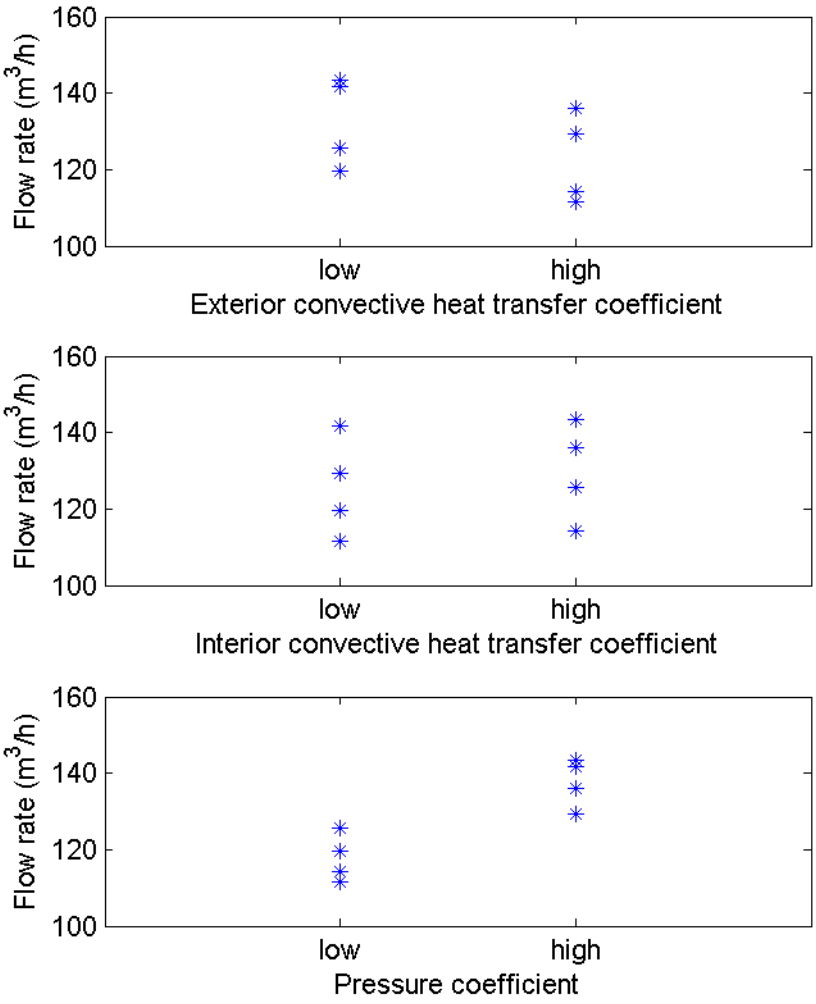

Figure 54. Scatter plots of summer averaged air flow rates depending on the parameters studied

Table 20. ANOVA analysis results for averaged flow rate in the no occupancy period.

Source	Sum Sq.	d.f.	Mean Sq.	F	Prob>F
X1	193.82	1.00	193.82	22.5272	0.13
X2	35.41	1.00	35.41	4.1154	0.29
X3	799.05	1.00	799.05	92.8714	0.07
X1*X2	0.49	1.00	0.49	0.0568	0.85
X1*X3	0.00	1.00	0.00	0.0000	1.00
X2*X3	0.03	1.00	0.03	0.0037	0.96
Error	8.60	1.00	8.60		
Total	1037.41	7.00			

Temperature increase of the air flow rate inside the OVF

The results of the sensitivity analysis of the estimated parameters on the increase of the temperature of the air flowing through the OVF when the inner opening is open and the OVF is in natural ventilation mode are now analized. This temperature increase is related to the additional heat provided by the OVF in the winter and with the additional heat loads that the free cooling suffers in the summer. The natural ventilation mode was established during the non occupancy period

The temperature increase was mainly affected by the internal and external convection heat transfer coefficients, Figure 55, Figure 56. The pressure coeffcient did not have any noticeable effect on this temperature increase, as it can be seen in the ANOVA analysis, Table 21.

During the winter season, Figure 55, a high external convection heat transfer coefficient means that more heat is transferred from the exterior layer of the OVF to the ambient air, so the temperature increase of the air inside the air gap decreased. The internal convection heat transfer coefficient had the opposite effect. A high internal convection heat transfer coefficient made more heat be transferred to the air flow through the OVF, thus raising the temperature increase. As deduced from the correspondent ANOVA analysis, the effect of the external convection heat transfer coefficient was greater than that of the internal convection coefficient, Table 21. During the summer the same behavior was observed, Figure 56, though the effect on the temperature increase was lower, Table 22. This could be due to the fact the in the summer the ventilation normally takes place with low temperature air, usually at night or in the early morning, so a big temperature increase was not expected. The effect of the convective coefficients was not expected to influence much the temperature increase.

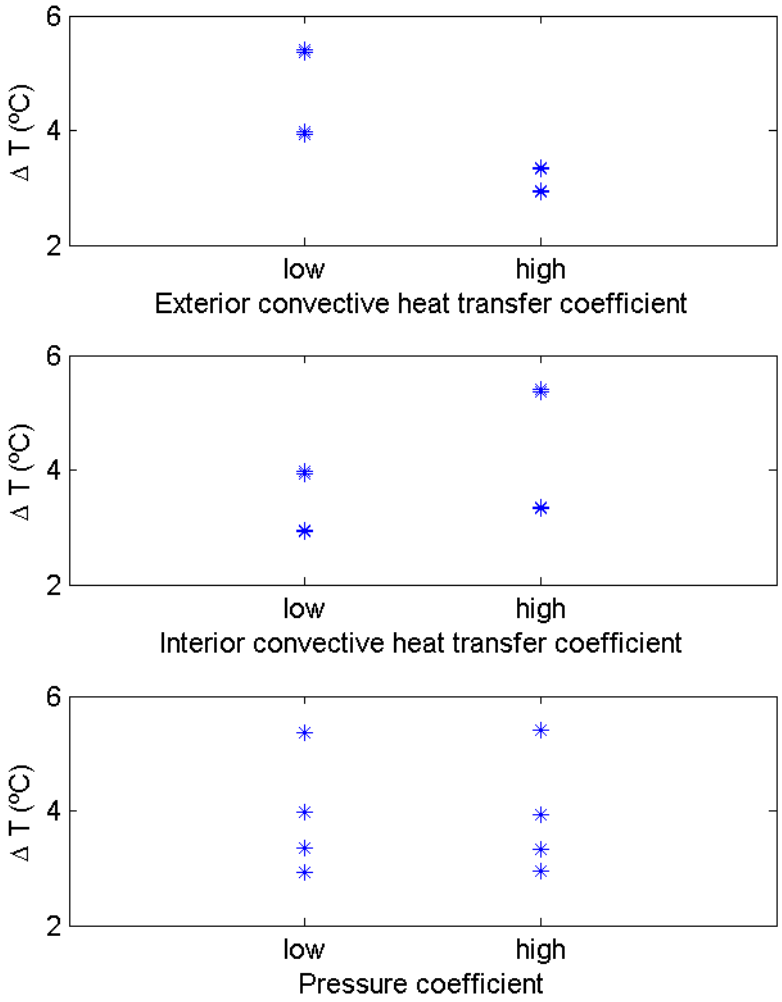

Figure 55. Scatter plots of winter averaged temperature rise in the OVF depending on the parameters studied

Table 21. ANOVA analysis results for averaged temperature rise in the OVF in the no occupancy period in winter.

Source	Sum Sq.	d.f.	Mean Sq.	F	Prob>F
External convective coefficient(X1)	4.67	1.00	4.67	3828.6994	0.0103
Internal convective coefficient(X2)	1.68	1.00	1.68	1376.6466	0.0172
Pressure coefficient(X3)	0.00	1.00	0.00	0.0017	0.9739
X1*X2	0.54	1.00	0.54	442.6525	0.0302
X1*X3	0.00	1.00	0.00	0.0865	0.8179
X2*X3	0.00	1.00	0.00	0.2877	0.6866
Error	0.00	1.00	0.00		
Total	6.89	7.00			

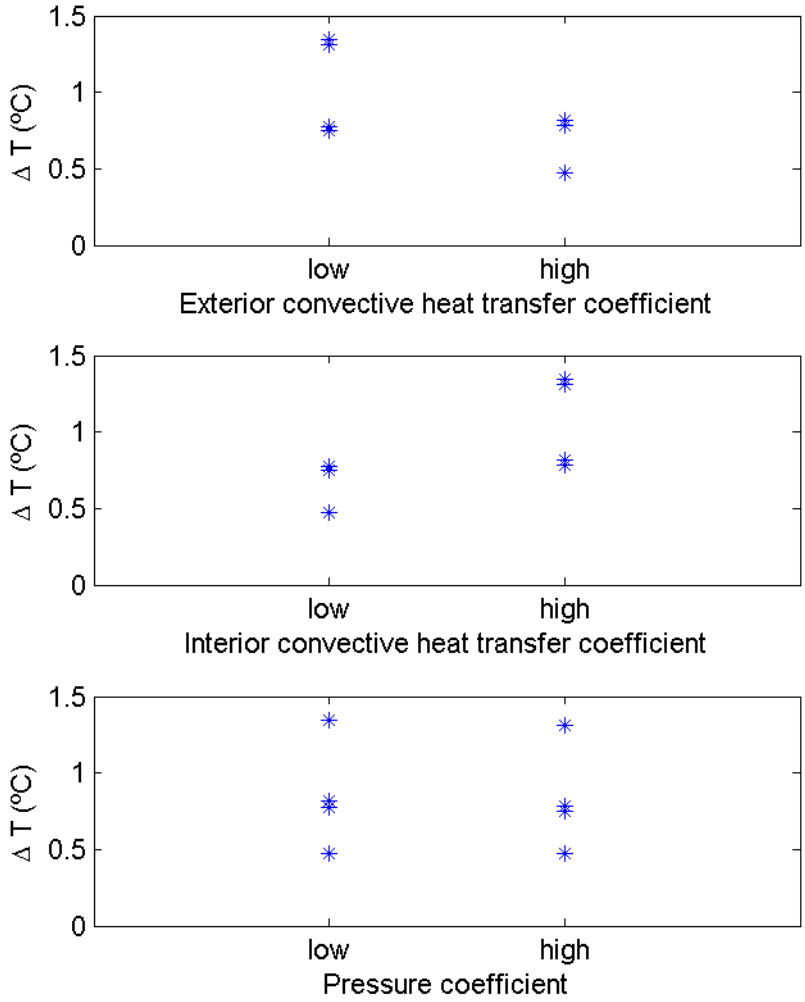

Figure 56. Scatter plots of summer averaged temperature rise in the OVF depending on the parameters studied

Table 22. ANOVA analysis results for averaged temperature rise in the OVF in the no occupancy period in summer.

Source	Sum Sq.	d.f.	Mean Sq.	F	Prob>F
External convective coefficient(X1)	0.34	1.00	0.34	3204.5922	0.0112
Internal convective coefficient(X2)	0.40	1.00	0.40	3808.6008	0.0103
Pressure coefficient(X3)	0.00	1.00	0.00	8.7003	0.2081
X1*X2	0.03	1.00	0.03	266.4886	0.0389
X1*X3	0.00	1.00	0.00	1.4063	0.4460
X2*X3	0.00	1.00	0.00	0.9326	0.5111
Error	0.00	1.00	0.00		
Total	0.76	7.00			

In summary, the results indicated that both internal and external convection heat transfer coefficients have an noticeable impact on the simulation outputs when using a OVF. From the energy saving point of view the convection heat transfer coefficients are the parameters that have a greater effect on the heating, and cooling demand. The pressure coefficient affects mainly the ventilation flow rate through the OVF, which affects indirectly the heating and cooling demands. Convection heat transfer coefficients are difficult to estímate parameters as they are a function of many variables: velocity field, boundary layer temperature field, flow regime,etc. Since the energy savings due to the preheating of air inside the façade is not too high, a poor estimation of these parameters could lead to a high uncertainty in the model predictions. Therefore, these parameters should be measured or calculated in conditions similar to the real situation.

4.3.4 SENSITIVITY ANALYSIS OF DESIGN PARAMETERS

In this section the results of the sensitivity analysis of the basic design parameters on the model outputs is presented. There were two parameters analysed: the global heat transfer coefficient of the insulation layer of the OVF and the absortivity of the external surface of the steel plate layer of the OVF. For this study the cases were those presented in Table 11. The results are presented as scatter plots and the ANOVA results are also presented in this section.

Heating demand

In Figure 57 the variation of the heating demand as a function of the insulation and abosortivity levels is shown. The heating demand was mainly affected by solar absortivity. The more radiation was absorbed by the steel plate, the more heat was transferred to the ventilation air, so the ventilation heat load decreased. At the same time, a better insulation also lowered the heating demand, though in a slightly way. The

results from the ANOVA analysis, Table 23, shows that the solar absortivity accounted for 80% of the variability of the heating demand.

The impact of the absortivity on the cooling demand in the summer was more noticeable, whereas the effect of the insulation was negligible respect to the former, Figure 58 Table 24. The effect of raising the solar absortivity was equal to rise the cooling load and thus the cooling demand. In the summer, solar radiation was greater and the solar absortivity implied an important increase on the thermal load. The insulation level had no appreciable effect on the variation of the energy demand in the summer.

The effect of solar absortivity on the cooling energy demand has a bigger impact on the total energy demand, and therefore a high solar absortivity reduces the energy savings per year. Thus, ventilating through the OVF in the summer must be avoided, using other channels to introduce fresh air in the building that do not imply a preheat process.

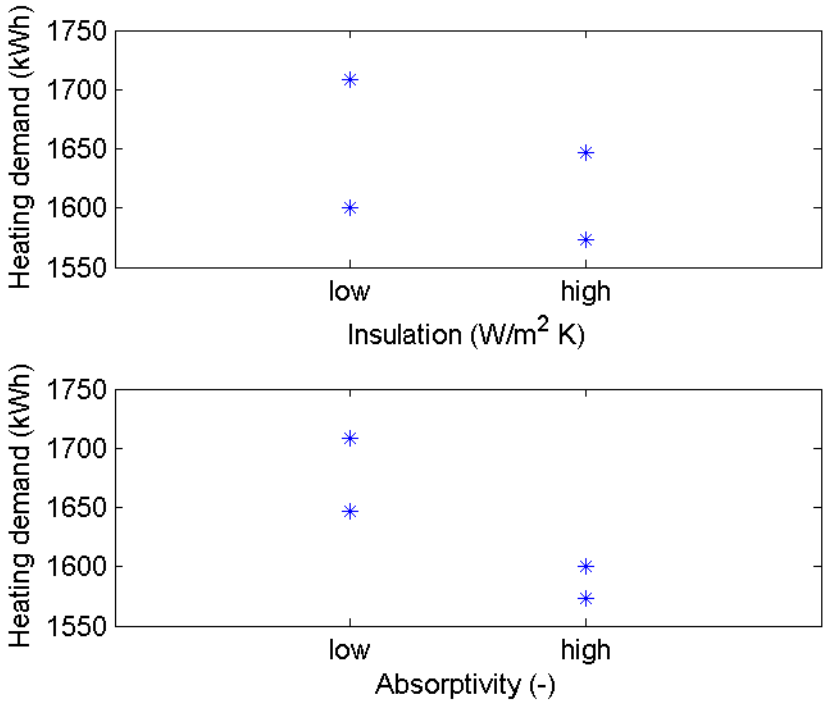

Figure 57. Scatter plots of yearly heating demand depending on the parameters studied

Table 23. ANOVA analysis results for heating demand

Source	Sum Sq.	d.f.	Mean Sq.	F	Prob>F
Insultation (X1)	2008.78	1.00	2008.78	6.96	0.2306
Absorptivity (X2)	8198.18	1.00	8198.18	28.41	0.1181
Error	288.52	1.00	288.52		
Total	10495.48	3.00			

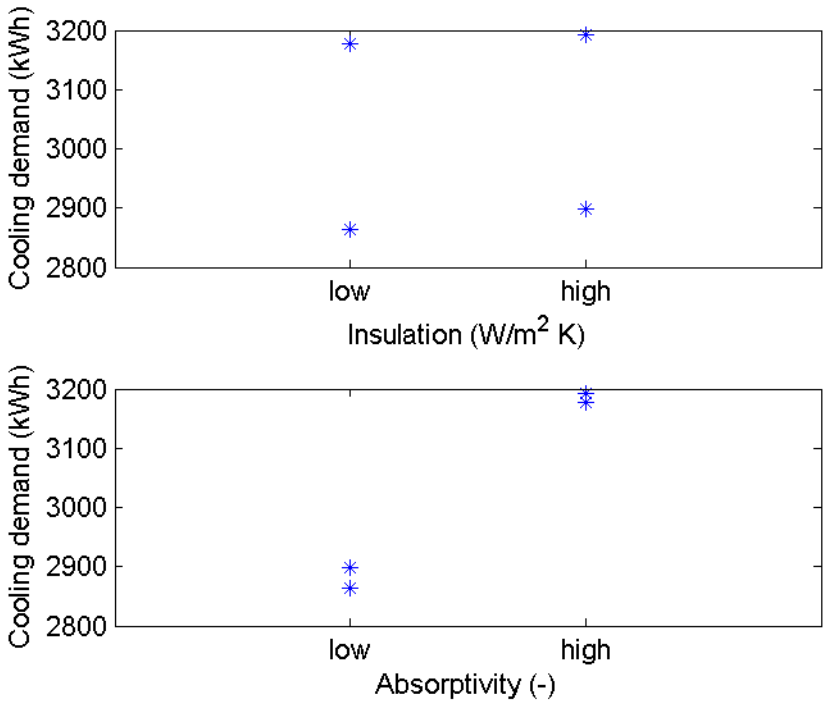

Figure 58. Scatter plots of yearly cooling demand depending on the parameters studied

Table 24. ANOVA analysis results for cooling demand

Source	Sum Sq.	d.f.	Mean Sq.	F	Prob>F
Insultation (X1)	579.51	1.00	579.51	5.77	0.2512
Absorptivity (X2)	91644.00	1.00	91644.00	911.93	0.0211
Error	100.49	1.00	100.49		
Total	92324.00	3.00			

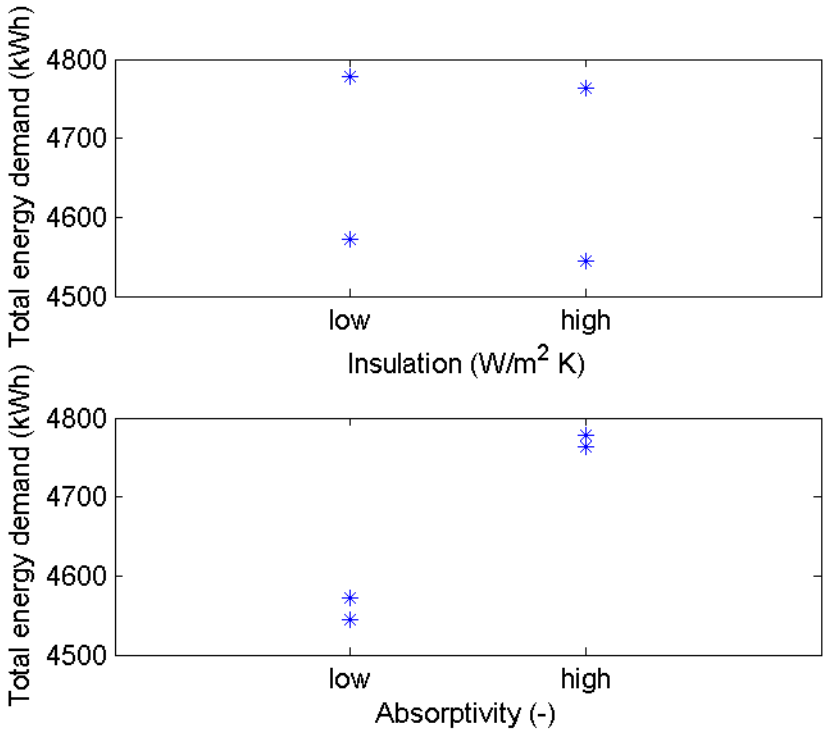

Figure 59. Scatter plots of yearly total energy demand depending on the parameters studied

Table 25. ANOVA analysis results for total energy demand

Source	Sum Sq.	d.f.	Mean Sq.	F	Prob>F
Insultation (X1)	430.41	1.00	430.41	8.8820	0.21
Absorptivity (X2)	45021.96	1.00	45021.96	929.0740	0.02
Error	48.46	1.00	48.46		
Total	45500.83	3.00			

Average room temperature in the non occupancy period

From Table 26 and Table 27 it can be deduced that the impact of the insulation and solar absortivity on the average temperature in the non occupancy period was negiglible. It can be highlighted, however, the fact that a high absortivity was related with lower average room temperatures in the non occupancy period, but the decrease was less than 0.5ºC. This lack of dependence could be due to the fact that the incoming energy in the ventilation air was a consecuence of the outdoor-indoor temperature difference rather than the energy absorbed from the OVF steel plate layer.

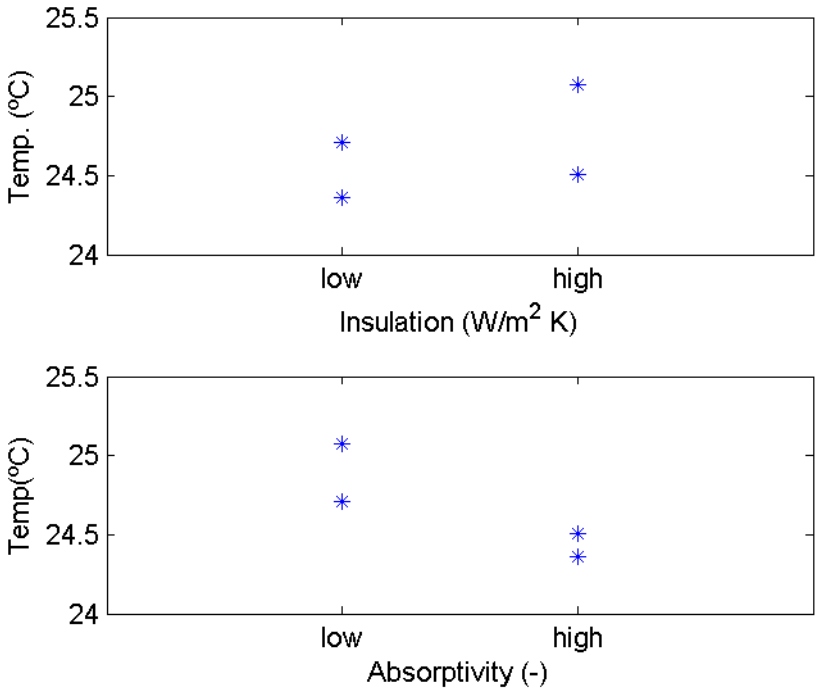

Figure 60. Scatter plots of winter mean temperature of the room depending on the parameters studied.

Table 26. ANOVA analysis results for averaged room temperature in the no occupancy period during winter.

Source	Sum Sq.	d.f.	Mean Sq.	F	Prob>F
Insultation (X1)	0.06	1.00	0.06	5.5619	0.26
Absorptivity (X2)	0.21	1.00	0.21	18.0958	0.15
Error	0.01	1.00	0.01		
Total	0.28	3.00			

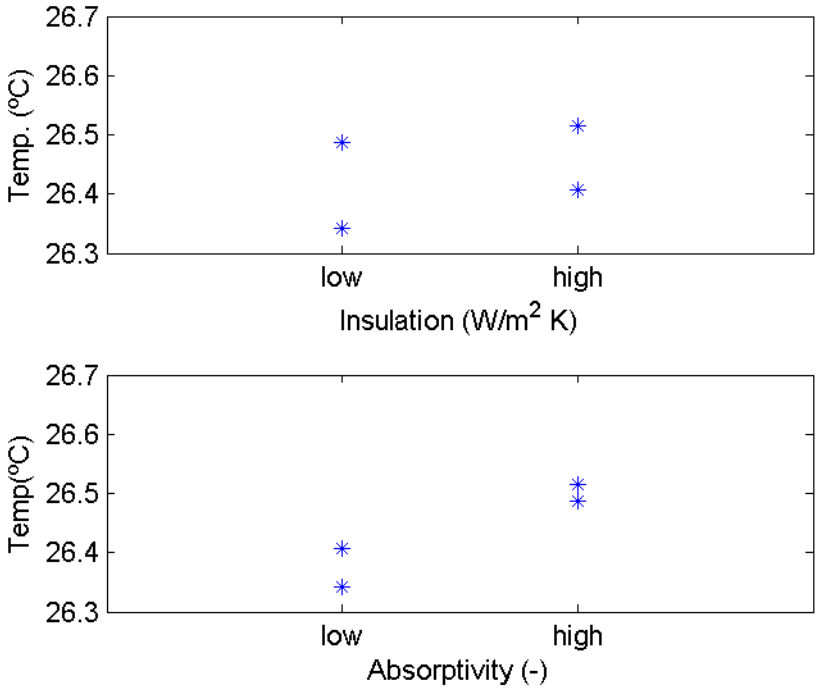

Figure 61. Scatter plots of summer mean temperature of the room depending on the parameters studied.

Table 27. ANOVA analysis results for averaged room temperature in the no occupancy period during summer.

Source	Sum Sq.	d.f.	Mean Sq.	F	Prob>F
Insultation (X1)	0.00	1.00	0.00	5.72	0.2522
Absorptivity (X2)	0.02	1.00	0.02	43.89	0.0954
Error	0.00	1.00	0.00		
Total	0.02	3.00			

Ventilation flow rate during the non occupancy period

In Figure 62 it can be observed that the insulation level had a negligible impact on the ventilation flow rate in the non occupancy period. However, solar absortivity had an important impact. This impact was due to the fact that a high absortivity is related with more energy introduced in the room, and the hotter the air in the room the greater the stack effect and the greater flow rate. This effect was positive in the winter, whereas it had a negative effect on the cooling energy demand as it was pointed out before.

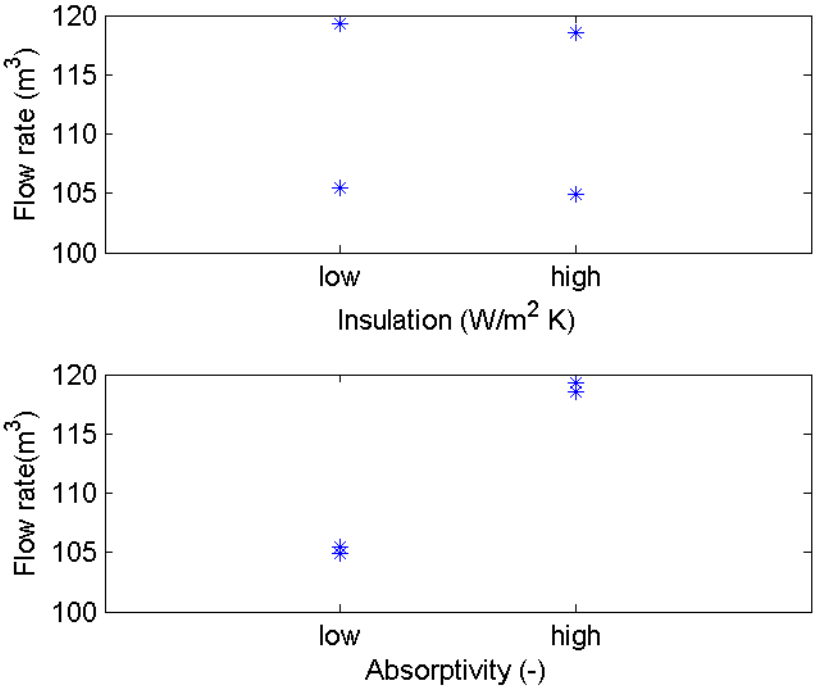

Figure 62. Scatter plots averaged air flow rates depending on the parameters studied

Table 28. ANOVA analysis results for averaged flow rate in the no occupancy period.

Source	Sum Sq.	d.f.	Mean Sq.	F	Prob>F
Insultation (X1)	0.43	1.00	0.43	197.28	0.0452
Absorptivity (X2)	189.22	1.00	189.22	86059.37	0.0022
Error	0.00	1.00	0.00		
Total	189.65	3.00			

Temperature increase of the air flow rate inside the OVF

In Figure 63 it can be observed that solar absortivity had an important impact on the temperature increase of the air flow going in the room in the non occupancy period during the winter. However, the insulation level had no apreciable effect. Heat absorption and transfer from the external steel plate layer is key for the preheating of the ventilation air, as it was highlighted previously.

During the summer the ventilation strategy consisted in introducing air at the lowest temperature possible during the night and early morning. This made none of the

parameters studied had a major effect on the heating of the ventilation air. Although a clear increase in the air temeperature can be observed, the value of this increment was very low, less than 0.3ºC.

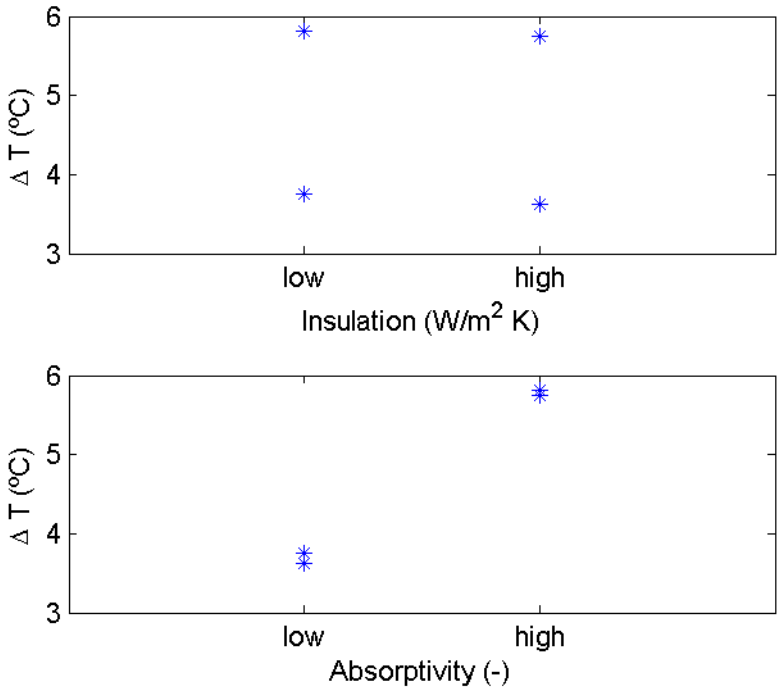

Figure 63. Scatter plots of winter averaged temperature rise in the OVF depending on the parameters studied

Table 29. ANOVA analysis results for averaged temperature rise in the OVF in the no occupancy period in winter.

Source	Sum Sq.	d.f.	Mean Sq.	F	Prob>F
Insultation (X1)	0.01	1.00	0.01	13.70	0.1680
Absorptivity (X2)	4.39	1.00	4.39	6816.47	0.0077
Error	0.00	1.00	0.00		
Total	4.40	3.00			

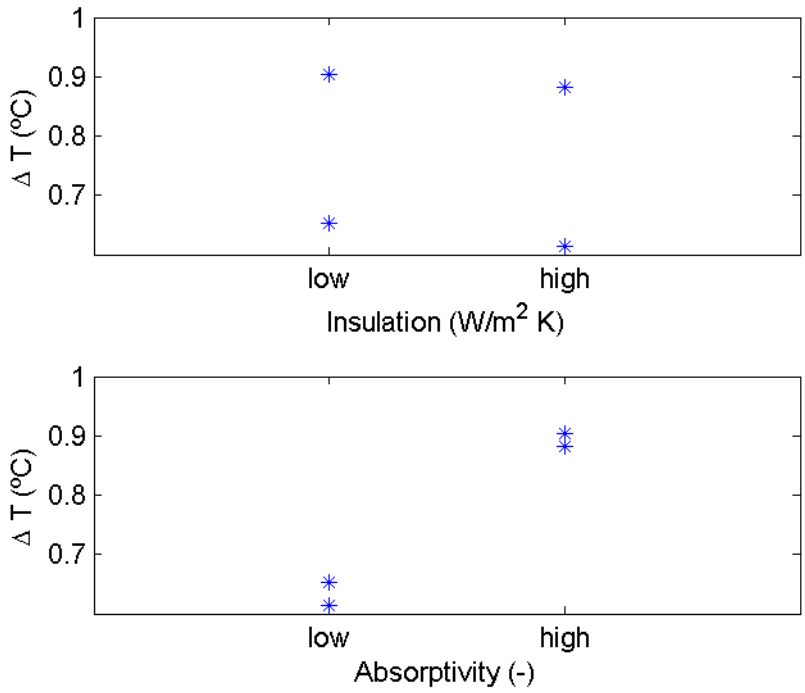

Figure 64. Scatter plots of summer averaged temperature rise in the OVF depending on the parameters studied

Table 30. ANOVA analysis results for averaged temperature rise in the OVF in the no occupancy period in summer.

Source	Sum Sq.	d.f.	Mean Sq.	F	Prob>F
Insultation (X1)	0.00	1.00	0.00	13.50	0.1691
Absorptivity (X2)	0.07	1.00	0.07	1003.57	0.0201
Error	0.00	1.00	0.00		
Total	0.07	3.00			

As a conclusión it can be said that the basic design of an OVF the insulation level is not a determinant parameter regarding energy consumption, although a better insulation would improve the total energy demand slightly. The insulation lowers mainly the heating demand. In the summer the insulation does nt play an important role in the cooling demand. The solar absortivity of the external surface of the OVF is shown key parameter for reducing the heating load in the winter, whereas it was found

counterproductive in the summer. The capacity of heating the ventilation air depends on the solar absortivity. It would be necessary to built two different ventilation channels: one for the summertime and other for the cold season, making it pass through the OVF. Furthermore, a high absortivity improves the natural ventilation during the non occupancy period, thus improving even more the heating savings.

Therefore the basic design should include a good insulation layer and a high absortivity external layer. The ratio of solar absortivity to long wave emissivity should be high too. Another opening should be made on the facade to by-pass the OVF when ventilating in the hot season.

It has to be pointed out that the internal load in the building used in this study is very high (35 people). That means any other thermal load could result of lower importance in comparison with it. So the variation of these parameters could be of greater importance in other kind of building use.

4.4 CONCLUSIONS

In this section a control system for an OVF was designed with mechanical ventilation air passing through the air gap during the occupation period. This was found convenient in the winter but not in the summer. The rest of the time the OVF opens or closes for natural ventilation depending on the external conditions. This allows the OVF to smooth indoor temperatures, thus reducing the heating or cooling energy consumption the next day.

In the estimated parameter study it was found that convection coefficients had greater impact on the energy consumption than the pressure coefficient. The pressure

coefficients affects indirectly the energy consumption through the air flow rate in natural ventilation.

The level of insulation of the inner layer of the OVF was found not to be determinant, whereas the absortivity of the outer surfaces was found to be a key parameter for preheating the ventilation air and reducing the heating energy consumption. It could also increase the cooling energy demand if the ventilation air flows through the OVF in the summer period.

From the design parameters study it was concluded that for a basic desing the OVF shoud include a proper insulation layer and an external layer with an outer surface with high solar absortivity and low long wave emissivity.

5. CONCLUSIONS AND FUTURE WORK

The main objectives of this study were proving that an OVF can meet the requirements of ventilation of a building and if any energy savings can be obtained by using an OVF in different operation modes. Also, the performance of an OVF under different climatic conditions and the sensitivity of the system to some of the most important paramenters were other goals to achieve.

For this purpose, two field experiences were carried out. The first one using a PASLINK test cell with a module of OVF installed on one of its sides and using constant flow rate mechanical ventilation. The second one was an OVF module installed on the façade of a real building and operating in natural ventilation mode. In both experiments the façade operated under real weather conditions, which were measured with the corresponding meteorological sensors. The experimental modules were outfitted with the necessary equipment for monitorizing the themal and air flow variables needed for the study of their performance. The recorded data was post processed and analyzed, and the results were discussed.

From these data, the dependency of the discharge coefficient of an OVF on the different driving forces was studied. It was an attempt to quatify with a single factor the ventilation that can be achieved with an OVF as a function of the weather conditions and other factors. However, it was found further research would be needed to achieve this goal with enough accuracy.

Also, in order to assess the performance of an OVF under other conditions that weren’t easy to get experimentally, a numerical model of the OVF was created and validated according to the experimental data. Sets of simulations using the model of a

real secondary school builing were carried out and the output data were post processed and analyzed conveniently. A basic control system was established from the simulations results. The performance of the OVF in different climatic zones and the sensitivity of the model to the variation of estimated and design parameters was realized and analized.

The results of this work yielded that an OVF could provide buildings with some natural ventilation independently of their climatic zone. However the volume of ventilation air achieved was not enough to meet the requirements of the local regulations in none of the cases, and thus mechanical ventilation was needed for this purpose. Natural ventilation can support the mechcanical ventilation system. The main ventilation driving forces were the wind pressure, the stack effect in the building and the buoyancy of air inside the OVF air gap.

The discharge coefficient relates the pressure difference between the intlet and outlet openings. It was found that the discharge coefficient depends on the temperature difference between outdoor and indoor and on the temperature of the air inside the OVF. Therefore the discharge coefficient could be use a a parameter to characterized an OVF design, but still the results weren't conclusive and more accurate data are needed.

The pressure coefficient was found a determinant parameter for the case of wind driving force prevalency. The urban environment and the height at which the inlet façade opening was located were the most influential external parameters for the pressure coefficient. It was also found that the buoyancy due to the temperature difference between the air inside the façade and the ambient air could be negligible respect to wind forces or the stack effect of the whole building. In the exhaust operation mode, i.e. the PASLINK experiment, wind forces and buoyancy inside the OVF were

found the main driving forces. However, in the case of the façade installed on a real building and in the secondary school building simulations they were wind forces and the building stack effect.

The results showed that the heating energy consumption could be reduced through two effects. The first effect was the reduction of the heating demand due to the preheating of ventilation air in the OVF in the occupancy periods. Air temperature rises of around 10ºC were found. The second one was the ventilation thorugh the OVF with air at a convenient temperature. This temperature has to be set previously in the control system. Cooling energy savings could also be achieved by natural ventilation at low temperatures. In these cases the OVF didn't play a key role. However ventilation through the OVF with hot weather was found to be counterproductive for reducing the cooling energy consumption.

There weren't found major differences in the performance of the OVF in the different climatic zones studied. Preheating of ventilation air during the winter reduced the heating load around 6%. Lower winter severity climates showed slightly greater heating load reductions. In the summer, ventilation of the room through the OVF is not recommended as it worsens the cooling energy demand.

It can be concluded from the sensitivity analysis that the external and internal convection heat transfer coefficient should be well estimated as they influence importantly the energy demand simulated. The pressure coefficient was also found an important parameter for the prediction of the air flow rate, but its influence depends on the prevalency of the wind driving force. The absortivity of the external layer was found a key parameter for absorbing the solar radiation and transfer it to the ventilation air. The insulation level of the façade was not found essential for the thermal performance

of the façade although this could be due to the high internal thermal loads present in the study.

Future work

The analsys of the performance of an OVF is a complicated matter. In the heated air cavity the fluid dynamics and heat transfer problems are strongly coupled, especially when buoyancy forces are significant. Moreover, buildings are exposed to the variation of wind and solar radiation, which are variables highly unpredictable and that also vary along the year and from one year to the next. Many studies could be carried out to try to understand deeply the performance of OVF's and to obtain trustworthy energy saving figures. Among these studies, the following are proposed:

- A more extensive monitorization campaing should be done in order to evaluate the sensitivity of the system to the variation of other design parameters. This would also allow to validate a more exhaustive numerical model.
- A more precise study about the dependency of the discharge coefficient could be done in a more controlled environment to isolate conviently each driving force.
- A detailed study of the flow regime inside the façade. A CFD study of the velocity field with different air cavity dimensions and aspect ratios would give useful information about the convection heat transfer coefficients.
- In a more macroscopic way, a comparative study about the heating and cooling demand of two identical rooms with and without OVF would yield more realistic energy saving results.
- A study of the ventilation energy savings by monitorizing the energy consumption of the ventilation system.

- The energy savings for other types of buildings with other types of activities should be researched, as internal loads play an important role in the thermal behavior of buildings.

ACKNOWLEDGEMENTS

The present study has been realized within the Spanish National Plan for R+D: “Integration of constructive systems of active ventilated facades for ensuring efficient energy consumption and indoor air quality. Implementation on non-residential buildings”, Ref. BIA2006-15398-C04-04, Ministry for Science and Education, Government of Spain.

The PASLINK cell test were carried out thanks the Building Quality Control Laboratory of the Vasque Country Government in Vitoria (Spain).

The measurements on the experimental module of OVF were possible thanks to the Indoor Environmental Engineering Laboratory of the Department of Civil Engineering of the Aalborg University.

REFERENCES

[1] PEREZ-LOMBARD, L.; ORTIZ, J.; POUT, C. A review on buildings energy consumption information. **Energy and Buildings,** v. 40, n. 3, p. 394-398, 2008 2008. ISSN 0378-7788. Disponível em: < <Go to ISI>://WOS:000252604700026 >.
[2] DIRECTIVA 2002/91/CE del Parlamento Europeo y del Consejo de 16 de Diciembre de 2002, Relativa a la Eficiencia Energética de los Edificios. (2002).
[3] Transport, D.G. f. (2009). EU energy and transport in figures. Pocketbook 2009.
[4] US DEPARTMENT OF ENERGY, Energy & Renewable Energy (2006). *BUILDINGS ENERGY DATABOOK*
[5] REAL DECRETO 314/2006, de 17 de marzo, por el que se aprueba el Código Técnico de la Edificación.
[6] B.F. Yu, Z. H. (2009). Review of research on air-conditioning systems and indoor air quality contrl for human health. International Journal of Refrigeration , 32, 3-20.
[7] Saelens, D. (2002) Energy performance assessment of single Storey multiple-skin facades. PhD. Thesis. Katholic Universiteit Leuven
[8] Loncour X, Deneyer A, Blasco M, Flamant G, Wouters P. Ventilated Double Facades. Belgian Building Research Institute Department of Building Physics, Indoor Climate & Building Services; 2004.
[9] Kim YM, Kim SY, Shin SW, Sohn JY. Contribution of natural ventilation in a double skin envelope to heating load reduction in winter. Building and Environment. 2009;44:2236-44.
[10] Gratia E, De Herde A. Greenhouse effect in double-skin facade. Energy and Buildings. 2007;39:199-211.
[11] Marinosci C, Strachan PA, Semprini G, Morini GL. Empirical validation and modelling of a naturally ventilated rainscreen facade building. Energy and Buildings. 2011;43:853-63.
[12] Mingotti N, Chenvidyakarn T, Woods AW. The fluid mechanics of the natural ventilation of a narrow-cavity double-skin facade. Building and Environment. 2011;46:807-23.
[13] Mei L, Infield D, Eicker U, Fux V. Thermal modelling of a building with an integrated ventilated PV facade. Energy and Buildings. 2003;35:605-17.
[14] Patania F, Gagliano A, Nocera F, Ferlito A, Galesi A. Thermofluid-dynamic analysis of ventilated facades. Energy and Buildings. 2010;42:1148-55.
[15] WOUTERS, P. et al. THE USE OF OUTDOOR TEST CELLS FOR THERMAL AND SOLAR BUILDING RESEARCH WITHIN THE PASSYS PROJECT. Building and Environment, v. 28, n. 2, p. 107-113, Apr 1993. ISSN 0360-1323. Disponível em: < <Go to ISI>://WOS:A1993LG71900002 >.
[16] ZOLLNER, A.; WINTER, E. R. F.; VISKANTA, R. Experimental studies of combined heat transfer in turbulent mixed convection fluid flows in double-skin-facades. International Journal of Heat and Mass Transfer, v. 45, n. 22, p. 4401-4408, Oct 2002. ISSN 0017-9310. Disponível em: < <Go to ISI>://000177570500002 >.
[17] Kalyanova, Olena ; Zanghirella, Fabio ; Heiselberg, Per ; Perino, Marco ; Jensen, Rasmus Lund. /Measuring Air Temperature in Glazed Ventilated Facades in the Presence of Direct Solar Radiation.I: Proceedings of Roomvent 2007. red. / Olli Seppänen ; Jorma Säteri. FINVAC ry, 2007.
[18] ASHRAE. Airflow Around Buildings. ASHRAE Handbook-Fundamentals 2005. Chap. 16.
[19] Chiu YH, Etheridge DW. External flow effects on the discharge coefficients of two types of ventilation opening. Journal of Wind Engineering and Industrial Aerodynamics. 2007;95:225-52.
[20] Loveday DL, Taki AH. Convective heat transfer coefficients at a plane surface on a full-scale building facade. International Journal of Heat and Mass Transfer. 1996;39:1729-42.
[21] Chiu YH, Etheridge DW. External flow effects on the discharge coefficients of two types of ventilation opening. Journal of Wind Engineering and Industrial Aerodynamics. 2007;95:225-52.
[22] Costola D, Blocken B, Hensen JLM. Overview of pressure coefficient data in building energy simulation and airflow network programs. Building and Environment. 2009;44:2027-36.
[23] KARAVA, P.; STATHOPOULOS, T.; ATHIENIKIS, A. K. Wind Driven Flow through Openings-A Review of Discharge Coefficients. **International Journal of Ventilation,** v. 3, n. 3, p. 12, 2004. ISSN 1473-3315.
[24] HEISELBERG, P.; SANDBERG, M. Evaluation of Discharge Coefficients for Window Openings in Wind Driven Natural Ventilation. **International Journal of Ventilation,** v. 5, n. 1, p. 10, 2006.

[25] ANDERSEN, K. T. Theory for natural ventilation by thermal buoyancy in one zone with uniform temperature. **Building and Environment,** v. 38, n. 11, p. 1281-1289, Nov 2003. ISSN 0360-1323. Disponível em: < <Go to ISI>://000184652100003 >.
[26] LARSEN, T. S.; HEISELBERG, P. Single-sided natural ventilation driven by wind pressure and temperature difference. **Energy and Buildings,** v. 40, n. 6, p. 1031-1040, 2008. ISSN 0378-7788. Disponível em: < <Go to ISI>://000254067500009 >.
[27] CHU, C. R. et al. Turbulence effects on the discharge coefficient and mean flow rate of wind-driven cross-ventilation. **Building and Environment,** v. 44, n. 10, p. 2064-2072, Oct 2009. ISSN 0360-1323. Disponível em: < <Go to ISI>://000266901100007 >.
[28] KARAVA, P.; STATHOPOULOS, T.; ATHIENITIS, A. K. Airflow assessment in cross-ventilated buildings with operable facade elements. **Building and Environment,** v. 46, n. 1, p. 266-279, Jan 2011. ISSN 0360-1323. Disponível em: < <Go to ISI>://000282407600027 >.
[29] CHIU, Y. H.; ETHERIDGE, D. W. External flow effects on the discharge coefficients of two types of ventilation opening. **Journal of Wind Engineering and Industrial Aerodynamics,** v. 95, n. 4, p. 225-252, Apr 2007. ISSN 0167-6105. Disponível em: < <Go to ISI>://000245062200001 >.
[30] COSTOLA, D.; ETHERIDGE, D. W. Unsteady natural ventilation at model scale - Flow reversal and discharge coefficients of a short stack and an orifice. **Building and Environment,** v. 43, n. 9, p. 1491-1506, Sep 2008. ISSN 0360-1323. Disponível em: < <Go to ISI>://000257007900008 >.
[31] ASHRAE. Ventilation and Infiltration. In: (Ed.). **ASHRAE Handbook-Fundamentals**, 2005. cap. 27,
[32] BALDINELLI, G. Double skin facades for warm climate regions: Analysis of a solution with an integrated movable shading system. **Building and Environment,** v. 44, n. 6, p. 1107-1118, Jun 2009. ISSN 0360-1323. Disponível em: < <Go to ISI>://000264310200002 >.
[33] PATANIA, F. et al. Thermofluid-dynamic analysis of ventilated facades. **Energy and Buildings,** v. 42, n. 7, p. 1148-1155, Jul 2010. ISSN 0378-7788. Disponível em: < <Go to ISI>://000278425400023 >.
[34] Incropera FP, Witt DDD, Bergman TL, Lavine AS. Fundamentals of Heat and Mass Transfer: Wiley; 2006.
[35] HEISELBERG, P.; SVIDT, K.; NIELSEN, P. V. Characteristics of airflow from open windows. **Building and Environment,** v. 36, n. 7, p. 859-869, Aug 2001. ISSN 0360-1323. Disponível em: < <Go to ISI>://000169515000009 >.
[36] SAWACHI, T. et al. Wind Pressure and Air Flow in a Full-Scale Building Model under Cross Ventilation. **International Journal of Ventilation,** v. 2, n. 4, 2004.
[37] Jiru TE, Haghighat F. Modeling ventilated double skin facade - A zonal approach. Energy and Buildings. 2008;40:1567-76.
[38] Chan ALS, Chow TT, Fong KF, Lin Z. Investigation on energy performance of double skin facade in Hong Kong. Energy and Buildings. 2009;41:1135-42.
[39] Haase M, da Silva FM, Amato A. Simulation of ventilated facades in hot and humid climates. Energy and Buildings. 2009;41:361-73.
[40] Kim YM, Lee JH, Kim SM, Kim S. Effects of double skin envelopes on natural ventilation and heating loads in office buildings. Energy and Buildings. 2011;43:2118-26.
[41] Solar Energy Laboratory UoW-M, GmbH TE, CSTB, TESS. TRNSYS 16 Reference Manual 2004.
[42] Palyvos JA. A survey of wind convection coefficient correlations for building envelope energy systems' modeling. Applied Thermal Engineering. 2008;28:801-8.
[43] Zanghirella F, Perino M, Serra V. A numerical model to evaluate the thermal behaviour of active transparent facades. Energy and Buildings. 2011;43:1123-38.
[44] GRATIA, E.; DE HERDE, A. Natural ventilation in a double-skin facade. **Energy and Buildings,** v. 36, n. 2, p. 137-146, Feb 2004. ISSN 0378-7788. Disponível em: < <Go to ISI>://000189122300006 >.
[45] BALOCCO, C. A simple model to study ventilated facades energy performance. **Energy and Buildings,** v. 34, n. 5, p. 469-475, Jun 2002. ISSN 0378-7788. Disponível em: < <Go to ISI>://WOS:000175636100006 >.
[46] BONHOTE, P.; EPERON, Y.; RENAUD, P. Unglazed coloured solar absorbers on facade: Modelling and performance evaluation. **Solar Energy,** v. 83, n. 6, p. 799-811, Jun 2009. ISSN 0038-092X. Disponível em: < <Go to ISI>://WOS:000266893400003 >.
[47] WARGOCKI, P. et al. The effects of classroom air temperature and outdoor air supply rate on the performance of school work by children. **Indoor Air 2005: Proceedings of the 10th International Conference on Indoor Air Quality and Climate, Vols 1-5**, p. 368-372, 2005 2005. Disponível em: < <Go to ISI>://WOS:000233831200079 >.
[48] SHENDELL, D. G. et al. Associations between classroom CO2 concentrations and student attendance in Washington and Idaho. **Indoor Air,** v. 14, n. 5, p. 333-341, Oct 2004. ISSN 0905-6947. Disponível em: < <Go to ISI>://WOS:000223538700005 >.

[49] LÓPEZ, F. P. et al. Experimental analysis and model validation of an opaque ventilated facade. **Building and Environment,** v. 56, n. 0, p. 265-275, 2012. ISSN 0360-1323. Disponível em: < http://www.sciencedirect.com/science/article/pii/S0360132312001096 >.
[50] Real Decreto 1027/2007, de 20 de julio, por el que se aprueba el Reglamento de Instalaciones Térmicas en los Edificios
[51] KARAVA, P. et al. **Experimental study of the thermal performance of a large institutional building with mixed-mode cooling and hybrid ventilation**. ***Building and Environment,*** v. 57, p. *313-326*, 2012.
[52] PFAFFEROTT, J.; HERKEL, S.; WAMBSGANSS, M. Design, monitoring and evaluation of a low energy office building with passive cooling by night ventilation. **Energy and Buildings,** v. 36, n. 5, p. 455-465, May 2004. ISSN 0378-7788. Disponível em: < <Go to ISI>://WOS:000221826000007 >.
[53] GRATIA, E.; DE HERDE. Guidelines for improving natural daytime ventilation in an office building with a double-skin facade. **Solar Energy,** v. 81, n. 4, p. 435-448, 2007b. ISSN 0038-092X. Disponível em: < <Go to ISI>://000246746600001 >.
[54] BECKER, R.; GOLDBERGER, I.; PACIUK, M. Improving energy performance of school buildings while ensuring indoor air quality ventilation. **Building and Environment,** v. 42, n. 9, p. 3261-3276, Sep 2007. ISSN 0360-1323. Disponível em: < <Go to ISI>://WOS:000246650600014 >.
[55] GRATIA, E.; BRUYERE, I.; DE HERDE, A. How to use natural ventilation to cool narrow office buildings. **Building and Environment,** v. 39, n. 10, p. 1157-1170, Oct 2004. ISSN 0360-1323. Disponível em: < <Go to ISI>://WOS:000223517900003 >.
[56] JI, Y.; LOMAS, K. J.; COOK, M. J. Hybrid ventilation for low energy building design in south China. **Building and Environment,** v. 44, n. 11, p. 2245-2255, Nov 2009. ISSN 0360-1323. Disponível em: < <Go to ISI>://WOS:000268426800007 >.
[57] PRAJONGSAN, P.; SHARPLES, S. Enhancing natural ventilation, thermal comfort and energy savings in high-rise residential buildings in Bangkok through the use of ventilation shafts. **Building and Environment,** v. 50, p. 104-113, Apr 2012. ISSN 0360-1323. Disponível em: < <Go to ISI>://WOS:000299720800010 >.
[58] ANTVORSKOV, S. Introduction to integration of renewable energy in demand controlled hybrid ventilation systems for residential buildings. **Building and Environment,** v. 43, n. 8, p. 1350-1353, Aug 2008. ISSN 0360-1323. Disponível em: < <Go to ISI>://WOS:000257131200003 >.
[59] YAO, R. et al. Assessing the natural ventilation cooling potential of office buildings in different climate zones in China. **Renewable Energy,** v. 34, n. 12, p. 2697-2705, Dec 2009. ISSN 0960-1481. Disponível em: < <Go to ISI>://WOS:000269711300021 >.
[60] ARTMANN, N.; MANZ, H.; HEISELBERG, P. Climatic potential for passive cooling of buildings by night-time ventilation in Europe. **Applied Energy,** v. 84, n. 2, p. 187-201, Feb 2007. ISSN 0306-2619. Disponível em: < <Go to ISI>://WOS:000242521700006 >.
[61] YANGA, L. et al. Investigating potential of natural driving forces for ventilation in four major cities in China. **Building and Environment,** v. 40, n. 6, p. 738-746, Jun 2005. ISSN 0360-1323. Disponível em: < <Go to ISI>://WOS:000227416300002 >.
[62] SANTAMOURIS, M.; SFAKIANAKI, A.; PAVLOU, K. On the efficiency of night ventilation techniques applied to residential buildings. **Energy and Buildings,** v. 42, n. 8, p. 1309-1313, Aug 2010. ISSN 0378-7788. Disponível em: < <Go to ISI>://WOS:000278906700017 >.
[63] SHERMAN, M. H.; WALKER, I. S. Meeting residential ventilation standards through dynamic control of ventilation systems. **Energy and Buildings,** v. 43, n. 8, p. 1904-1912, Aug 2011. ISSN 0378-7788. Disponível em: < <Go to ISI>://WOS:000292786500012 >.